PREPARATION AND CHARACTERISATION OF Pt-Ru/C CATALYSTS FOR DIRECT METHANOL FUEL CELLS

Dissertation

Submitted in partial fulfilment of the requirements for the degree of

Masters of Science in Chemical Engineering

Prepared by:

Colleen Jackson

Prepared for:

Dr. Olaf Conrad

Dr. Pieter B.J. Levecque

Department of Chemical Engineering

Centre for Catalysis Research

National Hydrogen Catalysis Competence Centre

University of Cape Town

August 2014

SYNOPSIS

The direct methanol fuel cell (DMFC) is identified as a promising fuel cell for portable and micro fuel cell applications. One of the major benefits is that methanol is an energy dense, inexpensively manufactured, easily stored and transported, liquid fuel (Hamann *et al*., 2007). However, the DMFC's current efficiency and power density is much lower than theoretically possible. This inefficiency is predominantly due to the crossover of methanol from the anode to the cathode, Ru dissolution and Ru crossover from the anode to the cathode. In addition, the DMFC has a high manufacturing cost due to expensive catalyst costs and other materials. Catalyst expenses are further increased by catalyst loading due to low activity at the anode of the DMFC (Zhang, 2008). Hence, with increasing activity and stability of the Pt-Ru/C catalyst, catalyst expenditure will decrease due to a decrease in catalyst loading. In addition, performance will increase due to a reduction in ruthenium dissolution and crossover. Therefore, increasing the activity and stability of the Pt-Ru/C catalyst is paramount to improving the current DMFC performance and viability as an alternative energy conversion device.

Pt-Ru/C catalyst synthesis method, precursors, reduction time and temperature play a role in the activity for methanol electro-oxidation and stability since these conditions affect structure, morphology and dispersivity of the catalyst (Wang *et al.*, 2005). Metal organic chemical deposition methods have shown promise in improving performance of electro-catalysts (Garcia & Goto, 2003). However, it is necessary to optimise deposition conditions such as deposition time and temperature for $Pt(acac)_2$ and $Ru(acac)_3$ precursors.

This study focuses on a methodical approach to optimizing the chemical deposition synthesis method for Pt-Ru/C produced from $Pt(acac)_2$ and $Ru(acac)_3$ precursors. Organo-metallic chemical vapour deposition (OMCVD) involved the precursor's vapourisation before deposition and a newly developed method which involved the precursors melting before deposition. An investigation was conducted on the effects of precursor's phase before deposition. The second investigation was that of the furnace operating temperature, followed by an exploration of the furnace operating time influence on methanol electro-oxidation, CO tolerance and catalyst stability. Lastly, the exploration of the Pt:Ru metal ratio influence was completed.

It was found that the catalyst produced via the liquid phase precursor displayed traits of a high oxide content. This led to an increased activity for methanol electro-oxidation, CO tolerance and catalyst stability despite the OMCVD catalyst producing smaller particles with a higher electrochemically active surface area (ECSA).

The furnace operating temperature of the reactor played a significant role in catalyst activity and stability as high temperatures caused sintering of the catalyst particles and higher degrees of alloying. However, the lowest temperature in the study did not have the highest activity or stability but rather 350 °C was found to be the favoured operating temperature. This gives a firm indication that an optimum degree of alloying and catalyst morphology was found at this temperature. The furnace operating time of the reactor does not have a noteworthy influence on particle size or degree of alloying but affected ECSA, as a longer time in the reactor resulted in a lower ECSA and a less active and stable catalyst. This finding confirms that catalyst morphology is affected by reactor conditions and the preferred operating time in the reactor is the shortest time in this study of 30 minutes.

An interesting result was found in the Pt:Ru metal ratio investigation, as the ratio showing the best result for that of CO tolerance was different from that for methanol electro-oxidation. A higher degree of alloying was found in catalysts with a higher ruthenium ratio and ECSA decreased as platinum content increased. The methanol oxidation onset potential was similar across the Pt:Ru ratio range of 40:60 – 60:40, whilst CO oxidation onset potential had a clear minimum at 50:50. This indicates the CO oxidation onset potential is more sensitive to changes in Pt:Ru ratio than methanol oxidation. The second criterion for methanol oxidation activity is mass activity at 0.5 V vs. RHE ($\mu A/m^2$) and chronoamperometry experiments, which showed a Pt:Ru ratio of 50:50 to be the best performing.

These findings indicate a profound dependence of the methanol electro-oxidation activity on catalyst composition, particle size and morphology, and therefore CO tolerance and stability on reactor operating conditions, preparation method and Pt:Ru ratio. This study adds knowledge and some insight into catalyst preparation methods which could assist in enhanced catalyst design and improved catalyst activity for DMFC purposes.

ACKNOWLEDGEMENTS

I have been incredibly fortunate to have done my masters in the HySA Catalysis group. It has been a new, exciting and inspiring experience. I am deeply grateful to all who have supported and guided me through these 18 months.

To Olaf Conrad, your knowledge and passion for fuels cells and electrochemistry was both intimidating and inspiring! Thank you for accepting me into the master's degree and giving me such an amazing opportunity. I will forever appreciate your open door policy as a supervisor, as well as your continuous guidance and patience throughout my 'ups' and especially my frustrating 'downs'. Your friendly (and Tigger-like) persona made the HySA group a cheerful work environment.

I would especially like to thank Pieter Levecque for his unsurpassable ability to duplicate himself so he can be there for every one of his students as if they were his only responsibility. I couldn't have done it without you and I owe sincere gratitude for the day-to-day guidance and approachable, caring nature.

To Shiro Tanaka, I have thoroughly enjoyed the side project in which you involved me. Thank you for pushing me beyond my thesis work and into the exciting world of research.

Walter Böhringer, Eric Van Steen, Chris Woolard, Nabeel Hussain and Sue Harrison for providing the coursework which helped adequately prepare me for my thesis, thank you.

Thank you to my friend Susan Taylor for first encouraging me to join HySA, helping me in the labs when I first started and always being there when I needed help.

To all the friendly faces in HySA and Catalysis, it has been an absolute pleasure working with, and around you for the past 18 months.

Thank you to Mohamed Jaffer and Miranda Waldron in the Electron Microscope Unit for their efficiency in analysing my samples, as well as going out of their way to help in urgent situations.

Most importantly I would like to thank my boyfriend Douglas Whistance. Your unfailing love, support, interest, patience and understanding throughout this journey will forever be appreciated. Your motivational talks, proof reading and encouragement helped get me to the finish line.

Last, but certainly not least, I'd like to thank my family, parents and sisters for their support throughout my studies.

TABLE OF CONTENTS

LIST OF FIGURES

LIST OF TABLES

NOMENCLATURE

Symbols

Symbol	Unit	Description
A	Å	Lattice constant
d_P	nm	Diameter platinum particle
$d_{spacing}$	Å	d-spacing
$I_{crossover}$	$mol.min^{-1}cm^{-2}$	Rate of methanol permeation
L_{Pt}	g	Platinum loading on electrode
l_{os}	Å	Platinum on carbon d-spacing
l, m, n	-	Lattice planes
n_{rev}	-	Theoretical efficiency
v_i	-	Stoichiometric coefficients
x_{Ru}	-	Ruthenium faction in Pt-Ru particles
X	wt %	Weight percent contribution
θ	radians	Bragg angle
β	-	Peak width

ρ	m^3/g	density
τ	nm	Average crystallite size
λ	nm	X-ray wavelength

Constants

Constant	Value	Unit	Description
F	96 485	C/mol	Faraday's constant
k	0.9	-	Scherrer equation shape factor
Q_f	210	$\mu C/cm^2$	Hydrogen adsorption charge on platinum

GLOSSARY

Abbreviation	Description
ad	adlayer
ads	Adsorption
ACS	Advanced carbon supports
APU	Auxiliary power units
CVD	Chemical vapour deposition
CL	Catalyst layer
CNT	Carbon nano-tubes
CV	Cyclic voltammetry
DFA	Debye function analysis
DFT	Density function theory
DL	Double layer
DMFC	Direct methanol fuel cell
ECSA	Electrochemically active surface area

emf	Electromotive force
EXAFS	Extended X-ray adsorption fine structure
fcc	Face centred cubic
GDL	Gas diffusion layer
MeOH	Methanol
OMCVD	Organo-metallic chemical vapour deposition
OMCLD	Organo-metallic chemical liquid deposition
ORR	Oxygen reduction reaction
PEM	Polymer electrolyte ion-exchange membrane
PEMFC	Polymer electrolyte ion-exchange membrane fuel cell
Pt/C	Platinum supported on carbon
Pt-Ru/C	Platinum and ruthenium supported on carbon
RHE	Reversible hydrogen electrode
SEM	Scanning electron microscope
SA	Surface Area
TEM	Transmission electron microscope

TGA	Thermogravimetric analysis
upd	Under potential deposition
XANES	X-ray adsorption near edge structure
XRD	X-ray diffraction

1. INTRODUCTION

The need for sustainable energy and alternative energy sources is increasing as fossil fuels are depleting, and the move towards 'green' energy is underway. Since there is no burning of fuel in fuel cells, they are considered to be a clean process and have been proposed as an alternative energy source to conventional methods (Zhang, 2008).

Conventional methods convert fuel into thermal energy by burning the fuel in oxygen. The thermal energy is then converted into mechanical energy, usually via a turbine. Finally, the mechanical energy is converted into electrical energy. Fuel cells convert chemical energy directly into electrical energy by electro-chemically reacting a fuel with oxygen. Since this is a shorter energy pathway, the process is potentially more efficient than conventional methods (Behling, 2012). Another advantage of fuel cells is the silent operation due to few moving parts, which allows for easy maintenance (Zaidi & Rauf, 2009).

The most widely studied and promising fuel cell currently is the hydrogen polymer electrolyte membrane fuel cell (PEMFC), because the system can obtain a high efficiency and the only side product is water. However, the hydrogen fuel cylinders are too large and heavy to be viable in portable applications. For portable applications it is important to have a dense fuel that is rich in hydrogen in order to reduce the weight and size of the fuel tank. Secondly, a significant hurdle is the development of a reasonably priced and safe hydrogen infrastructure and distribution network to replace the petroleum and diesel based system (Liu & Zhang, 2009). The disadvantages of hydrogen technology initiated the research into an alternative fuel cells to be used with Direct Alcohol Fuel Cells (Gao *et al.,* 2012).

Methanol has been considered to be the most promising alcohol for portable and micro fuel cell applications since methanol is a liquid under atmospheric conditions, synthesized easily and inexpensively, and has a theoretical specific energy density of 6 $kWh.kg^{-1}$ (Hamann *et al*., 2007). Therefore a Direct methanol fuel cell (DMFC) is a promising alternative to conventional batteries, which have a much lower specific energy density of 0.6 $kWh.kg^{-1}$. This would translate into a longer battery life and more power available on portable devices. In addition, the DMFC would have the advantage of instantaneous refueling, unlike the rechargeable battery which requires hours to restore power. Moreover, methanol production is a mature technology and can be stored and distributed by adapting the current petroleum and diesel infrastructure (Zhang, 2008).

Despite the many advantages of DMFC's over hydrogen PEMFC's, the drawbacks of DMFC's are the high cost of materials used in fabrication, the crossover of methanol from the anode to the cathode,

ruthenium dissolution and crossover from the anode to the cathode, low efficiency and low power density (Zhang, 2008). Due to the low activity of the catalyst at the anode, catalyst loading at the anode is approximately ten times that of the catalyst loading in a hydrogen PEMFC. The high catalyst loading increases mass transfer limitations which further decreases the efficiency at the anode (Shah, 2007).

Carbon supported Pt-Ru catalysts are considered to currently be the best catalysts for the anode of the DMFC because of their tolerance of the carbon monoxide intermediate of the methanol oxidation reaction and activity towards the water split reaction (Aricò *et al.,* 2001). These Pt-Ru/C catalysts are usually prepared by chemical reduction of H_2PtCl_6 and $RuCl_3$ precursors with an atomic ratio of $Pt_{0.5}Ru_{0.5}$ (1:1) (Wang *et al.*, 2005). However, it has been proposed that catalyst precursors containing chloride have lower activity and stability than non-chloride precursors since the chloride deactivates the active sites on the catalyst (Zhao *et al*., 2005). This optimum ratio of Pt:Ru, morphology, degree of alloying and particle size is highly contested since optimum conditions are easily influenced by slight variations in preparation methods (Wang *et al.*, 2005).

The wet chemical method is the most common catalyst synthesis method, this method involves the impregnation of precursors in solution while mixing, followed by chemical reduction using a reducing agent. The catalyst is then washed, dried, calcined and activated (Liu *et al*., 2006). The Organo-Metallic Chemical Vapour Deposition (OMCVD) synthesis method has many advantages over wet synthesis. Namely, it is a 'one-step' process which is less time consuming since it allows lengthy stages, involved in the wet chemistry method, to be avoided (Thurier & Doppelt, 2008). In addition, the mixing of catalyst precursors in the OMCVD method occurs in the vapour phase. This allows for small particle production, excellent film uniformity and an enhanced level of control over metal loading, since the decomposition occurs at the same time and in a more controlled manner (Zhao *et al*., 1989). The CVD process is a promising catalyst synthesis method because small particles are produced which show excellent electrochemical properties in PEMFC's (Garcia & Goto, 2003).

The aim of this study was to investigate the characteristics and electrochemical performance for methanol oxidation of Pt-Ru/C catalysts prepared by OMCVD method and a new method which involves precursor deposition before vapourisation. The effect of varied precursor deposition phases, synthesis times (30 minutes - 8 hours deposition time), synthesis temperature (300 - 700 °C) and Pt:Ru ratios (9:1 – 5:5) was investigated.

2. LITERATURE REVIEW

2.1. Direct Methanol Fuel Cell Technology

The direct methanol fuel cell (DMFC) produces electrical energy directly from liquid methanol in a fuel cell to produce water and carbon dioxide.

2.1.1. Fuel Cell Operation

A DMFC consists of two electrodes, the cathode and the anode, which are both in contact with a proton conducting electrolyte between them. The present day DMFC electrolyte is a polymer electrolyte ion-exchange membrane (PEM). The electrodes usually consist of 3 layers, the catalyst layer, the diffusion layer, and backing layer. The most typical catalyst used at the cathode is Pt, and Pt-Ru alloy at the anode which can be supported by carbon or unsupported catalysts (Liu & Zhang, 2009). The purpose of the catalytic layer is to decrease the activation energy of the half reaction and conduct protons and electrons while being gas permeable, water regulating and corrosion stable.

Methanol and water are fed into the anode where the oxidation reaction occurs on the catalyst surface to produce carbon dioxide, protons (H^+) and electrons (e^-). The electrons travel up the current collector; through the external electrical circuit to the cathode and the protons cross the electrolyte from anode to cathode. At the cathode the electrons and protons react with oxygen to form water.

The half reactions at the electrodes are as follows:

$$Anode: \quad CH_3OH + H_2O \rightarrow 6H^+ + 6e^- + CO_2 \qquad \text{Equation 1}$$

$$Cathode: \quad \frac{3}{2}O_2 + 6H^+ + 6e^- \rightarrow 3H_2O \qquad \text{Equation 2}$$

$$Overall\ Reaction: \quad CH_3OH + \frac{3}{2}O_2 \rightarrow 2H_2O + CO_2 \qquad \text{Equation 3}$$

DMFC systems are promising alternative portable power systems for electronic devices such as laptops, mobile phones, medical devices and auxiliary power units (APU). There are multiple institutes which have developed DMFCs of varying output power densities such as Motorola Labs (12-27 $mWcm^{-2}$), Samsung Advanced Institute of Technology (23 $mWcm^{-2}$) and Korea Institute of Energy Research (121-207 $mWcm^{-2}$) (Liu & Zhang, 2009). In addition to portable applications, DMFCs could fill a role in transportation systems since they are comparable, and in some ways superior, to the hydrogen PEM fuel cell mainly due to ease of storage and transport (Liu & Zhang, 2009).

The DMFC setup is as shown below:

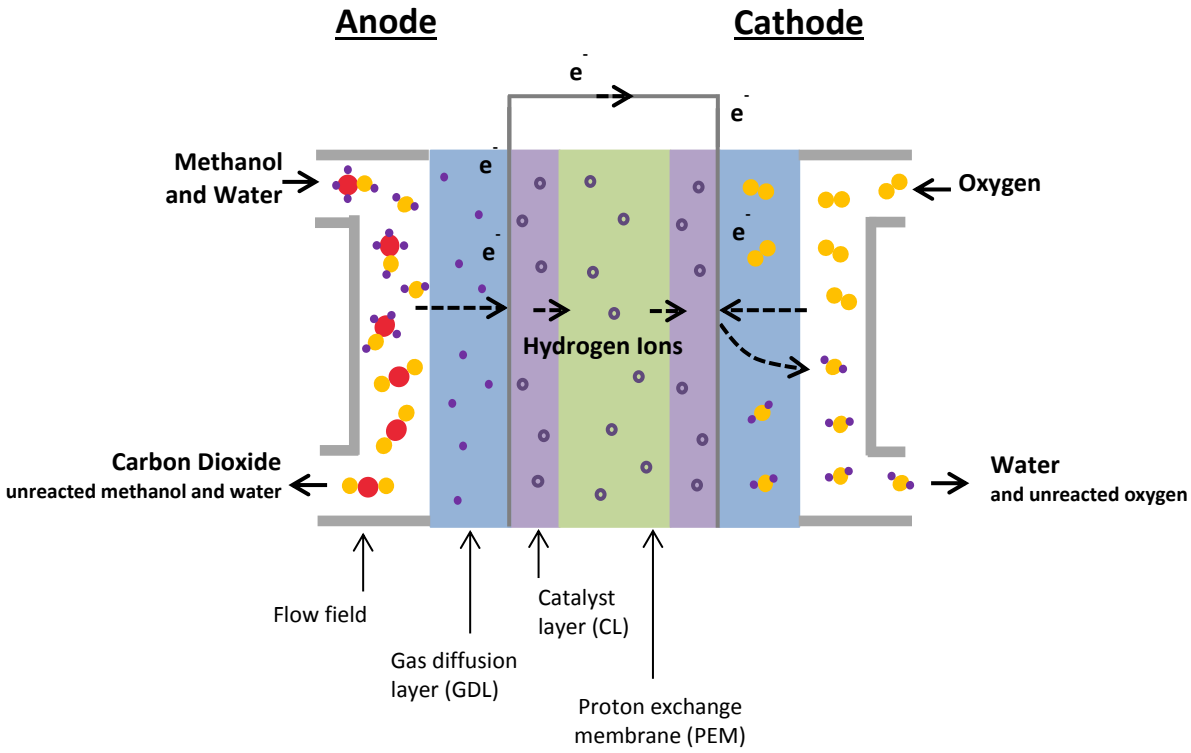

Figure 2-1: Schematic of DMFC operation.

2.1.2. Thermodynamic Efficiency

One of the drives behind research into DMFCs is due to the high theoretical efficiency of the system to produce 6 kWh/kg_{MeOH} of electrical energy in a fuel cell. This theoretical energy density is derived from thermodynamic efficiencies calculated using the half reactions in equations 1 and 2.

The enthalpy of the reaction is calculated by the equation:

$$\Delta H^0 = \Sigma v_i H_{i,products} - \Sigma v_i H_{i,reactants} \qquad \text{Equation 4}$$

$$\Delta H^0 = -727\ kJ/mol$$

The entropy of the reaction is calculated by the equation:

$$\Delta S^0 = \Sigma v_i S_{i,products} - \Sigma v_i S_{i,reactants} \qquad \text{Equation 5}$$

$$\Delta S^0 = 0.81\ kJ/(K.mol)$$

The Gibbs free energy is thus calculated by enthalpy and entropy values since:

$$\Delta G^0 = \Delta H^0 - T\Delta S^0 \qquad \text{Equation 6}$$

Where T=298.15 K

$$\Delta G^0 = -702\ k\,J/mol$$

The electromotive force (emf) is calculated by:

$$emf = -\frac{\Delta G^0}{nF} = 1.21\ V \qquad \text{Equation 7}$$

Where n = 6 e^- and F is Faradays Constant= 96 485 $C.mol^{-1}$

The thermodynamic efficiency is calculated by:

$$\eta_{rev} = \frac{\Delta G^0}{\Delta H^0} = 0.964 \qquad \text{Equation 8}$$

The theoretical efficiency of the DMFC is therefore 96.4% at 25 °C, 1 atm and pure O_2 feed at the cathode. This efficiency is higher than the hydrogen fuelled PEFC's theoretical efficiency which is calculated to be 83%. Current DMFC performance is far from the theoretical efficiency due to methanol crossover, ruthenium dissolution, ruthenium crossover, and inefficiency of Pt-Ru/C catalyst at the anode (Zhang, 2008).

2.1.3. Current DMFC Efficiency

The open circuit voltage of a DMFC with a polymer electrolyte is considerably lower than the thermodynamic potential or reversible potential difference, mainly due to methanol crossover and ruthenium dissolution. The methanol crossover causes a mixed potential at the cathode and 'irreversible adsorption of intermediate species at the electrode potentials close to the reversible potential' (Liu & Zhang, 2009). The polarization curve of a polymer electrolyte DMFC is shown in Figure 2-2.

In the presence of methanol, the onset potential of the oxygen reduction reaction (ORR) is below 0.9 V vs. reversible hydrogen electrode (RHE), however in the absence of methanol the reversible potential is 1.23 V vs. RHE.

The kinetic limitations of the reaction are the methanol oxidation reaction and ORR compete with each other, with methanol oxidation as preference at the cathode. No current is registered above 0.9 V vs. RHE due to this phenomenon (Liu & Zhang, 2009). In addition, at high currents mass transport negatively effects cell potential due to CO_2 removal from the anode and flooding at the cathode. Flooding at the cathode is primarily due to methanol and water crossover, and partially due to water formation at the electrode.

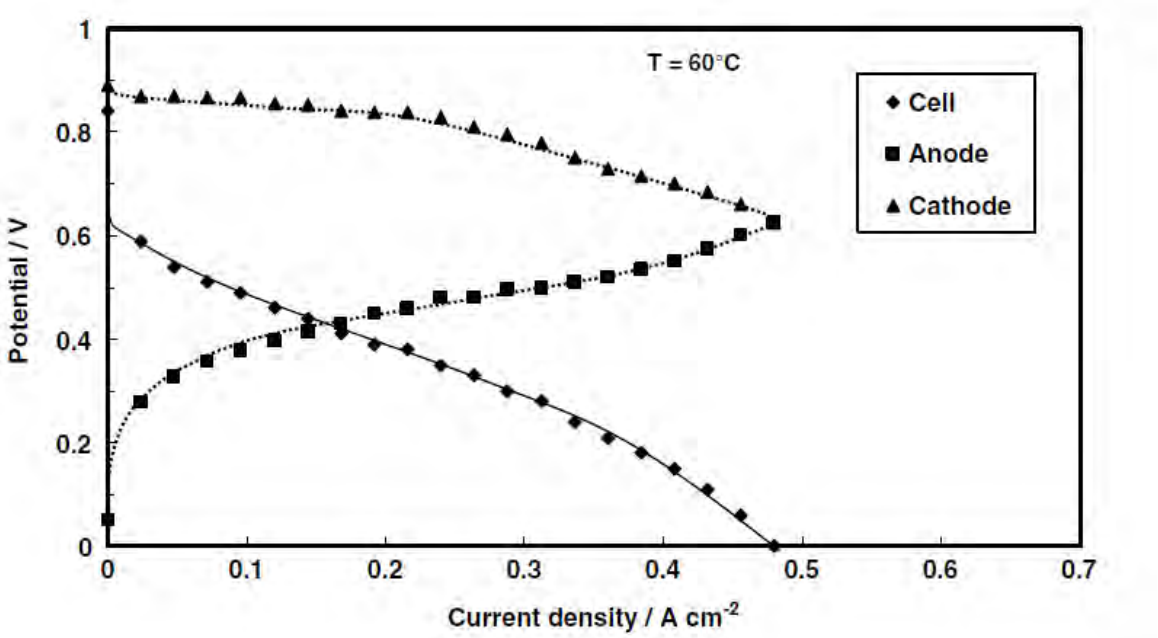

Figure 2-2: Single cell and in situ half-cell electrode polarizations for a DMFC operating at 60 °C, ambient pressure, 1 M CH_3OH at the anode and air feed at the cathode (Zhang, 2008).

The methanol crossover can be calculated from the CO_2 concentration at the cathode since almost complete methanol oxidation of the methanol which crossed over will take place at high electrochemical potentials. From the methanol crossover, the equivalent current lost from this can be calculated using Faraday's Law:

$$I_{crossover} = n_{MeOH\ crossover} \times 6 \times F \qquad \text{Equation 9}$$

Where methanol crossover is a rate of methanol permeation per geometric electrode area and time (Liu & Zhang, 2009).

Since the activity of the Pt-Ru/C catalyst is low, the catalyst loading in a DMFC anode is ten times that of the anode in hydrogen PEMFC. This increased loading introduces mass and heat transfer limitations which further decreases the cells' efficiency. This inefficiency is mainly attributed to the formation of Ru ions and the subsequent dissolution in solution. The dissolved metal leads to an activity loss at the anode, and the ability of Ru ions to travel through the membrane and deposit on the cathode negatively affects the cathode activity (Piela *et al.*, 2004). Ruthenium dissolution is described in more detail in section 2.3.4.

2.2. DMFC Anode Catalysts

Platinum based catalysts are the standard catalysts for DMFC operations, this section outlines mechanisms for methanol oxidation and CO oxidation on Pt while outlining the importance of alloys in enhancing the activity for both reactions.

2.2.1. Catalysts for Methanol Oxidation Activity

The low activity of the anode electro-catalyst is the major factor limiting the DMFC performance and the practical development of the fuel cell (Vielstich *et al.*, 2003). The detailed mechanism of methanol oxidation has been widely studied by a variety of methods and experimental procedures, finding that electro-oxidation of methanol on pure platinum begins with three steps of dehydrogenation at low potentials followed by, CO-like species chemisorption, OH or H_2O like species adsorption, an interaction between the CO-like and OH-like species followed by CO_2 evolution. The rate determining step is dependent on the reaction temperature and the catalyst surface structure (Liu & Zhang, 2009).

The mechanism for this reaction on pure platinum is as follows:

$$CH_3OH + Pt \rightarrow Pt - CH_2OH + H^+ + e^- \qquad \text{Equation 10}$$

$$Pt - CH_2OH \rightarrow Pt - CHOH + H^+ + e^- \qquad \text{Equation 11}$$

$$Pt - CHOH \rightarrow Pt - COH + H^+ + e^- \qquad \text{Equation 12}$$

$$Pt - COH \rightarrow Pt - CO + H^+ + e^- \qquad \text{Equation 13}$$

The splitting of water on platinum occurs by the following equation; however this is a slow reaction and it requires high activation energy:

$$Pt + H_2O \rightarrow Pt - OH + H^+ + e^- \qquad \text{Equation 14}$$

The CO_{ads} acts as a poison on the platinum surface because of the strong adsorption on the surface and does not readily react to form CO_2 as shown the in the equation below:

$$Pt - OH + Pt - CO \rightarrow 2Pt + CO_2 + H^+ + e^- \qquad \text{Equation 15}$$

Due to the strong CO adsorption and slow water splitting reaction on platinum, platinum alloys supported on carbon black are the current state of the art electro-catalysts for methanol oxidation (Liu & Zhang, 2009). The electro-catalytic activity of platinum for methanol oxidation and CO oxidation is known to be improved by second metals such as Ru or Sn (Aricò *et al.,* 2001). Ruthenium alloyed with platinum has a low activation energy for CO oxidation and the water split reaction due

to the metal interactions. Therefore when ruthenium is alloyed with platinum the activity for methanol oxidation is higher than pure platinum.

Methanol oxidation on Pt-Ru catalysts is partially understood. The initial dehydrogenation of methanol in understood to primarily take part on Pt sites as shown in Equation 10, 11, 12 and 13, however the water split and CO oxidation is suggested to go one of two ways. Some researchers believe the CO can migrate from the platinum active site to the ruthenium active site, if the ruthenium is close to the platinum originally suggested by Watanabe & Motoo (1975). Another theory is if ruthenium is close enough to platinum, this interaction reduces the strong interaction between CO and platinum and thus the CO will react faster to form CO_2 (Gasteiger *et al.*, 1994a). The two theories are shown below:

$$Ru - OH + Ru - CO \rightarrow 2Ru + CO_2 + H^+ + e^- \qquad \text{Equation 16}$$

$$Ru - OH + Pt - CO \rightarrow Pt + Ru + CO_2 + H^+ + e^- \qquad \text{Equation 17}$$

2.2.2. Catalysts for CO Tolerance

CO electro-oxidation on a monometallic Pt surface is a well understood reaction, described by linearly adsorbed CO and CO oxidation on Pt (100) and Pt (110) surface sites (Dhar *et al.*, 1987). The rate of CO oxidation at low coverage is high whilst the rate of CO oxidation decreases at high coverage, indicating the rate of CO oxidation is dependent on coverage and thus involves the use of adjacent surface (Zhang, 2008).

$$Pt + CO \rightarrow Pt - CO_{ads} \qquad \text{Equation 18}$$

$$Pt + H_2O \rightarrow Pt - OH_{ads} + H^+ + e^- \qquad \text{Equation 19}$$

The understood mechanism on Pt is described below (redrawn from Gilman, 1964):

$$CO_{dissolved} + Pt \rightarrow \underset{\mid}{CO} \qquad\qquad H_2O + Pt \rightarrow \underset{\mid}{H_2O}$$

$$\underset{\mid}{Pt} \qquad\qquad \underset{\mid}{Pt}$$

$$\underbrace{CO}_{\mid} + \underbrace{H_2O}_{\mid} \rightarrow \overbrace{\underbrace{CO}_{\mid} - - \underbrace{H_2O}_{\mid}}^{\text{Adjacent Complex}} - - e^- \rightarrow \overbrace{\underbrace{CO}_{\mid} - - \underbrace{OH}_{\mid}}^{\text{Activated Complex}} + e^- + H^+$$

$$Pt \qquad Pt \qquad Pt \qquad Pt \qquad Pt \qquad Pt$$

$$CO - -OH \rightarrow CO_2 + e^- + H^+ + 2Pt$$
$$\quad | \qquad\quad |$$
$$\quad Pt \qquad Pt$$

The adsorption of CO and H_2O in the first step is rate controlled by diffusion to the metal site, thus this step is rapid for surfaces with less coverage than at equilibrium. The second step is the electron-transfer step. This step is rate determining provided there is a fixed concentration of reactant pairs. The last step is the final electron-transfer step, which is fast in relation to step two (Gilman, 1964). The activation energy for this reaction is significantly reduced with the presence of Ru, which is the primary reason Pt-Ru alloys are employed for CO tolerance catalysis.

CO adsorbs strongly to the surface of platinum and ruthenium to form a monolayer which can be removed by the following oxidation reaction (Zhang, 2008):

$$CO + H_2O \rightarrow CO_2 + 2H^+ + 2e^- \qquad \text{Equation 20}$$

The cyclic voltammogram in Figure 2-3 is an example of CO oxidation on a pure Pt surface.

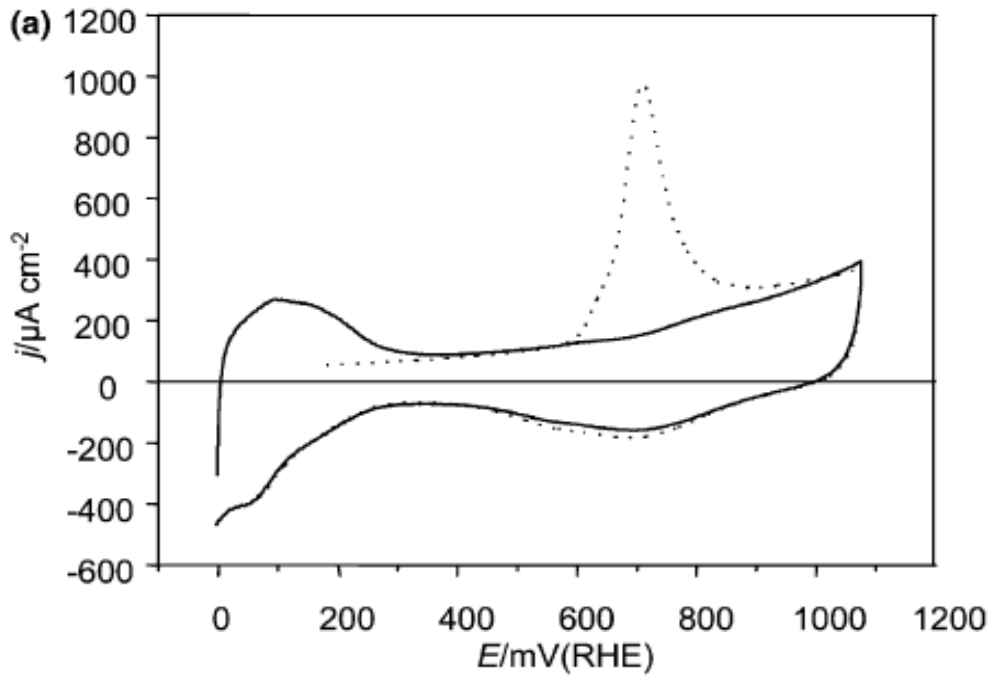

Figure 2-3: CO stripping voltammograms of Pt recorded in 0.1 M $HClO_4$ solution. First scan: dashed lines; second scan: solid lines (CO adsorbed for 3 min at 0.1 V vs. RHE, v = 5 $mV.s^{-1}$, T =293 K) (Vigier *et al.*, 2004).

CO oxidation on Pt-Ru/C catalysts is not completely understood, there are two accepted mechanisms for improved performance of CO oxidation on Pt-Ru surface. These two mechanisms are named the (1) bifunctional mechanism and (2) the direct mechanism, enabled by the ligand or electron effect. In order to remove CO_{ads} from the surface, an oxygenated species is required to react with CO_{ads} to produce CO_2, these two mechanisms are described in detail below.

(1) The bifunctional mechanism states the better performance of binary systems could be attributed to the promotional effect with ruthenium assisting in water activation (Giorgi *et al*., 2001):

$$Pt + CO \rightarrow Pt - CO_{ads} \qquad \text{Equation 21}$$

$$Ru + H_2O \rightarrow Ru - OH_{ads} + H^+ + e^- \qquad \text{Equation 22}$$

$$Pt - CO_{ads} + Ru - OH_{ads} \rightarrow Pt + Ru + CO_2 + H^+ + e^- \qquad \text{Equation 23}$$

The bifunctional mechanism aids in CO oxidation since hydrogen oxidation reaction occurs on free Pt sites between CO_{ads}, CO_2 liberation and CO re-adsorption. At low potentials CO re-adsorption rate is rapid in relation to CO_{ads} oxidation, thus the hydrogen oxidation reaction is hindered by CO_{ads} on to platinum sites. Therefore, a supply of OH species is necessary to increase the rate of CO_{ads} oxidation by a metal which does not adsorb CO. The bifunctional mechanism on Pt-Ru involves a 'Ru-OH type' species which is not completely understood (Zhang, 2008).

(2) The direct mechanism involves the reduction of the adsorption energy of CO on Pt by a 'ligand effect'. The theory describes that when Pt is alloyed with Ru, this results in a downward shift of the d-bands in the Pt, causing a less strongly adsorbed CO bond on the Pt sites. Since the CO_{ads} is not held as strongly by Pt sites, this allows for a higher rate of CO_{ads} oxidation (Zhao *et al.*, 2007).

Lu & Masel (2001) conducted an investigation of Ru deposited on Pt (110) using Temperature Programmed Desorption (TPD) in a UHV in order to determine the CO tolerance mechanism. Their findings were that Ru substantially affected the adsorption properties of Pt (110) surface since the binding energy of CO decreases. The exchange of ^{18}O into $H_2{}^{16}O$ is improved by a reduction in the activation barrier. In conclusion, the investigation yielded a total of approximately 200 mV reduction in CO activation barrier is achieved, with roughly 40 mV (20%) associated to the ligand effect and 160 mV (80%) reduction due to the bifunctional mechanism.

2.3. Pt-Ru/C Catalysts

As mentioned above, Pt-Ru/C catalysts are most commonly used in the anode of the DMFC due to the CO tolerance of ruthenium and activity for the water split reaction.

2.3.1. Pt-Ru Bimetallic Alloy Structure

Structural modifications due to metal interactions are caused in a Pt particle once Ru has been alloyed with the Pt. Vogel *et al*. (1997) studied the changes in particle structure and surface structure due to Pt-Ru alloying via in-situ XRD, Debye function analysis (DFA), X-ray absorption near edge structure (XANES) and extended X-ray adsorption fine structure (EXAFS). The best fit simulation was found to be half face-centered cubic (fcc) orientation and the other half multiply twinned decahedral particles.

Another study (Radmilović *et al.,* 1995) identified well-resolved (200) and (111) crystallographic planes with occasional (113) facets and twinned particles which resemble a cubo-octahedral shape in real space. High resolution transmission electron microscopy (HRTEM) micrographs clearly show the presence of these surfaces, as demonstrated in Figure 2-4 showing (111) and (200) crystal surfaces.

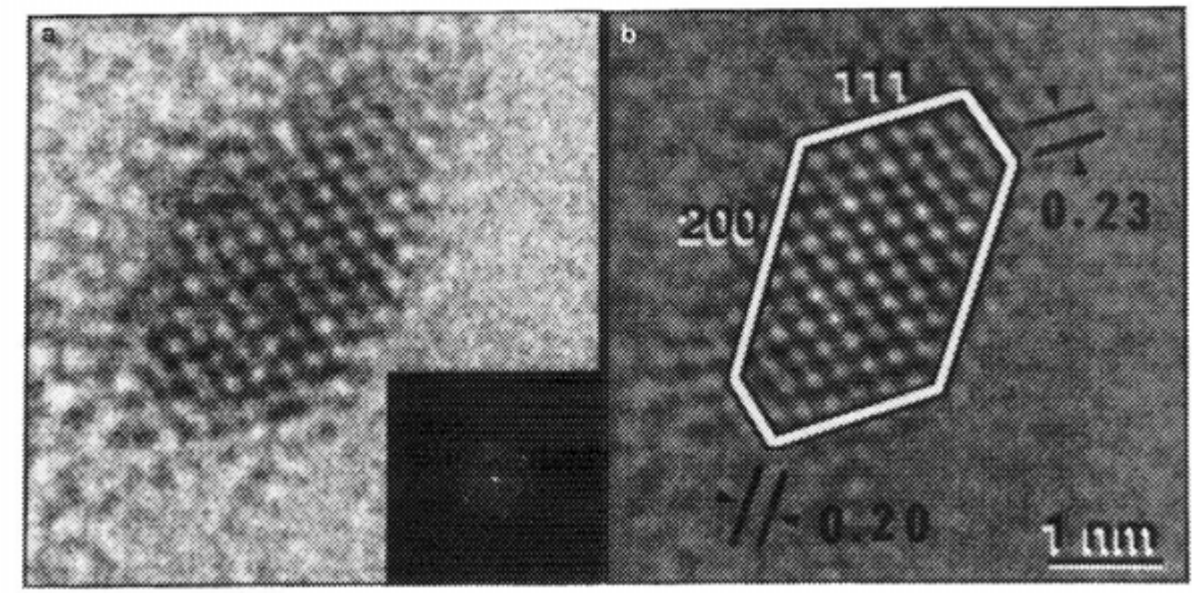

Figure 2-4: HRTEM micrograph of a Pt-Ru particle on the edge of the carbon support: (a) unfiltered image of asymmetric cubo-octahedral particle (b) Fourier filtered image (Radmilović *et al.,* 1995).

2.3.2. Pt-Ru/C Catalyst in DMFC

2.3.2.1. Temperature effect on Methanol Oxidation

Aricò *et al.* (2003) investigated the methanol oxidation behaviour of three Pt-Ru catalysts with varying metal concentrations on a carbon support with a temperature range of 80 - 130 °C.

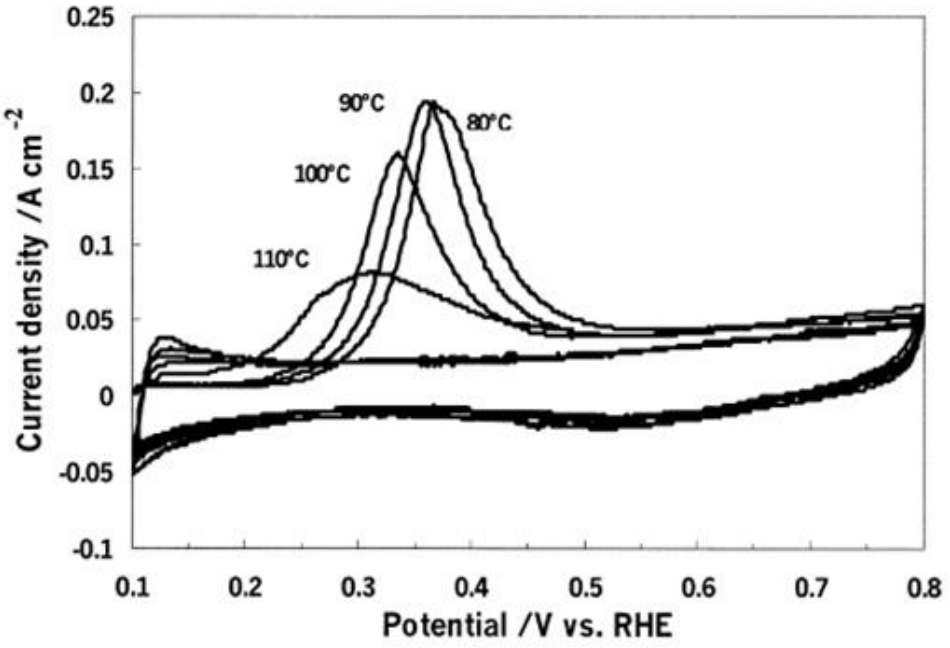

Figure 2-5: In situ CO stripping voltammetry on 85 wt% Pt-Ru/C catalyst at various temperatures under the DMFC configuration. Anode: 2% CO in Ar, 1 atm, adsorbed for 30 min. Cathode: H_2 feed, 1 atm (Aricò *et al.*, 2003).

As the temperature increases, the activation barrier for methanol oxidation is decreased and the peak potential is shifted towards the left. Although the activation barrier is decreased, as temperature increases above 90 °C there is a dramatic decrease in coverage of adsorbed methanolic species. However as temperature increases the physio-chemical properties of the alloy have much less influence on the methanol oxidation behaviour since the high temperatures reduce CO poisoning on the surface of the metals.

On the contrary, Gasteiger *et al.* (1994b) investigated the temperature dependence of methanol electro-oxidation on Pt-Ru alloys and concluded that the optimum Ru content increased with increasing temperature. In addition, the investigation showed as temperature increased the electro-oxidation of methanol increased significantly on Pt, Ru and Pt-Ru catalysts as demonstrated by potentiostatic oxidation graphs shown in Figure 2-6.

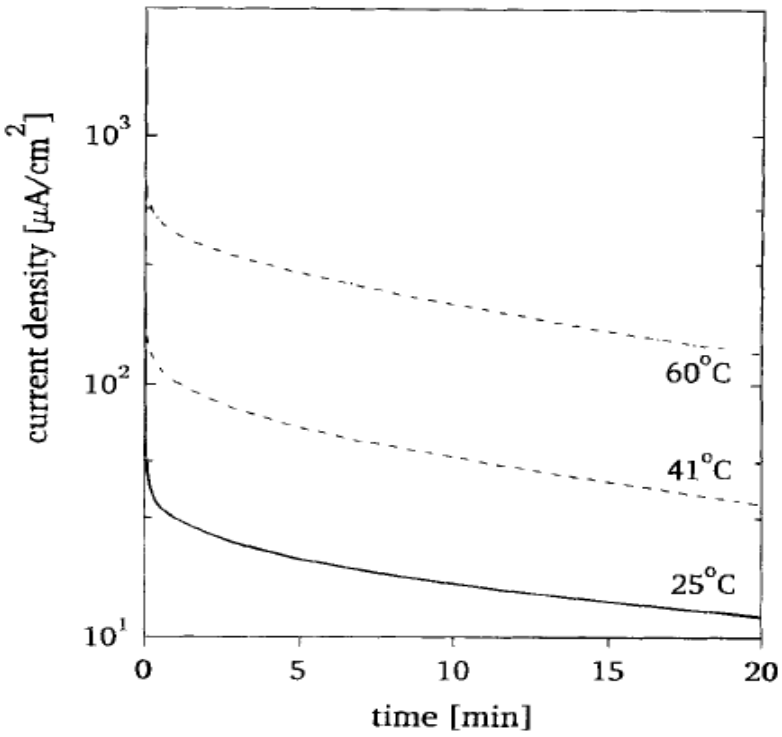

Figure 2-6: Potentiostatic oxidation of 0.5 M CH_3OH in 0.5 M H_2SO_4 at 25, 41, and 60 °C on sputter-cleaned Pt-Ru alloy electrodes with a Ru surface composition of 33 a/o. Potential was stepped from 0.075 to 0.4 V vs. RHE (Gasteiger *et al*., 1994b).

2.3.2.2. Pt:Ru composition effect on Methanol Oxidation

The subject of the optimal Pt:Ru ratio for methanol oxidation remains unclear due to many factors influencing the optimum and contradicting results from studies. There are multiple factors effecting the optimum composition of Pt-Ru/C in a DMFC such as co-catalytic effect, preparation method, surface morphology (e.g. roughness), presence of Ru oxides, presence and type of support, operating anode potential range, methanol concentration, and temperature (Zhang, 2008). Due to the multiple factors, many experiments geared at determining optimum composition of Pt-Ru catalysts for methanol electro-oxidation yield contradicting results.

Aricò *et al*. (2009) stated: 'The optimum Ru surface composition is preferable to the relevant synergism accomplished by a Pt-Ru surface with 50% atomic Ru in maximizing the product of OH coverage and intrinsic rate constant, assuming the surface reaction between CO_{ads} and OH_{ads} as rate determining step'.

Gasteiger *et al.* (1994b) described that at low temperatures, methanol oxidation occurs more readily on Pt-Ru alloys with Ru content of ≈ 10 atm%. As temperature is increased to moderate temperatures (around 60 °C) the ratio of Ru ≈ 33 atm% is preferred. At intermediate and high

temperatures, the rate determining step is the removal of OH from the catalyst surface. Since this occurs more readily on the Ru surface, a higher ratio of Ru is optimum for higher temperatures.

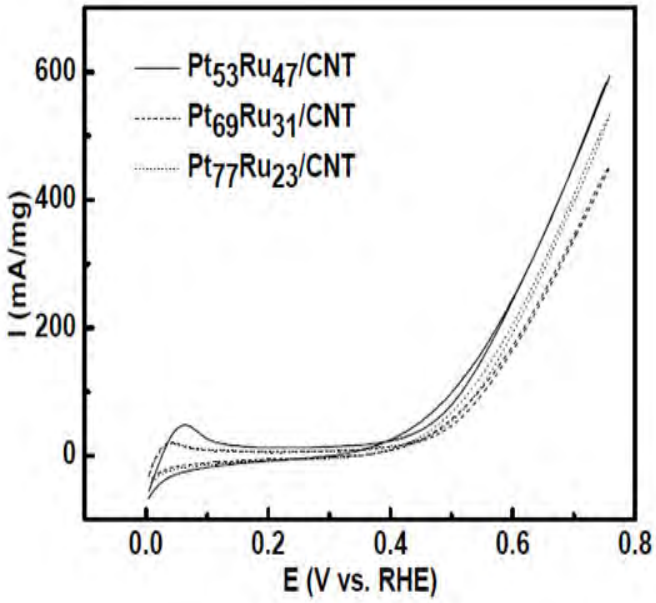

Figure 2-7: Cyclic voltammograms of methanol electro-oxidation on different Pt-Ru/CNT catalysts at 60 °C (Li & Xing, 2009).

Li & Xing (2009) found the optimum Pt:Ru ratio on carbon nano-tubes (CNT) for methanol oxidation with 2.0 M CH_3OH at 60 °C to be 50:50 atm%, shown in Figure 2-7 whilst Lizcano-Valbuena *et al.* (2002) suggested the optimum Pt:Ru ratio for methanol oxidation with 2.0 M CH_3OH at 25°C to be 75:25 atm%, shown in Figure 2-8.

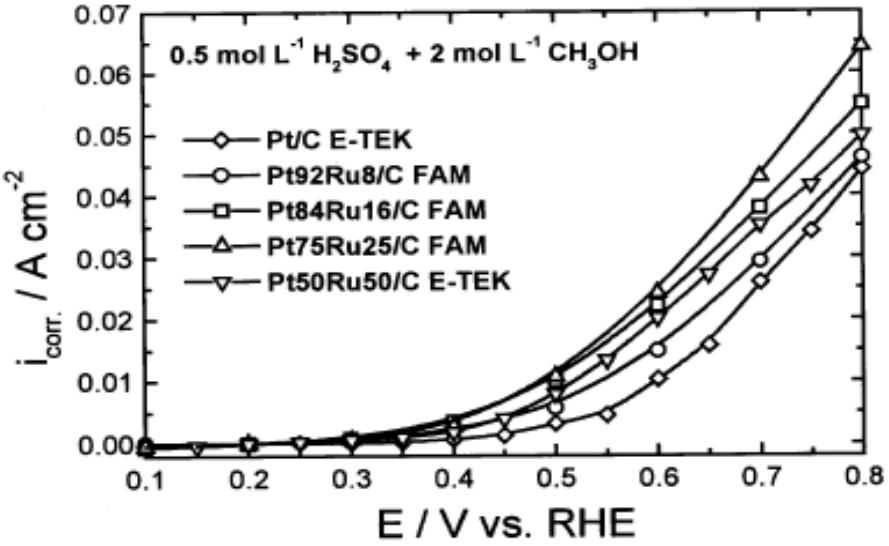

Figure 2-8: Current densities of the 20th min of chronoamperometric studies at several potentials in 2 M methanol solution in 0.5 M H_2SO_4 (Lizcano-Valbuena *et al.*, 2002).

Figures 2-7 and 2-8 demonstrate the temperature dependency of the optimum Pt-Ru ratio. However, there are many conflicting studies, such as Coutanceau *et al*. (2004) which concluded the optimal Pt:Ru ratio for temperature ranges of 50-110 °C with 1 M CH_3OH to be 80:20 atm%.

In addition to temperature dependence, the optimum Pt:Ru ratio is dependent on methanol concentration as demonstrated in Figure 2-9.

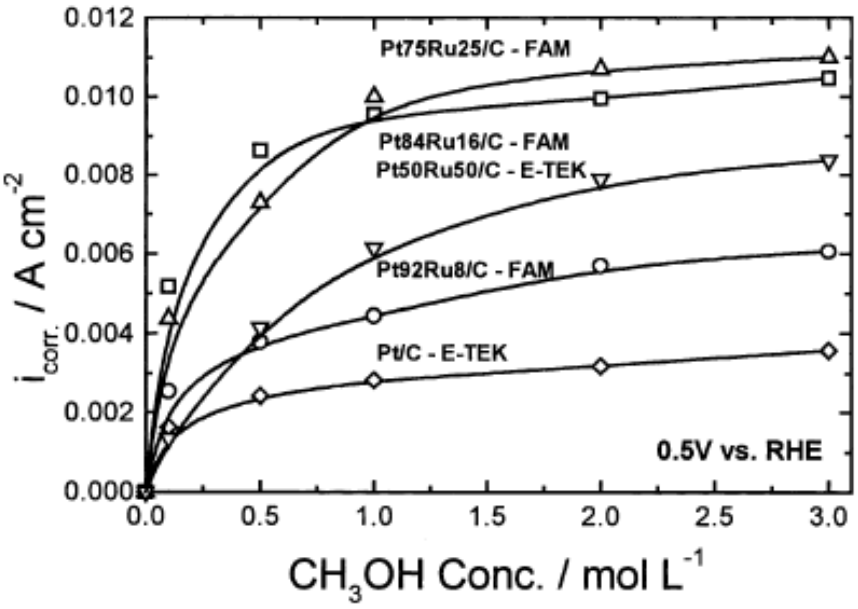

Figure 2-9: Current densities at the 30th minute of chronoamperometric studies at 0.5 V vs. RHE in different methanol concentrations in 0.5 M H_2SO_4 for all catalysts, corrected for cathodic current densities at the same potential in the absence of methanol (Lizcano-Valbuena *et al.,* 2002).

It is still widely debated if Pt-Ru alloys or Pt nanoparticles decorated with Ru nanoparticles show higher activity for methanol oxidation. Waszczuk *et al*. (2001) prepared Pt decorated with Ru nanoparticles using spontaneous deposition and compared it to Johnson Matthey commercial Pt-Ru alloy of the same elemental composition. The result showed double the oxidation current density for methanol oxidation compared to the homogeneous alloy. A separate study by Chrzanowski & Wieckowski (1998) prepared single crystals of Pt(111), Pt(100), Pt(110) and polycrystalline Pt decorated with Ru by electro-deposition which showed better activity, especially for Pt(111)/Ru with one order of magnitude higher than commercial Pt-Ru for methanol oxidation. To the contrary, Iwasita *et al*. (2000) investigated activities of different types of Pt-Ru catalysts for methanol oxidation, including ultra-high vacuum (UHV) cleaned Pt-Ru alloys, UHV evaporated Ru onto Pt (111), and adsorbed Ru on Pt (111). The results in Figure 2-10, show the Pt-Ru alloy prepared by UHV cleaning gives four times higher oxidation current density than the Pt(111)/Ru_{ad}.

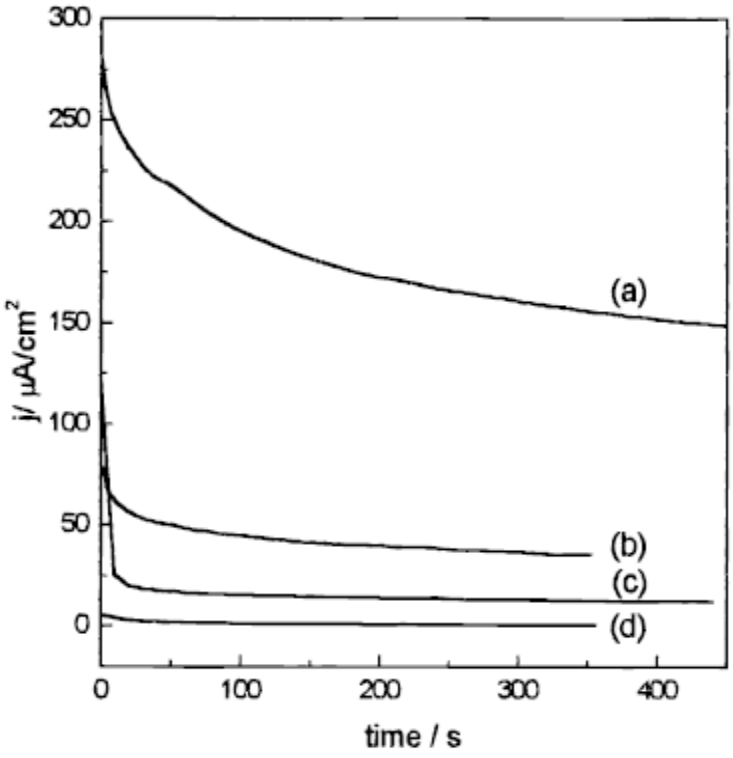

Figure 2-10: Chronoamperometry of different Pt-Ru electrodes at 0.5 V vs. RHE in 0.5 M CH_3OH and 0.1 M $HClO_4$. a) Pt-Ru alloy prepared by H_2 reduction, b) Pt(111)/Ru_{ad} prepared by spontaneous adsorption, c) Pt(111)/Ru prepared by evaporation, d) Pt(111) (Iwasita *et al*., 2000).

In addition, Bock *et al*. (2005) prepared Pt-Ru alloys and Ru adlayer/Pt catalysts and found significantly lower methanol oxidation activity for Ru adlayers on Pt and interestingly concluded that catalysts containing RuO_2 had pointedly higher methanol oxidation activity than other catalysts. It should be noted that preparation methods in this investigation include high temperature treatment, emphasising the importance of method preparation in catalyst performance.

One focus of Bock *et al*. (2005) was the role of RuO_2 in methanol oxidation performance. Other investigations involving Ru oxides and oxo-hydroxide (RuO_xH_y) have been conducted describing the essentiality of these Ru compounds in improved methanol oxidation activity (Long *et al.,* 2000) (Rolison *et al.,* 1999) (Frelink *et al*., 1995a, 1995b & 1996). Long *et al*. (2000) investigated methanol oxidation on Pt-Ru, Pt-RuO_2 and Pt-RuO_xH_y attributed the enhanced activity of Pt-RuO_xH_y to its electron and proton conducting capabilities. The conducting properties of Pt-RuO_xH_y are key in performance for methanol oxidation as they promote the formation of Ru-OH which, by the bifunctional mechanism, aids in CO tolerance on Pt surfaces, and since Ru metal and anhydrous RuO_2 do not have these capabilities, they are not as active for methanol electro-oxidation (Rolison *et al.,* 1999). Frelink *et al.* have conducted ellipsometry studies of methanol oxidation on Pt-Ru and more

specifically Pt on Ru oxides (1995a), (1995b), and (1996), the studies suggested a disappearance of the Ru oxide film in methanol resulting in the following reaction proposal:

$$RuO + Pt - CO \rightarrow CO_2 + Pt + Ru \qquad \text{Equation 24}$$

Furthermore, Frelink *et al.* (1996) investigated oxide formation on Pt-Ru via Energy-dispersive X-ray spectroscopy (EDS) analysis resulting in one type of oxide: $(PtRu)O_x(HSO_4)$ with x ≈ 2 and y ≈ 4.

Lasch *et al*. (2003) investigated the role of Ru oxides on methanol oxidation at low temperatures. Results yielded that RuO_2 content increased with temperature, transforming from hydrous Ru oxides to all of the Ru presenting as RuO_2 at temperatures above 773 K. It was concluded that, in order to have a high activity for methanol oxidation, alloyed Pt-Ru and hydrous Ru oxides are favourable.

The optimum weight % metal loading on a carbon support between 10 and 90 wt% at different temperatures was investigated by Neergat *et al*. (2002), which showed across 25 to 65 °C the optimum weight % metal loading to be 60 wt% in 1 M H_2SO_4 and 1 M CH_3OH with Pt-Ru (1:1) ratio. This result was reiterated by Liu & Zhang (2009) which investigated 45, 50, 55, 65, 70 and 75 wt% in a solution of 0.5 M H_2SO_4 and 1 M CH_3OH to find 65 wt% shows the highest surface specific activity for methanol oxidation, while 60 wt% showed the best MEA performance.

Morphology has further implications on the optimum composition, however this is more difficult to determine and quantify. The alloying effect allows the methanol oxidation rate to be faster since Ru can be incorporated into the Pt structure, allowing the interaction between metals and therefore improve performance by the bifunctional mechanism and/or the direct mechanism. The discrepancies in optimum composition between experiments conducted under the same conditions can probably be attributed to different preparation methods resulting in varying morphologies or surface structure. Hoster *et al.* (2001) established that rough Pt-Ru surfaces, surfaces with many defects such as steps and kinks, and surfaces formed by electro-deposition are more resistant to poisoning than smooth Pt-Ru surfaces of the same composition. It was also determined that well defined Pt (111) peaks in XRD can translate to higher methanol activity since Pt (111) has been identified as an active surface for methanol oxidation. In addition, a high ratio of Pt (111) surfaces has found to be produced by the formic acid reduction technique (Lizcano-Valbuena *et al.,* 2002).

2.3.3. CO tolerance of Pt-Ru

Ralph & Hogarth (2002) investigated the influence of alloyed and unalloyed $Pt_{50}Ru_{50}$ on CO tolerance. The catalysts compared were 20 wt% Pt/Vulcan XC72R, 20 wt% Pt and 10 wt% Ru/ Vulcan XC72R and 10 wt% Ru deposited on 20 wt% Pt/Vulcan XC72R. The peak potential for CO oxidation on Pt/C occurred at 0.58 V vs. RHE, 0.44 V vs. RHE for unalloyed $Pt_{50}Ru_{50}$ and the lowest peak potential

on alloyed $Pt_{50}Ru_{50}$ at 0.37 V vs. RHE. This evidence suggests the necessity of alloyed Pt-Ru in CO electro-oxidation as the incorporation of Ru into the Pt lattice improves CO tolerance and reduces the lattice spacing (Zhang, 2008).

The Pt:Ru composition studies have shown varying results for optimum ratios of Pt to Ru. This is most probably resulting from the synthesis process as the Ru incorporated into the Pt lattice is essential to increase CO tolerance (Zhang, 2008).

The influence of $Pt_{1-x}Ru_x$ composition was studied by Stevens *et al.* (2007) preparing different ratios of alloyed catalysts via magnetic sputtering. The alloyed catalysts were deposited through shadow masks onto 3M nanostructured thin-film catalyst support for testing in a PEMFC with reformate containing 50 ppm CO. It was suggested that Ru ranges of $0.2 < x < 0.9$ were more CO tolerant than Pt alone. In addition, researchers such as Gasteiger *et al.* (1995), Giorgi *et al.* (2001) and Lin *et al.* (1999) described the optimum ratio of Pt:Ru for CO tolerance to be 1:1.

Gavrilov *et al*. (2007) investigated different weight % metal loadings on carbon support for CO oxidation at 25 °C and 50 °C and demonstrated that 60 wt% metal loading is the optimum metal loading for both temperatures in 0.5 M H_2SO_4 solution. This is an interesting conclusion since the optimum wt% metal loading for methanol oxidation was likewise suggested to be 60 wt% metal.

It is well known that Ru in Pt-Ru/C catalysts often exists as ruthenium oxide or hydrous ruthenium oxide. Researchers seem to support the premise that ruthenium oxides enhance CO oxidation as shown by Over & Muhler (2003) and Kim *et al.* (2000) via UHV conditions shows the transformation of Ru (0 0 0 1) to an epitaxially grown RuO_2(1 1 0) film with a onefold under coordination during operation. This translates into CO molecules strongly adsorbed onto the oxide surface, which is shown by density function theory (DFT) calculations and experiments to be the most important elementary step.

2.3.4. Stability of Pt-Ru/C in DMFC

Catalyst crystallinity, particle surface composition and the oxidation state of the metals are susceptible to change during fuel cell operation (Zhang, 2008). Pt-Ru bimetallic electro-catalysts are known to undergo preferential leaching of Ru, especially when methanol is present in solution. This undesired reaction changes the composition of the catalyst and in turn affects the activity (Gancs *et al.,* 2006). In addition, Piela *et al.* (2004) concluded that Ru leaching occurs via the formation of thermodynamically unstable Ru oxide species. However, Ru in an alloyed Pt-Ru matrix is less prone to leaching, and good stability was found in catalysts with a high Ru content in Pt-Ru (Liu & Zhang, 2009).

Compton (1987) proposed a mechanism for the formation of RuO_2 gas, shown in Figure 2-12. This shows the Ru catalyst is sensitive to dissolution at high potentials causing the catalyst to platinize (Vielstich *et al.,* 2009). Ru is thermodynamically stable at potentials below 0.4 V, however experimentally a slow loss of Ru is seen at potentials lower than 0.4 V (Inaba, 2009). An example of Ru instability was shown by Inaba (2009) in Figure 2-11 for CV with potential limits of 0.05 and 0.6 V vs. RHE and CO stripping with potential limits of 0.05 and 0.8 V vs. RHE.

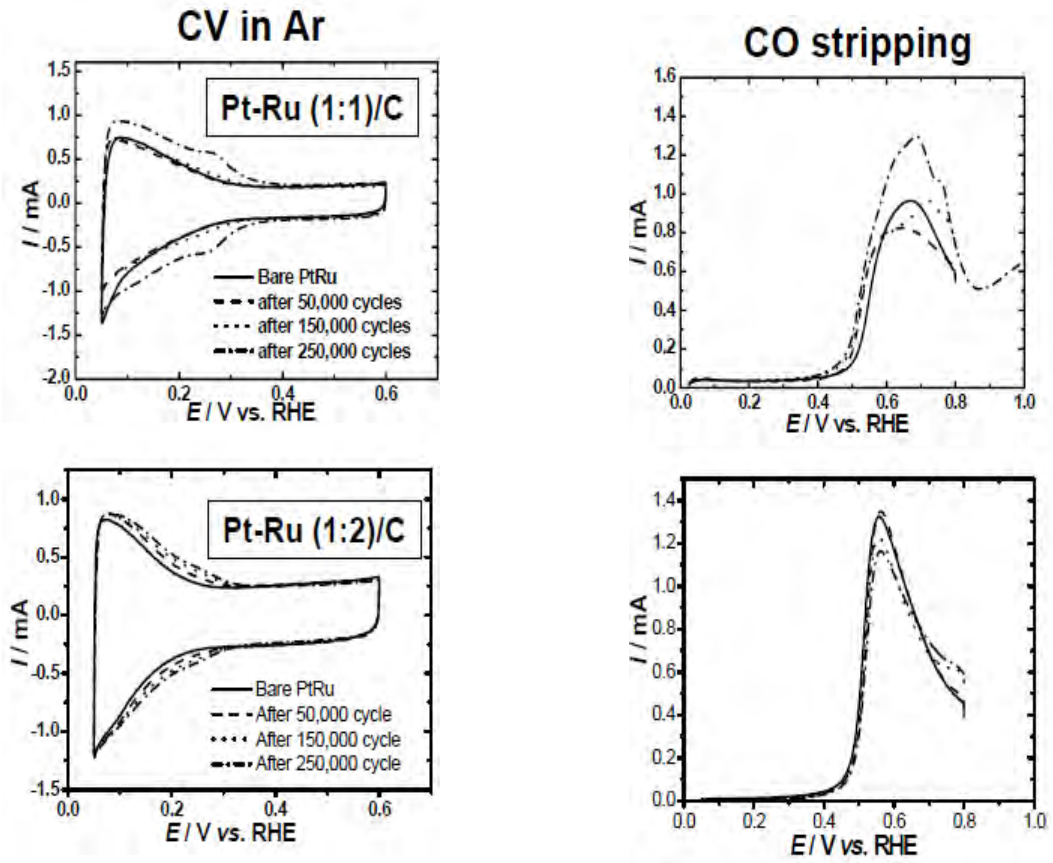

Figure 2-11: CVs and CO stripping voltammograms of commercially available Pt-Ru (1:1)/C and Pt-Ru (1:2)/C during potential cycling in the range of 0.05-0.6 V at 0.5 V/s in 0.5 M H_2SO_4 at 25 °C under Ar atmosphere (Adapted from Inaba, 2009).

Piela *et al.* (2004) investigated the role of Ru leaching in an operating DMFC using electrochemical testing in combination with X-ray fluorescence. The findings showed the impact of Ru dissolution in a DMFC is Ru crossing over the proton conducting Nafion membrane from the anode to the cathode. Once at the cathode, the Ru redeposits at the electrode resulting in the decline of oxygen reduction reaction rate. This phenomenon can occur at cell potentials as low as 0.4 mV. The oxygen reduction on Pt surfaces occurs at a minimum activity level after a Ru coverage 'threshold' on Pt is reached.

This lower limit of ORR activity at concentrations above the threshold is attributed to Ru adatoms' ability to reduce molecular oxygen at high overpotentials (Zhang, 2008) (Stamenkovic *et al.,* 2005).

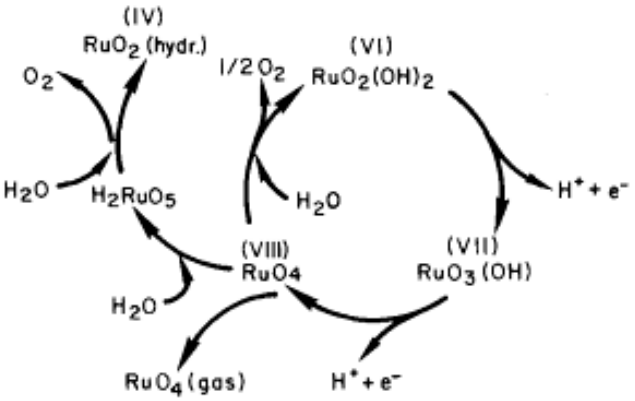

Figure 2-12: Model for oxygen evolution and corrosion reactions on Ru and RuO_2 electrodes (Compton, 1987).

Rotating disc electrode experiments conducted by Gancs *et al.* (2007) revealed that oxygen reduction at the cathode suffers a loss of 0.16 mV due to Ru contamination at the Pt cathode.

A review by Liu & Zhang (2009) showed the influence of catalyst support on Ru leaching from Pt-Ru in sulphuric acid with and without methanol. The investigation concluded that Cabot Pt-Ru/KB had far less Ru leaching than commercial Pt-Ru/C and Pt-Ru Black catalysts as shown in Table 2-1:

Table 2-1: Ru loss due to leaching of commercial Pt-Ru catalysts on varying supports (Liu & Zhang, 2009).

Commercial Catalyst	1M H_2SO_4	1M H_2SO_4 + 1M CH_3OH	1M H_2SO_4 + 3M CH_3OH
Cabot 60 wt% Pt-Ru/KB	0.2	3.80	2.90
Commercial 60 wt% Pt-Ru/C	0.1	12.0	13.6
Commercial 60 wt% Pt-Ru Black	0.1	10.7	12.3

In addition to leaching of Ru, Pt-Ru catalysts are susceptible to particle growth during operation in a DMFC, causing a decrease in surface area and thus a decrease in anode activity. Jeon *et al*. (2006) researched the current density dependence on performance degradation of DMFCs. The stability tests were conducted over 145 hours at each of the current densities of 100, 150, and 200 $mA.cm^{-2}$. The maximum power densities were 93.9, 79.9 and 55.1% of the initial value, and the particle size change from 3.3 nm to 3.4, 3.9, and 4.2 nm after operation for 100, 150, and 200 $mA.cm^{-2}$

respectively. The dissolution of Ru was seen to change the ratio of Pt:Ru from 53:47 to 54:46, 56:44 and 73:27 for MEAs after operation at 100, 150, and 200 $mA.cm^{-2}$ respectively. A similar investigation by Wang *et al*. (2008) in single cells at a current density of 100 $mA.cm^{-2}$ with operating hours of 117, 210, and 312 was conducted. It was seen by XRD that particle size increased from the original value of 2.8 to 3.0, 3.2, and 3.3 nm respectively.

It is evident that more stable Pt-Ru alloys are needed in a DMFC in order to reduce the loss of activity at the anode and at the cathode. Operating conditions and mechanisms of change to electro-catalysts during fuel cell operation was investigated by Knights *et al.*, 2004 which concluded that advanced electro-catalyst designs and enhanced water retention at the anode can reduce degradation of Pt-Ru due to dissolution of metals.

2.4. Catalyst Synthesis Methods

Pt-Ru/C is the most common catalyst for the anode of the DMFC. Several methods have been adopted to prepare catalyst materials for fuel cells, each with their own advantages and disadvantages, the most relevant methods to this study are summarised below.

2.4.1. Wet Synthesis Methods

The impregnation method is the most commonly used synthesis method due to its simple and straightforward technique for Pt-Ru catalyst preparation. The first step in wet chemical synthesis is an impregnation step which involves mixing the precursors with the carbon support in an aqueous solution to form a homogeneous mixture. The chemical reduction of the precursors follows the impregnation. The chemical reduction is carried out by liquid phase reducing agents such as $NaBH_4$, formic acid or gas phase reduction using hydrogen at high temperatures (Liu *et al*., 2006). This method is temperature dependent since this will affect the dispersivity, morphology and particle size which will, in turn, affect the activity of the catalyst.

2.4.2. Organo-Metallic Chemical Deposition

Organo-Metallic precursors can deposit on a substrate via two pathways, vapour deposition or liquid deposition.

2.4.2.1. Deposition from the Vapour Phase

Organo-Metallic Chemical Vapour Deposition (OMCVD), also known as Metal-Organic Chemical Vapour Deposition (MOCVD), is the formation of a thin solid film on a substrate material by a chemical reaction of vapour-phase metal-organic precursors (Jones & Hitchman, 2009). The OMCVD method of metal deposition on a substrate is executed in several different ways, including the

injection of the vapourised precursor with an inert gas into the reactor and a liquid delivery system of precursor and solvent sprayed onto the substrate. Another method involved the precursors' decomposition in the vapour phase in the reactor with an inert gas allowing for the metal to deposit on the surface of a substrate (Thurier & Doppelt, 2008).

A schematic of the OMCVD process is shown in Figure 2-13 and a detailed description of the process is as follows (Jones & Hitchman, 2009):

1) Evaporation and transport of precursors in the bulk gas flow region into the reactor.
2) Gas phase reactions of precursors in the reaction zone to produce reactive intermediates and gaseous by-products.
3) Mass transport of reactants to the substrate surface.
4) Adsorption of the reactants on the substrate surface.
5) Surface diffusion to growth sites, nucleation and surface chemical reactions leading to film formation.
6) Desorption and mass transport of remaining fragments of the decomposition away from the reaction zone.

OMCVD has many advantages over wet chemical methods since it is a 'one stage' process and avoids synthesis steps such as impregnation, washing, drying, calcination and activation. In addition, the surface is protected from poisoning and material transformations during the drying stage. The OMCVD method is therefore considered fast and economic because it eliminates time consuming stages when compared to wet chemistry methods (Thurier & Doppelt, 2008).

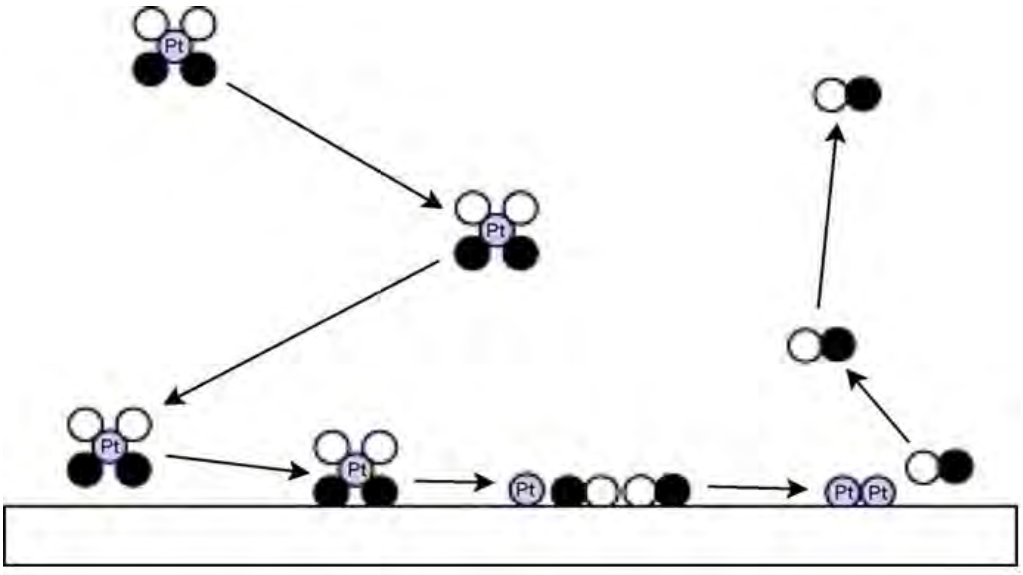

Figure 2-13: Schematic of Pt precursor in the OMCVD process (Thurier & Doppelt, 2008).

The CVD process is a promising catalyst synthesis method because small particles are produced which show excellent electrochemical properties in PEMFCs (Garcia & Goto, 2003).

An Overview of Chemical Vapour Deposition by Jones & Hitchman (2009) lists important precursor requirements as follows:

1) Adequate volatility to achieve acceptable growth rates at moderate evaporation temperatures.
2) Stability so that decomposition does not occur during evaporation.
3) A sufficiently large temperature ‘‘window’’ between evaporation and decomposition for film deposition.
4) High chemical purity.
5) Clean decomposition without the incorporation of residual impurities.
6) Good compatibility with co-precursors during the growth of complex materials.
7) Long shelf-life with indefinite stability under ambient conditions, i.e. unaffected by air or moisture.
8) Readily manufactured in high yield at low cost.
9) Non-hazardous or with a low hazard risk.

Suitable volatility is the main requirement for liquid and solid precursors and volatility needs to be enhanced by a reduction in intermolecular forces which lead to the formation of a dimer, oligomer or polymer. Thermal stability is important for long term storage at room temperature and the precursor should decompose at the evaporation temperature needed to achieve adequate gas phase transport as well as rapid decomposition at intended process conditions, and no decomposition prior to reaching conditions. (Jones & Hitchman, 2009).

Metal carbonyls and metal carbonyl derivatives are suitable for CVD due to high volatility, the zero-valent state of the metal centre and stability of the CO ligand after the dissociation from the metal. However, these compounds are highly toxic and have a high sensitivity to air, light and moisture (Bahlawane *et al.*, 2011).

2.4.2.2. Platinum (II) Acetylacetonate and Ruthenium (III) Acetylacetonate

Platinum (II) Acetylacetonate ($Pt(acac)_2$) is part of the β-diketonate family complexes. It has many advantages including: stability in air and water, as well as being relatively inexpensive (Thurier & Doppelt, 2008). In a vacuum, this precursor has a fairly low vapourisation temperature of 180 °C (Thurier & Doppelt, 2008) and a decomposition temperature of 210-240 °C (Battiston *et al.,* 2005). At atmospheric pressure, the precursor melting point is 250 °C and decomposes at around 265 °C

(Yoda *et al*., 2004). A β-diketonate is a compound of the form $M(CH_3COCHCOCH_3)_2$, where M is the metal. The molecular structure of $Pt(acac)_2$ is given below:

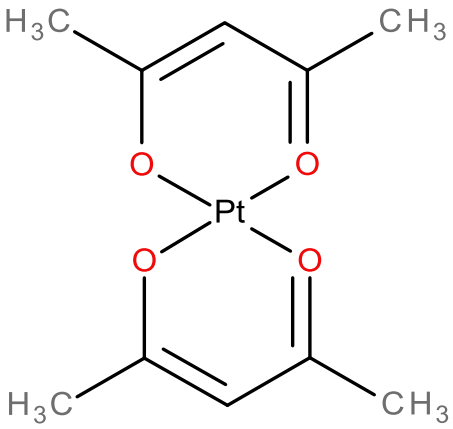

Figure 2-14: Molecular Structure of Platinum (II) Acetylacetonate.

The Pt-O_{acac} is the ligand which decomposes in order to deposit Pt metal on the substrate. The bond strength is 180 kJ/mol. Metal de-coordination does not take place, therefore a high metal purity is likely formed (Thurier & Doppelt, 2008).

Similarly, ruthenium (III) acetylacetonate ($Ru(acac)_3$) is part of the β-diketonate family complex. $Ru(acac)_3$ is a stable precursor (Igumenov *et al.,* 2007) with a vapourisation temperature of 160 °C (Morozova *et al.,* 2009) followed by decomposition at 220 °C in a vacuum (Green *et al.,* 1985). Under atmospheric conditions, $Ru(acac)_3$ has a melting point at 240 °C and decomposes at 285 °C (Igumenov *et al.,* 2007).

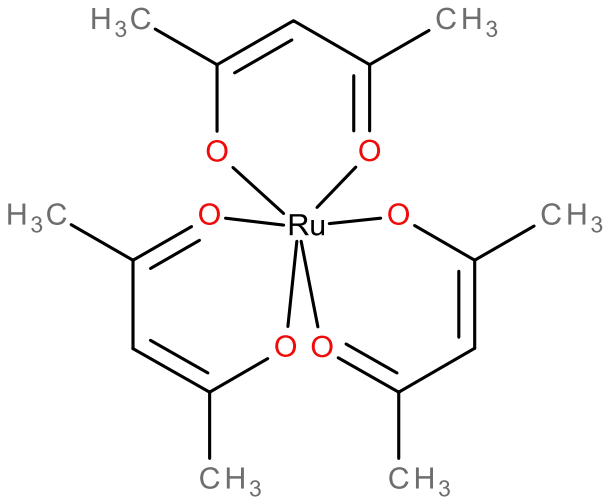

Figure 2-15: The Molecular Structure of Ruthenium (III) Acetylacetonate.

2.5. Catalyst Supports

Catalyst supports allow for fine dispersion and stability of small metal particles. The support provides access to a larger number of catalytically active sites and the support assists in reducing the surface energy of the metal to avoid agglomeration of particles (Auer *et al.*, 1998). A brief overview of typical supports for fuel cell catalysts is given below.

2.5.1. Carbon Black

Carbon blacks are produced by pyrolysis of a carbon source. Carbons are often used as support material due to their large surface areas, light weight, being suitable for decomposition of very active catalysts and relative stability in acidic and basic media (Zhang, 2008).

Vulcan XC-72R is the most commonly used carbon black support material for PEMFC and DMFC applications (Liu *et al*., 2006). Vulcan XC-72R is an extra conductive furnace black produced by Cabot and has been a standard in the plastic and fuel cell industry for many years (Vielstich *et al.*, 2003). Vulcan XC-72 has a surface area of $\sim$250 m^2 g^{-1} and has good chemical and physical cleanliness and good process ability, as well as low sulphur content and ionic contamination (Cabot Corporation, 2013).

2.5.2. Advanced Carbon Supports

Advanced Carbon Supports (ACS) is carbon supports which are structured in the nano-scale. Examples of ACS include nanotubes, nanowires and nanofibers.

Carbon nanotubes (CNT) have been investigated as supports for Pt-Ru alloy catalysts since the definitive graphitic surface structures and crystallinity enhances the catalyst activity (Li & Xing, 2009) due to excellent conduction (Wang *et al.*, 2007).

The structure of CNT allows for a high surface area and a large number of mesopores which results in a high metal dispersion. The main disadvantages of these supports is their tendency to clump together during manufacturing, difficulty in controlling their diameter and the high manufacturing cost, resulting in them being unsuitable for commercial production at this stage (Kotov, 2006).

2.5.3. Non-Carbon Supports

Carbon corrosion is one of the drawbacks of carbon as a catalyst support, therefore efforts have been made to investigate inorganic materials as catalyst supports.

Non-carbon supports such as metal-oxides (TiO_2 and WO_3) have been investigated as alternative support materials for Pt with promising results. In a study by Rajalakshmi *et al*. (2008), TiO_2 allowed for thermal and oxidation stability with respect to corrosion, and prevented agglomeration when

compared to carbon supports. However, the binding energy of Pt on oxide supports is significantly lower than that of Pt/C, meaning the oxide support catalysts are less thermodynamically stable (Sharma & Pollet, 2012).

2.6. Electrochemical Characterisation Techniques

2.6.1. Cyclic Voltammetry

Cyclic Voltammetry (CV) is a potentiodynamic electrochemical measurement which is often used to characterise the mechanism of electrode reactions, their kinetics and could be used to determine the electrochemically active surface area of a catalyst (Liu & Zhang, 2009).

In CV the potential of the working electrode is swept from a low potential limit to the upper potential limit and back again while the current response is measured (Liu & Zhang, 2009). The graph of current versus potential is called a cyclic voltammogram. Oxidation occurs on the forward sweep and produces a positive (anodic) current, while reduction occurs on the reverse sweep resulting in a negative (cathodic) current. Redox reactions occur at varying peak potentials depending on the activation energy required for the reaction to occur. Half-cell reactions with low activation energies occur at lower potentials, whereas high reaction energies occur at higher potentials. Thus a cyclic voltammogram is useful in identifying the potentials at which electrochemical reactions occur. The typical cyclic voltammogram of a polycrystalline Pt electrode is shown in Figure 2-16 in an acidic environment.

The region between 0.05 V and 0.4 V vs. RHE is known as the reversible hydrogen adsorption and desorption regions, which is attributed to the underpotential deposition (H_{UPD}) of a hydrogen monolayer in the negative-going sweep and the release of protons (H^+) in the positive-going sweep (Climent & Feliu, 2011). The reaction equation for the hydrogen electro-desorption reaction is as follows (Zhang, 2008):

$$Pt - H_{ads} \rightarrow Pt + H^+ + e^- \qquad \text{Equation 25}$$

The hydrogen electro-adsorption reaction on the reverse sweep is as follows (Zhang, 2008):

$$Pt + H^+ + e^- \rightarrow Pt - H_{ads} \qquad \text{Equation 26}$$

Individual peaks in the H_{UPD} positive sweep region labelled as Hw and Hs occur due to the energy associated with the desorption. Strongly adsorbed hydrogen will desorb at higher potentials (H_s), whereas weakly adsorbed hydrogen will desorb at lower potentials (H_w). Further studies have

reported H_w and H_s correspond to hydrogen electro-desorption from different surfaces of the platinum crystal (Zhang, 2008).

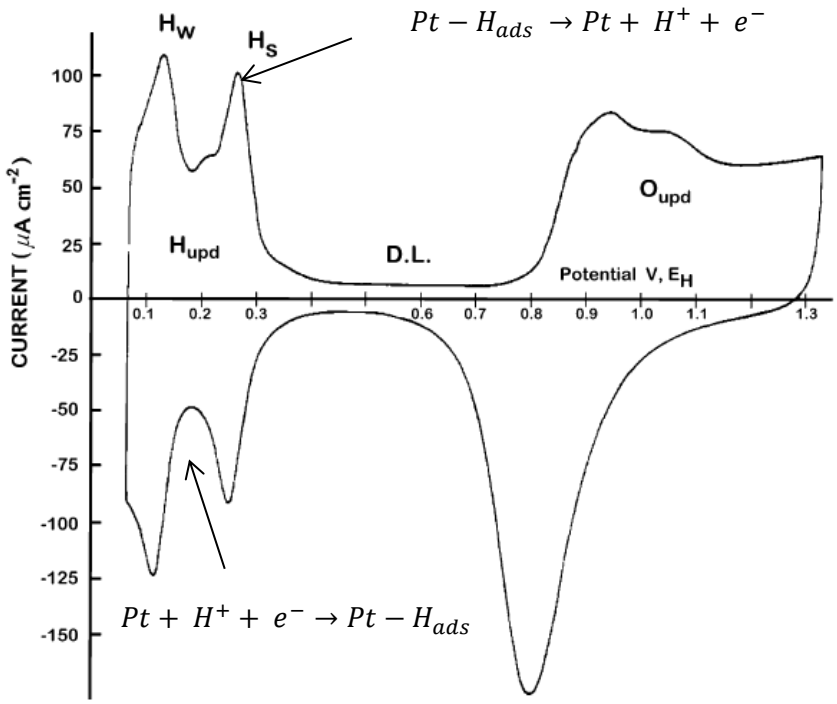

Figure 2-16: Typical Cyclic voltammogram of a polycrystalline Pt electrode in 0.5 M H_2SO_4, sweep rate 50 mV/s (Adapted from Climent & Feliu, 2011).

Kinoshita (1990) proposed a cubo-octahedral platinum particle model for ideal platinum nanoparticles. The cubo-octahedral model consists of Pt atoms comprising of eight (111) and six (100) crystal faces connected by edge and corner atoms.

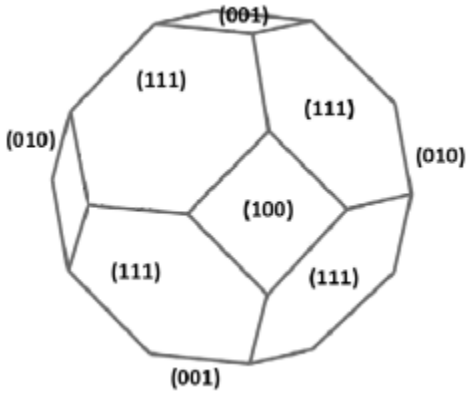

Figure 2-17: Model cubo-octahedral structure illustrating (111), (100) and (010) crystal faces and edge and corner atoms (Barnard, 2013).

Single crystal studies performed by Will (1965) investigated the hydrogen adsorption on the three main platinum faces (100), (111) and (110). The Pt surfaces "interact at different energies with the hydrogen atoms due to the different type and overlapping between the electronic local density of a site and the adsorbed hydrogen" (Climent & Feliu, 2011). Will (1965) observed that strongly adsorbed hydrogen was related to Pt (100) and Pt (110) orientation and weakly adsorbed hydrogen peak was mainly related to Pt (111) orientation. Thus, the hydrogen desorption peak associated with Pt(111) surface occurs at a potential ≈ 0.12 V vs. RHE, the Pt(110) surface occurs at a potential around 0.22 V vs. RHE and the Pt(100) surface at a higher potential of around 0.27 V vs. RHE (Zhang, 2008).

The featureless region with a small observed current between 0.4 and 0.8 V vs. RHE is attributed to double layer charging (DL) (Climent & Feliu, 2011). This is caused by the interaction between two phases at the interface, particularly the interface between an electrode and electrolyte solution. At this interface there exists a segregation of positive and negative charges by preferential adsorption of either positive or negative ions at the interface. Thus, a charge distribution is formed (Pletcher *et al.,* 2001). If peaks were to be observed in the region could be attributed to impurities such as heavy metal deposition (Climent & Feliu, 2011).

CV can also be used to determine the Electrochemically Active Surface Area (ECSA) by integrating the area under the adsorption (H_{upd}) or desorption regions, subtracting the DL of the cyclic voltammogram, can determine the total adsorbed or desorbed hydrogen charge on the platinum sites. The hydrogen adsorption charges associated with different Pt crystal surfaces were statistically combined to form an estimated hydrogen adsorption charge for a smooth polycrystalline platinum surface. This estimated charge has been found to be 210 $\mu C/cm^2_{Pt}$. Normalising the H_{upd} by the hydrogen adsorption charge allows for the number of sites which took part in the reaction to be determined. Therefore, the ECSA can be calculated using the following equation:

$$ECSA = \frac{Q_{Hupd}}{L_{Pt} Q_f} \qquad \text{Equation 27}$$

Where Q_{Hupd}= integrated area under the hydrogen adsorption/desorption peak after subtraction of the double layer.

L_{Pt} = platinum loading on the electrode

Q_f = 210 $\mu C/cm^2_{Pt}$

The region above 0.8 V vs. RHE on the cyclic voltammogram is related to oxygen adsorption and desorption on the platinum surfaces, known as O_{upd} (Climent & Feliu, 2011). The reactions associated with the region are shown below:

$$Pt + H - O - H \rightarrow Pt - O - H + H^+ + e^- \qquad \text{Equation 28}$$

$$Pt - O - H + H - O - H \rightarrow Pt - (O - H)_2 + H^+ + e^- \qquad \text{Equation 29}$$

$$Pt - (O - H)_2 \rightarrow Pt - O + H - O - H \qquad \text{Equation 30}$$

Reverse O_{upd}:

$$Pt - O + 2H^+ + 2e^- \rightarrow Pt + H - O - H \qquad \text{Equation 31}$$

However, it has since been shown that O_{UPD} does not occur at potentials less than 1.229 V vs RHE and the region between 0.9 – 1.2 V vs RHE is rather the formation of platinum oxides on the surface (Xing *et al.*, 2014).

Pt-Ru catalysts do not have a defined hydrogen adsorption-desorption region, due to a broad electric double layer region (Spinacé *et al.,* 2007), due to charging phenomenon. A pseudo-capacitance is a phenomenon associated with electrosorption and surface reactions at high-area electrode materials, the material 'stores charge indirectly through faradaic chemical processes but its electrical behaviour is like that of a capacitor' (Conway & Pell, 2003).

Since Ru favours oxygen species, an adlayer of water or dissociated water is present at the surface of the metal causing a pseudo-capacitance of Ru alloyed metals which is higher than Pt/C. As the particle size decreases resulting in an increase in surface area, this electric double layer capacitance enlarges (Han *et al.,* 2006). This pseudo-capacitance layer is larger for catalysts containing ruthenium oxide since this allows for more oxidation and reduction reactions to take place across the potentials (Sato *et al.,* 2000).

The typical cyclic voltammogram for a Pt-Ru/C catalyst is shown in Figure 2-18.

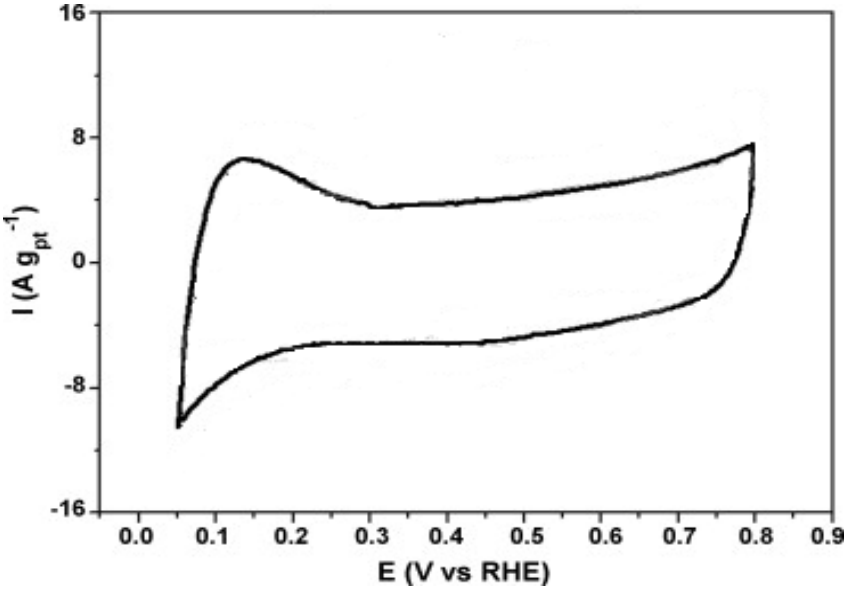

Figure 2-18: Typical cyclic voltammogram of Pt-Ru/C electro-catalyst in 0.5 M H_2SO_4 with a sweep rate of 10 mV s^{-1} (Adapted from Ribeiro *et al.*, 2010).

2.6.2. CO Stripping Voltammetry

CO stripping voltammetry is a potentiodynamic electrochemical measurement similar to that of CV. However, in CO stripping, a monolayer of CO is adsorbed on the surface, oxidised and subsequently desorbed. CO stripping voltammetry is a method used to determine the ECSA of a catalyst surface by measuring the peak area of the CO oxidation peak (Zhang, 2008). On a Pt surface this oxidation peak occurs between 0.76 and 0.95 V vs. RHE (Maillard *et al.*, 2005). On a Pt-Ru alloy surface the CO oxidation peak occurs at potentials 0.17 - 0.2 V lower (Zhang, 2008).

CO adsorbs strongly to the surface of Pt and Ru to form a monolayer which can be removed by the following oxidation reaction (Zhang, 2008):

$$CO + H_2O \rightarrow CO_2 + 2H^+ + 2e^- \qquad \text{Equation 32}$$

The first peak represents the CO_{ads} electro-oxidation, and the peak charge is due to the reaction above (Zhang, 2008). The ECSA determined is typically 1.4 times that of the ECSA calculated from the H_{upd} method. This is thought to be due to the contribution of the capacitance of the carbon support material for high surface area catalysts. Therefore, the carbon support contribution is subtracted from the layer charge, yielding similar results to that of the one obtained from H_{ups} (Mayrhofer *et al.,* 2008).

An example of CO stripping voltammograms is shown in Figure 2-19.

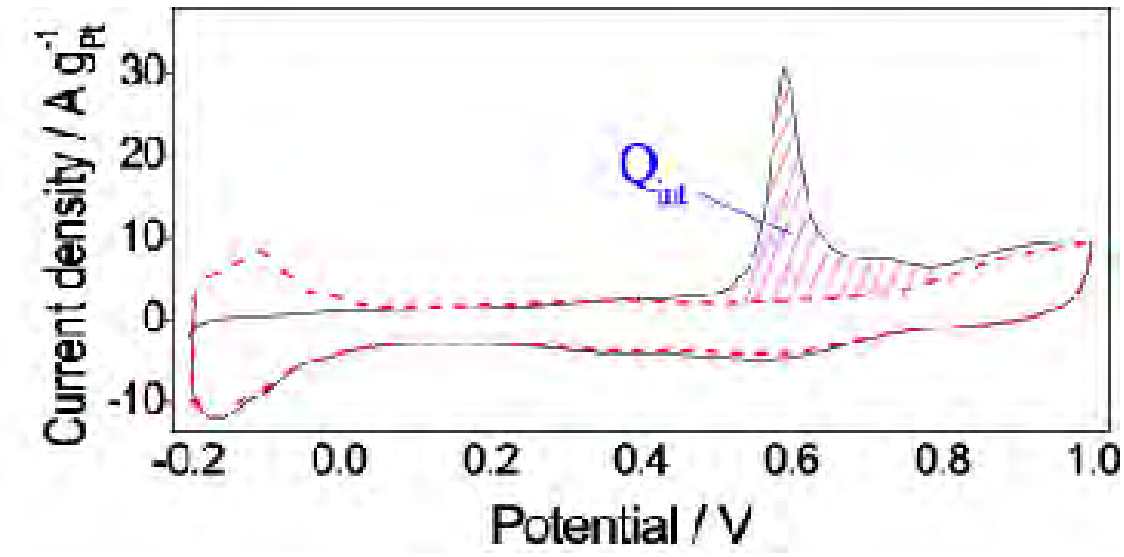

Figure 2-19: The CO stripping voltammograms of ECSA measurement for MWCNT-PDOP-PtNPs in 0.5 M H_2SO_4 at a sweep rate of 10 mV s^{-1} (Lin *et al.*, 2013).

In addition to the determination of ECSA, CO stripping can also be used to determine the morphology of particles as shown by Fabbri *et al.* (2014). It was shown that a morphology fingerprint of the surface can be produced to distinguish between isolated nanoparticles and extended surfaces.

2.6.3. Methanol Oxidation

The methanol oxidation mechanism as outlined in Equations 10-15 and 18-19, show the reactions are all oxidation reactions. This accounts for the oxidation curves on the forward sweep and reverse sweep shown in Figure 2-20.

Methanol chemisorption on Ru sites is a less favourable process than chemisorption on Pt sites, since methanol dehydrogenation occurs at potential values between 0.2 and 0.25 V vs. RHE on platinum sites. In addition, water discharge to form 'OH-like' species on Ru surfaces occurs at potentials below 0.2 V vs. RHE (Aricò *et al.,* 2001), whereas on Pt, the reaction occurs at much higher potentials of around 0.5 V vs. RHE (Gasteiger *et al.,* 1994b), which effectively blocks Ru sites for methanol chemisorption.

Although at high temperatures Ru can take part in methanol chemisorption, the oxygenated species chemisorption energy is much higher and therefore is preferred over methanol chemisorption (Aricò *et al.,* 2001).

A typical methanol oxidation cyclic voltammogram is represented in Figure 2-20:

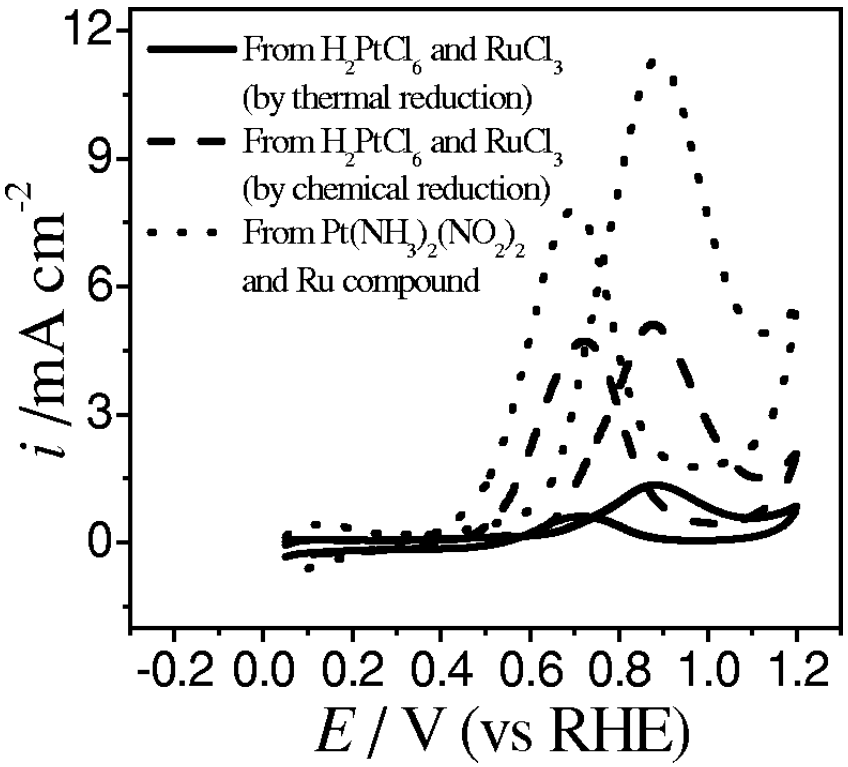

Figure 2-20: Cyclic voltammograms of methanol oxidation in an Ar saturated 0.5 M CH_3OH and 0.5 M H_2SO_4 electrolyte at 25 °C on Pt-Ru/C catalysts prepared from different methods and precursors (Wang *et al.,* 2005).

The oxidation peaks of the forward and reverse sweeps are not completed due to the low upper limit. In literature, this limit is inconsistent due to the lack of standardisation in this area. The upper limit is often below 0.8 V vs. RHE due to the instability of the Pt-Ru catalyst as discussed in section 2.3.4.

2.6.4. Chronoamperometry

Chronoamperometry is a quasi-steady state electrochemical potentiostatic technique which is useful to compare activities (Santos & Schmickler, 2011) and stability of a catalyst (Wang *et al.*, 2005).

Chronoamperometry is characterized by stepping the potential from one point on the voltammetric curve to a higher potential (oxidation) or lower potential (reduction) and monitoring the current response over time (Brett *et al.*, 1992). The first potential applied is below the equilibrium potential for the reaction. The potential is raised to a higher value (for oxidation) so that the reaction rate is controlled by mass transfer. At the start of the experiment, and during the first low potential step, the concentration of reactant at the surface of the electrode is equivalent to the bulk concentration. Once the potential has stepped to a higher potential, the concentration of reactant near the

electrode drops to zero due to the high reaction rate. As the reaction time continues, the reactant in the location around the electrode depletes causing the diffusion distance from the bulk solution to the electrode to increase and the concentration gradient to decrease. Since the concentration gradient decreases, the current declines over time (Zhang, 2008).

The experiment is not carried out for a duration longer than a few minutes since the reaction zone depletes quickly. Therefore a long period is not needed in order to analyse the mass transfer rate. In addition, over a long period of time convection due to a buildup of density gradients and environmental vibration is likely to influence results (Zhang, 2008).

Electro-catalysts stability testing is frequently evaluated using chronoamperometry as the decay in current over time can be related to the decay in activity over time and thus allows the catalytic activities of catalysts to be compared with a time component (Maiyalagan, 2008) (Yang *et al.,* 2007).

2.7. Physical Characterisation Techniques

Transmission Electron Microscopy (TEM), Energy-dispersive X-ray spectroscopy (EDX) coupled to a Scanning Electron Microscopy (SEM) and Thermogravimetric Analysis (TGA) and X-ray Diffraction (XRD) were used as physical characterization techniques. Standard methods were employed for TEM, SEM and TGA therefore only XRD will be discussed in more detail in this section.

X-ray Diffraction (XRD) is the process of focusing x-rays on a surface. These x-rays interact with the electrons in the matter and are scattered in various directions due to contact with the atomic electrons (Zhang, 2008). XRD allows for the analysis of crystallographic structure, alloying nature and crystallite size to be analysed.

When an x-ray source is applied to a material at an angle (θ), a diffraction pattern is specific to the compound observed. English physicists Sir W.H. Bragg and his son Sir W.L. Bragg developed a relationship in 1913 to explain why the cleavage faces of crystals appear to reflect X-ray beams at certain angles of incidence (θ).

The wave diffractions take place according to Bragg's Law:

$$n\lambda = 2d_{hkl}sin\theta \ (n = 1,2,3, \dots) \qquad \text{Equation 33}$$

Where: λ is the wavelength of the X-ray source, d is the lattice spacing, θ is the half-value of the diffraction angle, n is the order of the reflection.

The diffraction patterns are unique for the material's crystal structure and can therefore be used for identification of the compound.

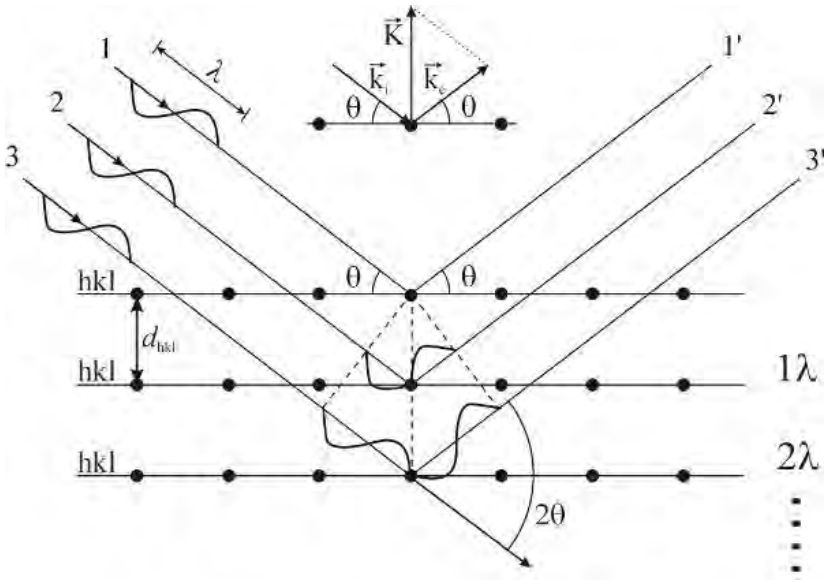

Figure 2-21: Illustration of X-ray diffraction (KU Leuven, 2010).

The average crystallite size is determined by using the Scherrer equation and a correction factor:

$$\tau = \frac{k\lambda}{\beta cos\theta} \qquad \text{Equation 34}$$

k is a dimensionless shape factor, usually assumed to be 0.9, β is the peak broadening of 2θ at half height and λ. Is the wavelength An estimate of crystallite size, if one assumes spherical powder particles, were made using the equation:

$$d_p = (\frac{4}{3}) \times \tau \qquad \text{Equation 35}$$

Where: τ is the volume-weighted length of the column perpendicular to the hkl plane, which is a measure of crystallite size, d_p is an estimation of crystallite size.

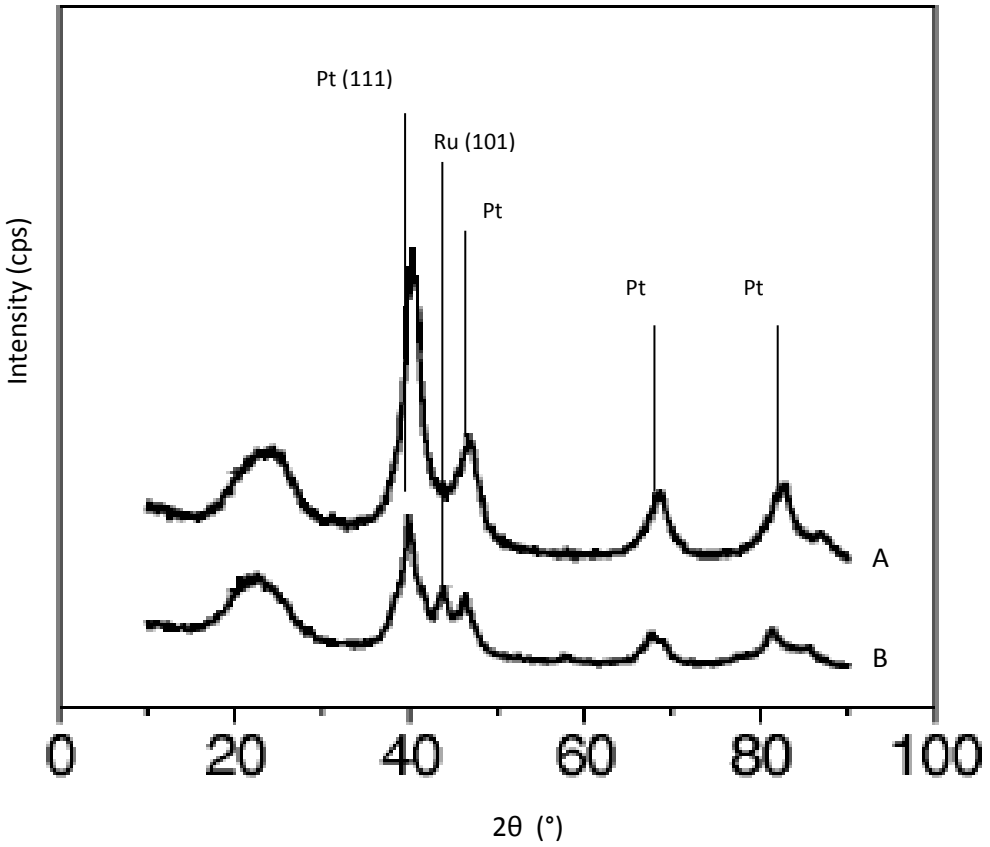

Figure 2-22: XRD pattern for Pt-Ru/C alloyed (A) and partially alloyed (B) (Adapted from Wang *et al.*, 2005).

The expected surface area of the catalyst can be calculated using the crystallite size from the XRD pattern in Equations 36 and 37 (Wang *et al*., 2005).

$$SA = \frac{6000}{\rho_{Pt-Ru} d_p} \qquad \text{Equation 36}$$

$$\rho_{Pt-Ru} = X_{Pt} p_{Pt} + X_{Ru} \rho_{Ru} \qquad \text{Equation 37}$$

Where SA is the estimated surface area, $\rho_{Pt\text{-}Ru}$ is the density of the Pt-Ru alloy, ρ_{Pt} is the density of platinum metal (21.45 g/cm^3), ρ_{Ru} is the density of ruthenium metal (12.45 g/cm^3) and ruthenium oxide has a density of 6.97 g/cm^3. The assumptions associated with Equations 36 and 37 are that the catalyst particles are spherical and a weighted density correlation is seen when the metals are mixed. In addition to these assumptions, an assumption is made when ruthenium exists as ruthenium oxide, the oxide species contributes to the active surface area of the catalyst as seen by Equation 24, and can therefore be included in the density of the overall catalyst particle.

To determine the degree of alloying a shift of peak position in the diffraction pattern and presence of Ru metal peaks is used. The typical alloyed Pt-Ru/C (A) and partially alloyed Pt-Ru/C (B) diffraction pattern is given in Figure 2-22.

The shift of the Pt crystallite diffraction peaks demonstrates the presence of an alloy. However, when the Ru (1 0 1) diffraction peak is absorbed atleast some of the Ru exists as a metal in unalloyed form.

For the Pt-Ru alloy, a more quantitative analysis of the degree of alloying can be employed. This is the study of the d-spacing, as indicated in Figure 2-22 as d_{hkl}. The d-spacing of a platinum lattice will decrease as smaller ruthenium atoms are included in the lattice structure (Watanabe *et al*., 1987). The decrease in d-spacing can be translated into the degree of Ru alloying by the following equations outlined by Antolini & Cardellini (2001):

$$A = d_{spacing} \times \sqrt{l^2 + m^2 + n^2} \qquad \text{Equation 38}$$

$$x_{Ru} = \frac{l_{os} - A}{k} \qquad \text{Equation 39}$$

Where A is the lattice constant, l_{os} is the lattice parameter of pure carbon supported Pt and k = 0.12452 Å.

Catalyst particles with no or little crystalline structure are called amorphous. This amorphous structure will show on an XRD curve as low intensity, broad peaks (Aricò *et al.,* 2002). Metal oxides such as platinum oxide, hydrous platinum oxide and ruthenium oxides often have an amorphous structure, therefore Pt-Ru catalysts often appear to have an amorphous XRD pattern if metal oxides are present (Aricò *et al.,* 2002) (Dinh *et al*., 2000).

3. OBJECTIVES AND HYPOTHESIS

An increase in activity and stability of the Pt-Ru/C catalyst will result in a decrease in catalyst expenditure due to a decrease in catalyst loading. In addition, performance will increase due to a reduction in ruthenium dissolution and crossover. Therefore, increasing the activity and stability of the Pt-Ru/C catalyst is paramount in improving the current DMFC performance and viability as an alternative energy source.

The activity for methanol electro-oxidation and stability of the Pt-Ru/C catalyst is largely affected by the catalyst synthesis method, precursors, reduction time and temperature. These parameters influence the structure, morphology, alloying and dispersivity of the catalyst which in turn affects methanol electro-oxidation activity and stability (Wang *et al.*, 2005).

The chemical deposition methods have shown promise in improving performance of electro-catalysts (Garcia & Goto, 2003). However, it is important to optimise method conditions such as operational time and temperature for $Pt(acac)_2$ and $Ru(acac)_3$ precursors in the reactor. To date, a methodical approach to optimizing the chemical deposition synthesis method for Pt-Ru/C has yet to be undertaken.

As evident from the literature review, the optimum Pt:Ru ratio is a much contested topic. It is therefore an important ratio to optimize for each researcher's method as slight variations could cause differing results (Zhang, 2008). The objectives of this study are therefore to:

I. Prepare Pt-Ru/C catalysts from $Pt(acac)_2$ and $Ru(acac)_3$ precursors by thermally induced chemical deposition to investigate which method produces well dispersed, alloyed, small catalyst particles.
II. Find optimal reactor operating time and temperature for catalyst preparation and study methanol oxidation activity.
III. Prepare Pt-Ru catalysts with different Pt:Ru ratios by the chemical deposition method to determine the optimal ratio for methanol oxidation.
IV. Determine if there is a correlation between methanol oxidation activity and carbon monoxide oxidation activity.

For this study, the following is hypothesised for the use of the chemical deposition method:

I. The chemical deposition method can be used to obtain alloyed Pt-Ru particles on a carbon support through a 'one-step' reaction.

II. The activity and stability of Pt-Ru/C catalysts can be optimized through the reactor operating temperature and time.

Factors which affect catalyst activity and stability were reviewed for this study. In addition to preparation in the reactor, reduction time and reduction temperature, the variation of the Pt:Ru ratio was also considered. Since methanol oxidation occurs on Pt sites and is enhanced by the introduction of Ru into the lattice, it is thus hypothesized that:

III. The activity of Pt-Ru/C catalysts can be optimized for methanol oxidation activity through variation of the Pt:Ru ratio.

4. EXPERIMENTAL PROGRAMME

The experimental programme below specifies the preparation, electro-characterisation and physical characterisation of Pt-Ru alloy on carbon catalysts prepared by metal-organic chemical deposition methods.

Table 4-1: List of Chemicals and Gases used for catalyst preparation and electrochemical characterisation

Chemical Formula	Chemical Name	Supplier	Purity Grade (%)
$Pt(acac)_2$	Platinum acetylacetonate	Sigma Aldrich	97
$Ru(acac)_3$	Ruthenium acetylacetonate	Sigma Aldrich	97
Vulcan XC72R-50	Carbon Black	Electrochem, Inc.	-
H_2SO_4	Conc. Sulphuric Acid	Sigma Aldrich	95-98
H_2O_2	Hydrogen Peroxide	Sigma Aldrich	35
C_3H_7OH	Iso-propanol	Kimix Chemicals	99.9
-	Nafion Solution	Ion-Power	5
CH_3OH	Methanol	Sigma Aldrich	99.9
Ar	Argon	Air Liquide	99.999
CO	Carbon Monoxide	Air Liquide	95
N_2	Nitrogen	Air Liquide	99.999
-	Synthetic Air	Air Products	-

4.1. Catalyst Synthesis by chemical deposition method

The Pt-Ru/C catalysts were prepared in a standard in-house reactor, designed based on literature and TGA data around temperatures and reactor atmosphere required. The precursor's masses were calculated by setting the specific wt% of metal on carbon, the Pt:Ru ratios desired and using a basis of 125 mg of Vulcan XC72R-50. An image of the reactor is shown in Figure 4-1.

A typical procedure is described below.

A 50 wt% Pt-Ru/C catalyst with a molar ratio of 50:50 was first prepared by weighing 125 mg of Vulcan XC72R-50, 166 mg $Pt(acac)_2$ and 168.2 mg $Ru(acac)_3$. The pre-weighed Vulcan and precursors were mixed using a mortar and pestle, loaded into the reactor and the reactor was sealed. The reactor was placed into a tubular furnace and an argon line was connected to the reactor. The furnace was programmed to heat to 100 °C, over a 30 minute period and hold at 100 °C for 30 minutes. The reactor was then sealed off from the argon and the furnace was heated to 350 °C, the

operating temperature, over a 60 minute period. The furnace was held at a temperature of 350 °C for a period of 4 hours. The reactor and furnace were left to cool to room temperature for 12 hours, after which the catalyst was removed and stored in a glass vial.

Figure 4-1: Reactor used for preparation of chemical deposition catalysts (Haynes alloy).

Synthesis atmosphere, times and temperatures were varied as shown in the table below:

Table 4-2: Synthesis conditions for each prepared catalyst

Catalyst	Atmosphere	Operating Temperature (°C)	Operating Time
1	Vacuum	350	4 hours
2	Argon	350	30 minutes
3	Argon	350	30 minutes
4	Argon	350	1 hour
5	Argon	350	2 hours
6	Argon	350	4 hours
7	Argon	350	6 hours
8	Argon	350	8 hours
9	Argon	300	4 hours
10	Argon	450	4 hours
11	Argon	600	4 hours
12	Argon	700	4 hours

Catalyst 3 is a remake of catalyst 2 in order to determine the reproducibility of the study. Different molar ratios were also investigated. The table below summaries the masses of $Pt(acac)_2$ and $Ru(acac)_3$ required for a 50 wt% Pt-Ru/C and different Pt:Ru molar ratios.

Table 4-3: Summary of masses of Vulcan XC72R-50, $Pt(acac)_2$ and $Ru(acac)_3$ for each catalyst of different ratios.

Pt:Ru Molar Ratio	Mass $Pt(acac)_2$ (mg)	Mass $Ru(acac)_3$ (mg)	Mass Vulcan XC72R-50 (mg)
90:10	238.3	26.8	125
80:20	223.1	56.5	125
75:25	214.9	72.6	125
60:40	187.3	126.5	125
50:50	166.0	168.2	125

4.2. Electrochemical Characterisation

Electrochemical characterisation was used to determine the activity for methanol oxidation, CO oxidation, ECSA and stability of the Pt-Ru/C catalysts. This section details the experimental setup, preparation and procedure employed in the electrochemical experiments.

4.2.1. Cell Setup

The electrochemical characterisation experiments were conducted in a typical three electrode electrochemical cell (Gamry Instruments). A glassy carbon electrode coated with catalyst ink was used as the working electrode, a Pt wire as a counter electrode and $Hg/HgSO_4$ reference electrode were used for the electrochemical experiments. All potentials were corrected and reported using the standard hydrogen electrode (SHE). A 0.5 M H_2SO_4 electrolyte solution was used for cyclic voltammetry experiments and prepared using 18.2 MΩ.cm deionised water and concentrated H_2SO_4. A 0.5 M H_2SO_4 and 1 M MeOH electrolyte solution was used for oxidation cyclic voltammetry, prepared using 18.2 MΩ.cm deionised water, concentrated H_2SO_4 and concentrated MeOH. The electrolyte solution for all electrochemical experiments was changed for each experiment/catalyst.

The glassware used was thoroughly cleaned before each experiment. The glassware was immersed in a solution of 1:1 hydrogen peroxide and concentrated sulphuric acid overnight prior to experiments, after which it's rinsed in 18.2 MΩ.cm deionised water. Care was taken when handling the H_2O_2/H_2SO_4, heavy duty rubber gloves and a face shield were used when handling the solution and glassware.

A 5 mm diameter glassy carbon electrode was used for all electrochemical characterisations and was thoroughly cleaned by polishing to a mirror finish in 1 µm followed by a 0.05 µm alumina suspension (Buehler) and rinsed by water prior to all experiments. The counter electrode was cleaned by burning off impurities over a flame for 20 seconds and rinsing with deionised water to cool down before placing in the cell.

Electrochemical characterisation sequence was cyclic voltammetry, followed by CO stripping, then methanol oxidation and finally chronoamperometry. In between CO stripping and MeOH oxidation, the electrolyte was changed. These experiments were done consecutively for each catalyst film and were carried out in a 5 hour period.

4.2.2. Catalyst Ink Preparation

A catalyst ink was prepared in a glass vial by adding 5 mg of the catalyst to 5.5 ml of 18.2 MΩ.cm deionised water, 1 mL of isopropanol and 50 µL of 15 wt.% Nafion® solution. The mixture was sealed in the vial, placed in a beaker of ice and ultrasonicated for 30 minutes. A micropipette was used to place 10 µL of the catalyst onto the working electrode (Pine Instruments). The electrode was left in air to dry, once the ink was dry the surface of the electrode was wetted using 18.2 MΩ.cm deionised water and lowered into the cell until the tip is submerged in the electrolyte by no more than 1 cm.

The metal on the electrode varied in accordance with the Pt:Ru ratio and is shown in the table below:

Table 4-4: Masses of Pt and Ru in the catalyst ink on the electrode.

Pt:Ru Ratio	Mass Pt (µg/cm^2)	Mass Ru (µg/cm^2)
90:10	17.3	1.93
80:20	15.4	3.85
75:25	14.4	4.81
60:40	11.6	7.70
50:50	9.63	9.63

4.2.3. Cyclic Voltammetry

Cyclic Voltammetry (CV) was used to clean the Pt-Ru/C catalyst surface of any impurities. The CV experiments were performed in an argon purged 0.5 M H_2SO_4 electrolyte solution. The cell was purged with argon for 30 minutes to deoxygenate the system before the working electrode was inserted into the cell. The potential of the working electrode was cycled between 0 and 0.7 V vs. SHE at 100 mV for 50 cycles, the scan rate was then reduced to 50 mV and cycled between 0 and 0.7 V

vs. SHE for 5 cycles. The CV curves could not be used to determine ECSA. Pt-Ru catalysts show a thick electric double layer, due to charging phenomenon. This leads to Pt-Ru not having a defined hydrogen adsorption-desorption region (Spinacé *et al.,* 2007).

4.2.4. CO Stripping Voltammetry

CO stripping voltammetry was used to determine the electrochemically active surface area (ECSA) of the Pt-Ru/C catalysts. The experiments were performed by initially purging the electrolyte with CO gas for 20 minutes while holding the potential of the working electrode at 0.1 V vs. SHE, where CO will absorb onto the catalyst surface in the form of Pt-CO and Ru-CO. The cell is subsequently purged with argon for 20 minutes while holding the potential at 0.1 V vs. SHE to ensure the remaining CO is only on the catalyst surface. The potential is then cycled, starting at 0.1 V vs. SHE to 0.8 V vs. SHE at 50 mV/s for 5 cycles.

The first cycle oxidises the surface CO to CO_2 while the last cycle is surface CO free which allows for the difference in area's to be integrated for charge. The ECSA was determined by assuming 420 $\mu C/cm^2_{Pt}$ per monolayer of CO adsorbed onto the surface metals and using the equation below. Since this value is valid for Pt surfaces it is not entirely accurate as Ru alloyed with Pt would have a slightly different adsorption charge. However, it is generally accepted in literature as suitable to compare catalysts.

$$ECSA\left(\frac{cm^2_{Pt}}{g_{Pt}}\right) = \frac{Charge\ (\mu C)}{420\frac{\mu C}{cm^2_{Pt}} \times Catalyst\ Loading\ (g_{Pt})}$$

4.2.5. Methanol Oxidation Cyclic Voltammetry

Methanol oxidation cyclic voltammetry was performed to compare the activity of the Pt-Ru/C catalysts for methanol oxidation. The CV experiments were carried out in an argon purged in 0.5 M H_2SO_4 and 1 M CH_3OH electrolyte solution. The cell was deoxygenated by purging the system with argon for 30 minutes before the working electrode was placed in the cell. The potential of the working electrode was cycled between 0 and 0.7 V vs. SHE at 20 mV for 5 cycles.

The activity of the Pt-Ru/C catalysts was reported in terms of onset potential and mass specific activity on the working electrode (A/g_{metal}) on the electrode and geometric surface area of the glassy carbon electrode (mA/cm^2) at a potential of 0.5 V vs. SHE on the forward sweep.

4.2.6. Chronoamperometry

Chronoamperometry was used to determine the stability of the Pt-Ru/C catalysts. The experiments were performed in an argon saturated 0.5 M H_2SO_4 and 1 M CH_3OH electrolyte solution. The cell was deoxygenated by purging the system with argon for 30 minutes before the working electrode was inserted into the cell. The potential was then set at 0.1 V vs. SHE and stepped to 0.5 V vs. SHE. The current was measured over a period of 30 minutes and reported in terms of mass of platinum on the working electrode (A/g_{metal}) on the electrode and geometric surface area of the glassy carbon electrode (mA/cm^2).

4.2.7. Standard Catalysts and Reproducibility

Two Pt-Ru/C commercial catalysts were used to establish a standard electrochemical activity and benchmark for all further electrochemical experiments for the Pt-Ru/C catalysts produced. Due to non-disclosure agreements, these catalysts will be referred to as commercial 1 (40 wt% Pt, 20 wt% Ru) and commercial 2 (30 wt% Pt, 23 wt% Ru). The commercial catalysts were used to determine the reproducibility of the electrochemical experiments and used as a benchmark for results obtained.

4.3. Physical Characterisation

Physical characterisation of the bimetallic catalysts were employed since an understanding of the structure, morphology, size and crystallinity of the Pt-Ru/C catalysts are vital in electrochemically active surface area, the activity for methanol oxidation and CO tolerance.

4.3.1. Transmission Electron Microscope (TEM)

Transmission Electron Microscope (TEM) was carried out at the Electron Microscope Unit at the University of Cape Town on a Tecnai G^2 electron microscope operating at 200 kV. A small amount of Pt-Ru/C catalyst was mixed with 2 ml of acetone and placed in an ultrasonic bath for 15 minutes. A drop of the solution was placed onto a carbon coated copper grid and the acetone was evaporated under a lamp for a few seconds before TEM analysis took place.

TEM was used to determine the particle size of the Pt-Ru nanoparticles and the dispersion of the metal on Vulcan XC72R-50. ImageJ 1.47v was used to measure 100 particles and an average is found.

4.3.2. Energy-dispersive X-ray spectroscopy (EDX)

Energy-dispersive X-ray spectroscopy (EDX) coupled to a Scanning Electron Microscopy (SEM) was carried out at the Electron Microscope Unit at the University of Cape Town on a FEI Field Emission Nova NanoSEM 230, using an Oxford X-Max detector and INCA software, at 30 kV. The samples were placed on a carbon paste and left to dry before analysis took place. This technique was used to determine the Pt:Ru ratio.

4.3.3. X-ray Diffraction (XRD)

X-ray Diffraction (XRD) was carried out on a Bruker D8 Advance diffractometer with a Co K_α radiation source operating at 40 kV. The Pt-Ru/C catalyst was placed in the sample holder and the x-ray angle was increased from 10° to 130° at 2° per minute.

XRD was used to determine the average crystallite size and Bruker Eva software was used to determine the d-spacing of the catalyst particles.

The average crystallite size was determined by using the Scherrer equation and correction factor:

$$\tau = \frac{k\lambda}{\beta cos\theta}$$

k is a dimensionless shape factor, usually assumed to be 0.9, β is the peak broadening of 2θ at half height and λ. Is the wavelength An estimate of crystallite size, if one assumes spherical powder particles, were made using the equation:

$$d = (\frac{4}{3}) \times \tau$$

Where: τ is the volume-weighted length of the column perpendicular to the hkl plane, which is a measure of crystallite size, d_p is an estimation of crystallite size.

4.3.4. Thermogravimetric Analysis (TGA)

Thermogravimetric Analysis (TGA) was carried out at the Department of Chemical Engineering at the University of Cape Town in a *METTLER TGA/sDTA851e Thermogravimetric Analyser*. A small amount of Pt-Ru/C catalyst sample (2-10 mg) was placed in an aluminium oxide (Al_2O_3) crucible. The sample is oxidised at 10°C per minute from 25°C to 800°C in 10 ml/min in synthetic air.

5. RESULTS AND DISCUSSION

Section 5 details the physical and electrochemical characterisation results of this study. Section 5.1 is the benchmarking section whereby two commercial catalysts are tested to offer the reader reference values for the catalysts prepared in this study. Commercial catalyst 1 is a 60 wt% Pt-Ru/C with a molar ratio of 1:1 while commercial catalyst 2 is a 54 wt% Pt-Ru/C with a molar ratio of 1:1.5. Section 5.2 covers the reproducibility of the study, as two catalysts were prepared and tested under the same conditions to show the reader the preparation method and electrochemical setup are working correctly and the results presented are herein reliable and reproducible. Section 5.3 is a TGA analysis of the precursors in order to determine the initial conditions of the reactor. Section 5.4 covers the precursor deposition phase for preparation under vacuum and argon. Section 5.5 is a detailed temperature profile of the furnace, which is an important parameter to consider when producing catalysts in the furnace. A systematic study was then conducted through various parameters, with each section influencing the subsequent experiments' parameters. Section 5.6 details the results collected for the physical and electrochemical characterisation of the catalysts prepared under argon and vacuum atmospheres. The results from section 5.6 are then carried through to section 5.7 which covers the reactor temperature influence on physical and electrochemical characteristics of the catalysts prepared. The results from the temperature study were considered in section 5.8 which discusses the influence of the operating time on the physical and electrochemical characteristics of the prepared catalysts. Section 5.9 talks to the influence of Pt:Ru ratio on the physical and electrochemical characterisation of the prepared catalysts. Section 5.10 details the comparison between the commercial catalysts and the best performing prepared catalyst.

5.1. Benchmarking

Benchmarking experiments were carried out on two commercial Pt-Ru/C catalysts using CO stripping voltammetry, methanol oxidation and chronoamperometry experiments. Commercial catalyst 1 is a 60 wt% Pt-Ru/C (Pt:Ru, 1:1) catalyst and commercial catalyst 2 is a 54 wt% Pt-Ru/C (Pt:Ru, 1:1.5) catalyst.

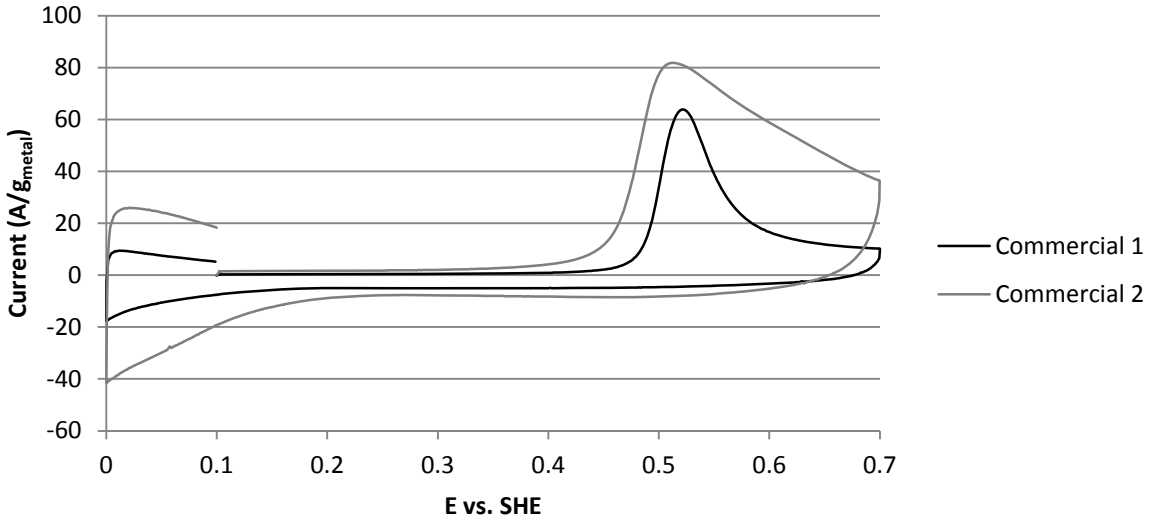

Figure 5-1: First sweep of CO stripping voltammograms of commercial catalysts 1 and 2.

Table 5-1: ECSA of commercial catalysts measured using CO stripping voltammetry.

Commercial catalyst	wt% Pt	ECSA (m^2/g)
Commercial 1	60	40.3
Commercial 2	54	105

Specifications of catalyst 2 were provided by the manufacturer wherein the active surface area of the catalyst, determined by CO adsorption, was stated to be 103.1 m^2/g_{cat}. This is close to the ECSA found by the electrochemical setup in this study and is an indication of the reliability of the electrochemical methods used in this study. Underneath are listed the CO oxidation, MeOH oxidation and chronoamperometry results.

Table 5-2: Electrochemical results for CO oxidation on commercial catalysts.

Commercial catalyst	Onset Potential (V vs. SHE)	Current at 0.5 V vs. SHE (A/g_{metal})	Current at 0.5 V vs. SHE (mA/cm^2)
Commercial 1	0.454	35.4	8.6
Commercial 2	0.400	77.8	8.6

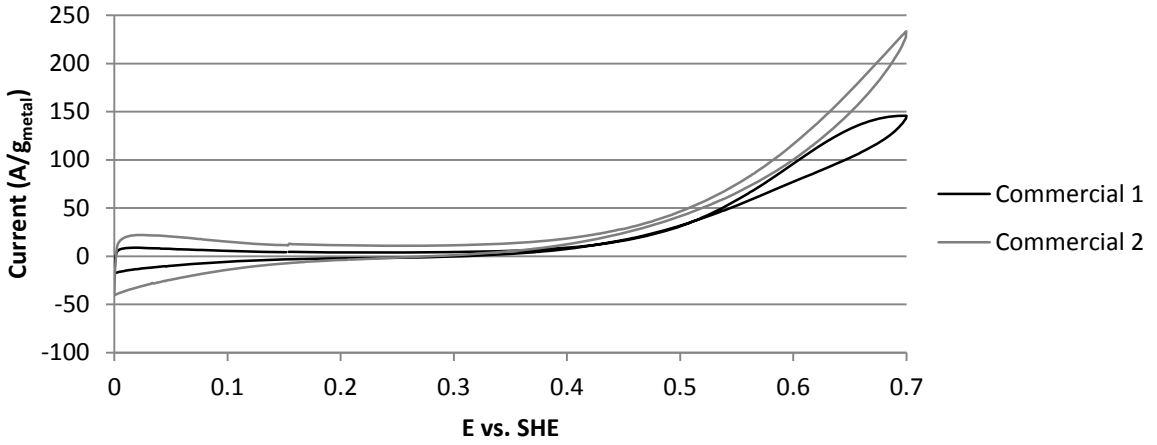

Figure 5-2: Methanol oxidation cyclic voltammograms of commercial catalysts 1 and 2.

Table 5-3: Electrochemical results for methanol oxidation on commercial catalysts.

Commercial catalyst	Onset Potential (V vs. SHE)	Current at 0.5 V vs. SHE (A/g_{metal})	Current at 0.5 V vs. SHE (mA/cm^2)
Commercial 1	0.328	31.2	7.6
Commercial 2	0.328	46.8	5.2

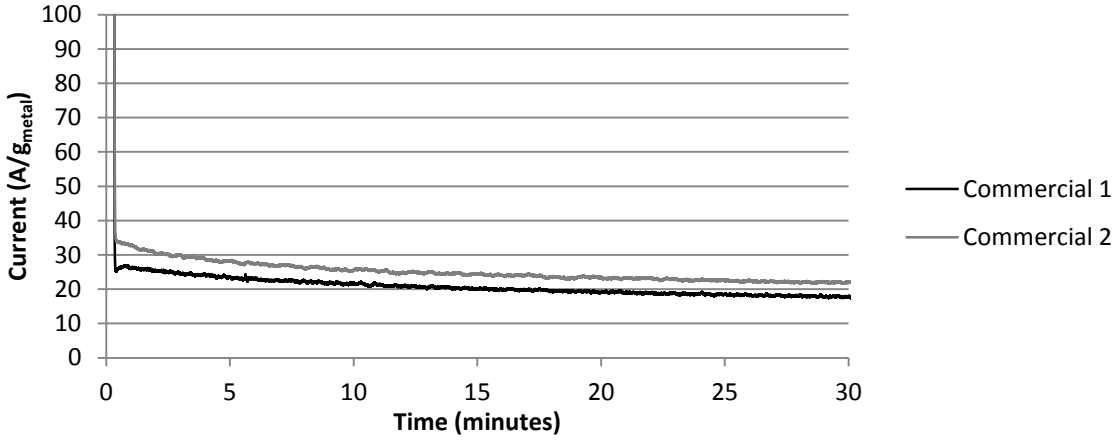

Figure 5-3: Chronoamperometry curves for commercial catalysts 1 and 2.

Table 5-4: Chronoamperometry results on commercial catalysts.

Commercial catalyst	Current at 30 minutes (A/g_{metal})	Drop in current (%)
Commercial 1	17.5	32.6
Commercial 2	21.9	34.9

The onset potentials and currents at 0.5 V vs. SHE for methanol oxidation and CO oxidation lie within a reasonable range for both catalyst 1 and catalyst 2. Combined with the ECSA value obtained for

catalyst 2 being similar to the catalyst specifications of 103.1 m^2/g_{Pt} this is a further indication that the experimental protocols developed for this study are reliable.

5.2. Reproducibility

Experimental repeats were performed throughout the project. The results shown below are an example of one of these experiments. Pt-Ru/C catalysts were produced under argon at 350 °C with a 30 minute operating time, 50 wt% total metal loading, with Pt:Ru of 50:50 to evaluate the reproducibility of the catalyst production method and testing. Physical and electrochemical characterisations of these catalysts are detailed below.

5.2.1. TEM and EDX

TEM images for the catalysts prepared under the same conditions are illustrated below:

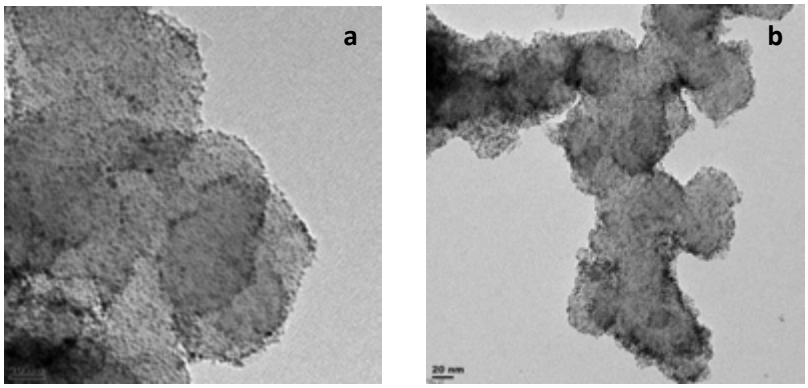

Figure 5-4: TEM images at 20 nm resolution of two Pt-Ru/C catalysts produced at 350 °C for 30 minutes under argon with a Pt:Ru ratio of 50:50.

The particle size measured from TEM images was found to be a) 2.60 nm and b) 2.18 nm. EDX analyses of Pt and Ru in total metal of the prepared catalysts are compared to expected results in the table below. The Pt and Ru metal percentages calculated from EDX results are within a reasonable range from the expected metal percentages.

Table 5-5: Expected Pt and Ru mol% in total metal compared to EDX analysis results of catalysts prepared under the same conditions.

Catalyst	Expected (mol%)		EDX result (mol%)	
	Pt	Ru	Pt	Ru
Catalyst a	50.0	50.0	52.0	48.0
Catalyst b	50.0	50.0	51.4	48.6

5.2.2. TGA

The TGA characterisation was used to determine the total metal loading of each catalyst. The table below details the expected versus TGA results on total metal loading. These results are close to the expected metal loading, emphasizing the reliability of the catalyst production method.

Table 5-6: Expected and TGA total metal loading of catalysts prepared under the same conditions.

Catalyst	Expected metal loading (wt%)	TGA metal loading (wt%)
Catalyst a	50.0	52.7
Catalyst b	50.0	51.7

5.2.3. XRD

XRD analysis was carried out on the catalysts prepared under the same conditions and the diffraction pattern is illustrated in Figure 5-5:

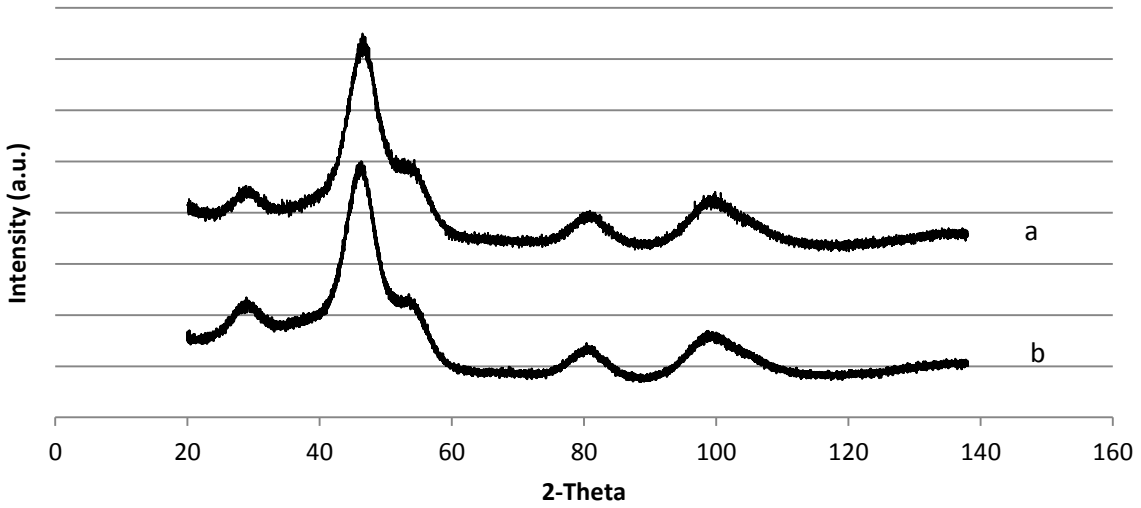

Figure 5-5: XRD graphs of Pt-Ru/C catalysts produced under the same conditions a) catalyst a and b) catalyst b.

The XRD curves are nearly indistinguishable. The Scherrer equation was used to calculate the average crystallite size for both catalysts, the data is displayed below:

Table 5-7: Particle size calculated using peaks (111) and (220) of XRD for catalysts prepared under the same conditions.

Catalyst	Average crystallite size (nm)
Catalyst a	2.24
Catalyst b	2.29

The lattice constant was calculated using the d-spacing of (111) and (220) peaks and the ruthenium atomic fraction in Pt-Ru was calculated using Vegard's Law for all prepared catalysts. The average lattice constant and ruthenium fraction included in the Pt-Ru structure is reported in Table 5-8.

Table 5-8: Average Lattice constant and Ru alloyed calculated using peaks (111) and (220) of XRD for catalysts prepared under the same conditions.

Catalyst	Average lattice constant	Average Ru atomic fraction in Pt-Ru (%)
Catalyst a	3.921	18.7
Catalyst b	3.922	18.5

5.2.4. CO Stripping Voltammetry

ECSA of the catalysts prepared under the same conditions were determined using CO stripping voltammetry and the results are shown in Table 5-9.

Table 5-9: ECSA and expected ECSA of catalysts made and tested under the same conditions.

Catalyst	Expected ECSA (m^2/g)	ECSA (m^2/g)
Catalyst a – run 1	224	270
Catalyst a – run 2	224	242
Catalyst b	220	263

The ECSA and CO oxidation results acquired for the two catalysts, including the two catalyst runs are within an acceptable range and demonstrate the reproducibility of the preparation method and electrochemical testing method. Electrochemical characterisation tests for CO oxidation activity were performed and the onset potential, current at 0.5 V vs. SHE normalized for total metal mass and finally intrinsic current at 0.5 V vs. SHE is reported.

Table 5-10: Electrochemical results for CO oxidation on catalysts prepared and tested under the same conditions.

Catalyst	Onset potential (V vs. SHE)	Current at 0.5 V vs. SHE (A/g_{metal})	Current at 0.5 V vs. SHE (mA/cm^2)
Catalyst a – run 1	0.386	44.8	1.4
Catalyst a – run 2	0.391	49.8	2.4
Catalyst b	0.394	47.1	2.3

5.2.5. Methanol Oxidation

Electrochemical characterisation tests for methanol oxidation activity were performed and the onset potential, current at 0.5 V vs. SHE normalized for total metal and finally intrinsic current at 0.5 V vs. SHE is reported.

Table 5-11: Electrochemical results for methanol oxidation on catalysts prepared and tested under the same conditions.

Catalyst	Onset potential (V vs. SHE)	Current at 0.5 V vs. SHE (A/g_{metal})	Current at 0.5 V vs. SHE (mA/cm^2)
Catalyst a – run 1	0.267	120	5.6
Catalyst a – run 2	0.271	109	5.3
Catalyst b	0.268	120	5.8

The methanol oxidation results shown in Table 5-11 show results within 10 % of one another, this confirmed the reproducibility of the production and testing method in its entirety.

5.2.6. Chronoamperometry

Chronoamperometry experiments were carried out on the catalysts prepared under the same conditions. The current after 30 minutes normalised for total metal mass and the percentage drop from 30 seconds to 30 minutes is reported in Table 5-12. These results, in accordance with the previous CO tolerance and methanol oxidation results are in an acceptable error margin of 10 %.

Table 5-12: Electrochemical results for methanol oxidation chronoamperometry on catalysts prepared and tested under the same conditions.

Catalyst	Current at 30 minutes (A/g_{metal})	Drop in current (%)
Catalyst a – run 1	66.9	37.9
Catalyst a – run 2	63.8	33.1
Catalyst b	70.8	35.4

5.2.7. Summary of Reproducibility

The data shown in this section speaks to the reproducibility of the catalyst preparation method and experimental setup. The results given are within a reasonable range of 10 % error and therefore it can be seen that the data in this work is reliable and reproducible.

5.3. TGA Analysis of Precursors

Thermogravimetric analysis (TGA) carried out on a $Pt(acac)_2$ sample and a $Ru(acac)_3$ sample in a nitrogen gas environment produced the following curves shown in Figure 5-6. The TGA analysis is used as an estimation of the decomposition window of $Pt(acac)_2$ and $Ru(acac)_3$ to determine the minimum operating temperature used in the furnace used to produce the catalysts.

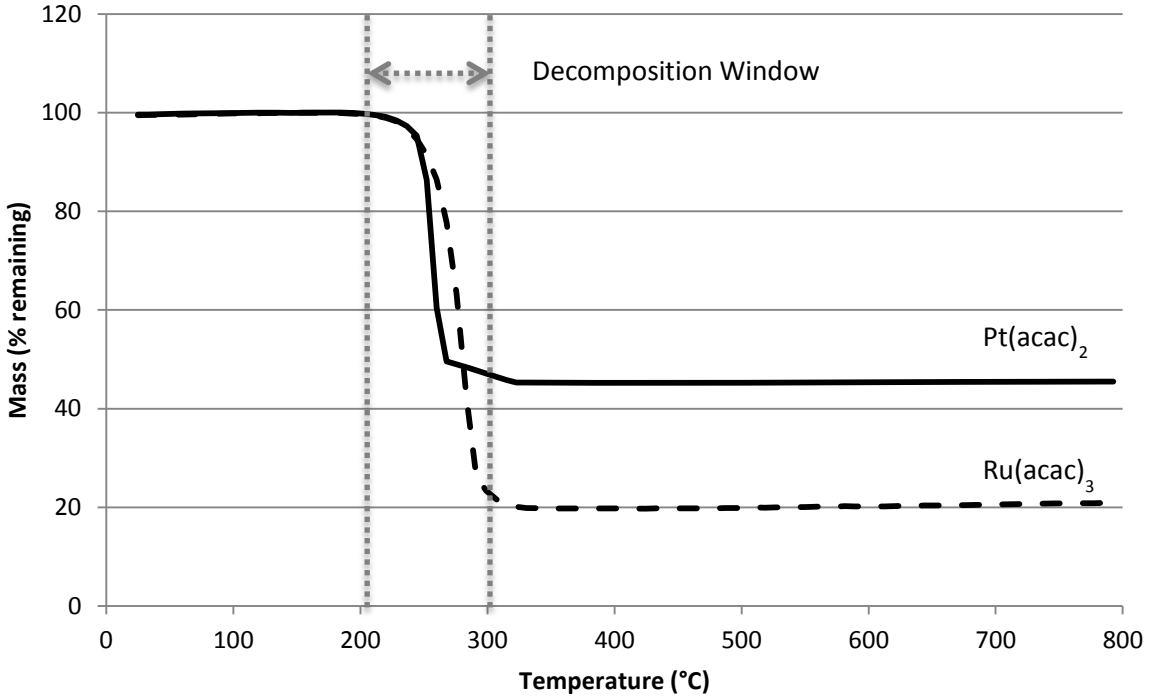

Figure 5-6: TGA curves of $Pt(acac)_2$ and $Ru(acac)_3$ measured under nitrogen at a heating rate of 10 °C/min.

The catalysts are produced under an argon and vacuum environment. The TGA curves give an indication of the decomposition window of both $Pt(acac)_2$ and $Ru(acac)_3$ in an inert environment. The curves show the majority of the decomposition takes place between ≈200 – 300 °C while a small amount of precursor decomposes between 300 - 500 °C, leaving behind platinum and ruthenium metal respectively. Table 5-13 details the weight contribution in the precursors.

Table 5-13: Weight contribution in $Pt(acac)_2$ and $Ru(acac)_3$.

Precursor	Molar weight	Metal loading (wt%)	Ligand weight contribution (wt%)
$Pt(acac)_2$	393.29	49.6	50.4
$Ru(acac)_3$	398.39	25.4	74.6

These findings are in line with the decomposition temperatures for $Pt(acac)_2$ and $Ru(acac)_3$ found in literature (Yoda *et al*., 2004 and Igumenov *et al.,* 2007). This gives an estimated temperature in which to run the furnace used to produce Pt-Ru/C catalysts by decomposition of $Pt(acac)_2$ and $Ru(acac)_3$ on a carbon substrate in an inert environment. Battiston *et al.* (2005) and Green *et al.* (1985) outline the decomposition temperature under a vacuum environment as ≈ 200 – 250 °C for $Pt(acac)_2$ and $Ru(acac)_3$.

5.4. Precursor Deposition Phase

When catalysts are produced under argon, it was discovered that precursor deposition occurred from the liquid phase. Precursor deposition from the liquid phase is an assumption which was made based on the phase diagram of the precursors used in this study. Assuming Clausius–Clapeyron relation:

$$Ln\,(P) = B - \frac{A}{T}$$

Where P is pressure in atmospheres, T is temperature in Kelvin, A and B are constants for each precursor (Morozona *et al.,* 2001)

Table 5-14: Clausius-Clapeyron constants for $Pt(acac)_2$ and $Ru(acac)_3$ (Morozona *et al.,* 2001).

Precursor	A	B
$Pt(acac)_2$	12737	20.19
$Ru(acac)_3$	15228	25.56

The vapourisation temperatures at atmospheric pressure can therefore be calculated, these were established to be 358 °C and 323 °C for $Pt(acac)_2$ and $Ru(acac)_3$ respectively. However, at atmospheric pressure, the $Pt(acac)_2$ melting point is 250 °C and decomposes at around 265 °C (Yoda *et al*., 2004) while $Ru(acac)_3$ has a melting point at 240 °C and decomposes at 285 °C (Igumenov *et al.*, 2007). Taking this information into account, the precursors are likely to melt and decompose before reaching the vapourisation temperature, therefore decomposition occurs from the liquid phase rather than the vapour phase.

Precursor deposition from the liquid phase is not a well-documented method, as literature is dominated by the OMCVD method. A similar method to liquid deposition is a method called Organo-Metallic Chemical Fluid Deposition (OMCFD). This method minimises the OMCVD by eliminating the precursor volatility constraints while retaining the coverage and transport properties since the precursor is mixed with a supercritical fluid (Long *et al.*, 2000).

The technique involves three stages, 'which are dissolutioning of the metallic precursor in the supercritical fluid phase, adsorption of the metallic precursor on the substrate and reduction of the metallic precursor to its metal form' (Erkey, 2008).

5.5. Furnace Temperature Gradient

A temperature gradient was conducted over the length of the furnace. The furnace thermocouples used to regulate the furnace are not placed in close proximity to the contact area and the heating is not uniform. Thus the furnace is overheated to temperatures above the set point in the center while areas on the edges are inadequately heated. Figure 5-7 details the actual temperature along the furnace for a range of set point temperatures.

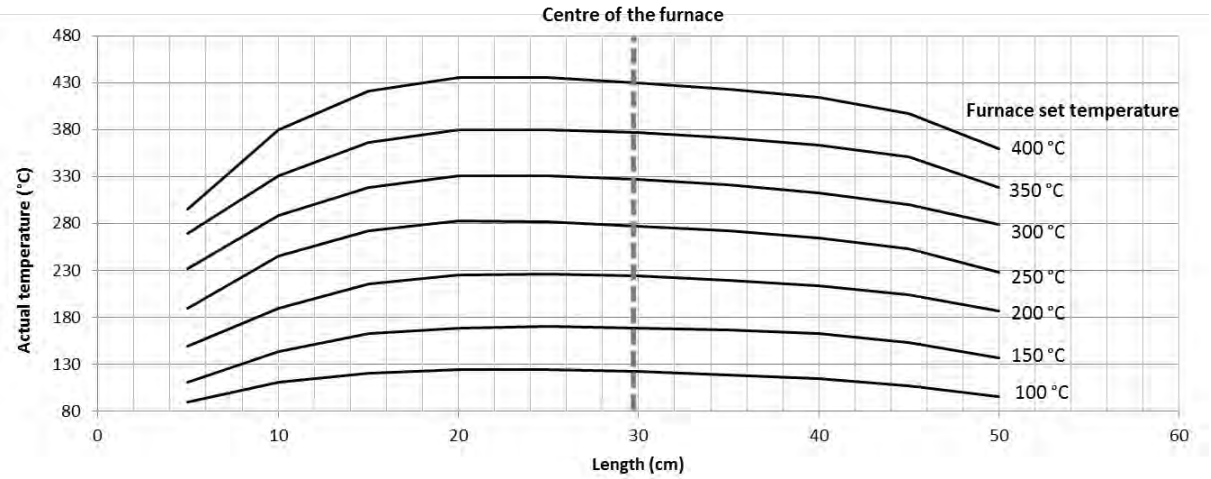

Figure 5-7: Temperature profile of the furnace used to produce catalysts by chemical deposition.

The figure above demonstrates the wide variation in temperature along the reactor and illustrates the importance of the position of the reactor in the furnace. Due to the above observations care was taken to always place the reactor at the same position. Furthermore, all set points reported in this work are corrected for the deviations indicated above.

5.6. Argon vs. Vacuum Reactor Atmosphere

Pt-Ru/C catalysts were produced under argon and vacuum atmospheres respectively. Each catalyst was made at 350 °C with an operating time of 4 hours, 50 wt% total metal loading, and a Pt:Ru molar ratio of 50:50. Physical and electrochemical characterisations of these catalysts are detailed below, followed by a summary in section 5.6.8.

5.6.1. TEM and EDX

TEM images for the catalysts prepared in varying atmospheres are illustrated below:

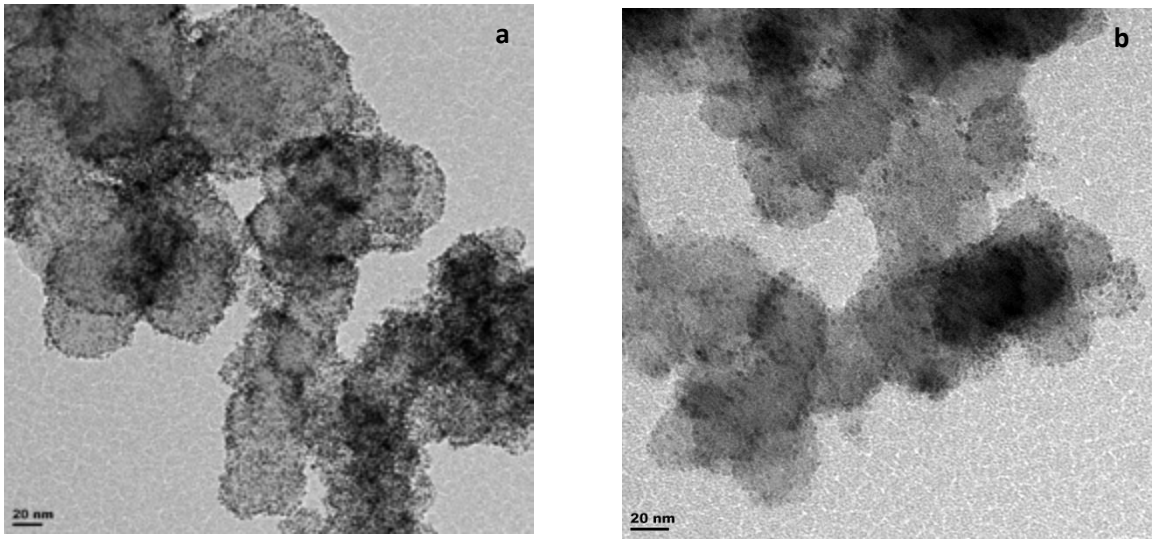

Figure 5-8: TEM images at 20 nm resolution of Pt-Ru/C catalysts produced at 350 °C for 4 hours under an a) argon atmosphere and b) vacuum atmosphere.

It is evident from the TEM images that both catalysts have good metal particle dispersion on the carbon support, however the catalysts produced under a vacuum atmosphere appear to be smaller.

The average particle size for the argon atmosphere prepared catalyst was 3.01 nm and the vacuum atmosphere prepared catalyst was 2.01 nm. The distribution of particle sizes is shown in Figure 5-9, this clearly demonstrates the vacuum catalyst particle size range is smaller than that of the argon catalyst. This is primarily due to the phase of the precursors during decomposition. As seen in the literature review, precursors at atmospheric pressure do not reach vapourisation temperature before deposition, while precursors in a vacuum atmosphere vapourise before deposition. The particle size of the vacuum prepared catalyst is smaller since the precursor deposits from the vapour phase, while the argon prepared catalyst is larger since the precursor it deposits from the liquid phase.

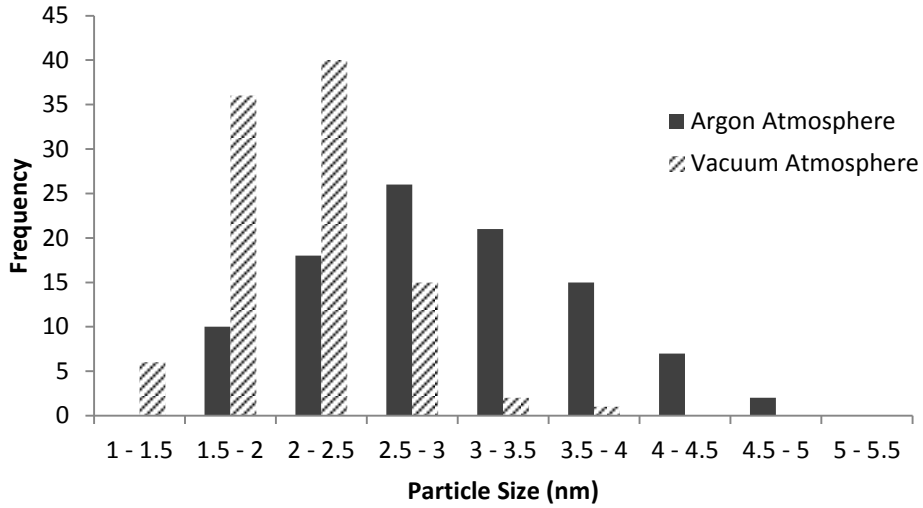

Figure 5-9: Particle size distribution graph of particles measured from TEM images of catalysts prepared under different atmosphere.

EDX analysis of Pt and Ru in total metal of the argon and vacuum prepared catalysts are compared to expected results in the table below. The Pt and Ru metal percentages calculated from EDX results are within a reasonable range from the expected metal percentages.

Table 5-15: Expected Pt and Ru mol% in total metal compared to EDX analysis results of catalysts prepared under different atmospheres.

Catalyst atmosphere	Expected (mol%)		EDX result (mol%)	
	Pt	Ru	Pt	Ru
Argon	50.0	50.0	53.6	46.4
Vacuum	50.0	50.0	52.5	47.5

5.6.2. TGA

The TGA characterisation was used to determine the total metal loading of each catalyst. The table below details the expected versus TGA results on total metal loading. These results are close to the expected metal loading, emphasizing the reliability of the catalyst production method.

Table 5-16: Expected and TGA total metal loading of catalysts prepared under different atmospheres.

Catalyst atmosphere	Expected metal loading (wt%)	TGA metal loading (wt%)
Argon	50.0	49.5
Vacuum	50.0	50.5

5.6.3. XRD

XRD analysis was carried out on the argon and vacuum atmosphere prepared catalysts and the diffraction pattern is illustrated in Figure 5-10, with Pt/C XRD graph as reference.

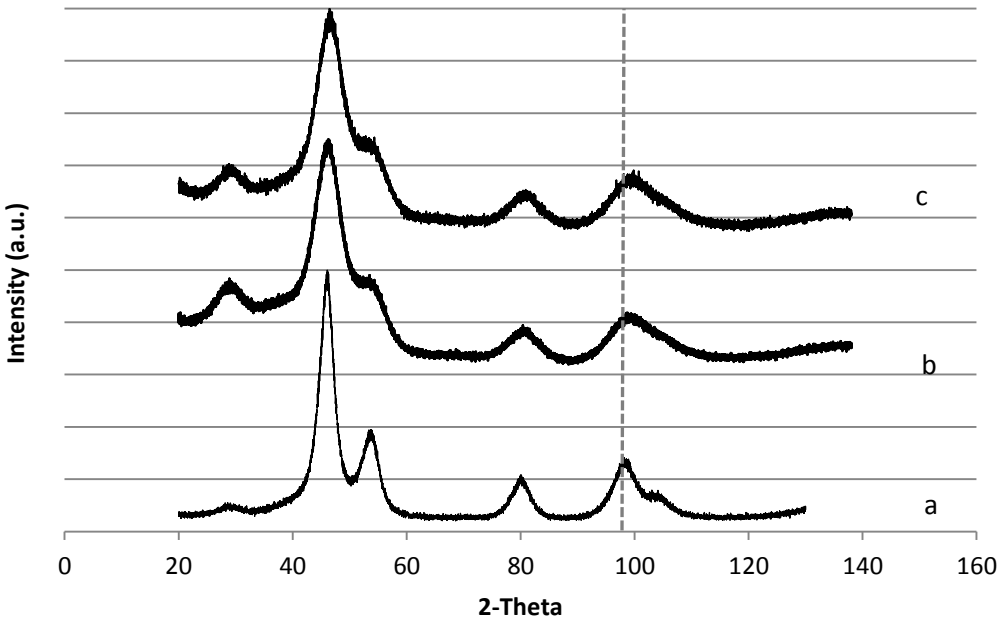

Figure 5-10: XRD graph of a) Pt/C catalyst and Pt-Ru/C catalysts produced at 350 °C for 30 minutes under b) argon and c) vacuum atmosphere.

The Pt/C XRD pattern has well defined peaks when compared to that of the Pt-Ru/C catalysts. In addition, the Pt-Ru/C catalyst peaks are slightly shifted to the right of the Pt/C peaks.

The Scherrer equation was used to calculate the average crystallite size in all the samples. The (111) and (220) peaks are used to calculate the average crystallite sizes, these peaks are indicated in Figure 2-22.

Table 5-17: Average crystallite size calculated using peaks (111) and (220) of XRD for catalysts prepared under different atmospheres.

Catalyst atmosphere	Average crystallite size (nm)
Argon	2.80
Vacuum	2.34

The lattice constant was calculated using the d-spacing of (111) and (220) peaks and the ruthenium atomic fraction in Pt-Ru were calculated using Vegard's Law for all prepared catalysts. The average lattice constant and ruthenium fraction included in the Pt-Ru structure is reported in Table 5-18.

Table 5-18: Average Lattice constant and Ru alloyed calculated using peaks (111) and (220) of XRD for catalysts prepared under different atmospheres.

Catalyst atmosphere	Average lattice constant	Average Ru atomic fraction in Pt-Ru (%)
Argon	3.914	25.3
Vacuum	3.923	17.6

The d-spacing of a platinum lattice will decrease as smaller ruthenium atoms are included in the lattice structure (Watanabe *et al*., 1987), this translates into a decrease in lattice spacing and lattice constant. Therefore it can be seen the lattice constant in inversely proportional to the ruthenium included in the platinum lattice since a decrease in lattice constant is due to an increase in ruthenium content in the lattice (Antolini & Cardellini, 2001). In addition, an increase in ruthenium in the platinum lattice is illustrative of the degree of alloying in the catalyst. The increase in ruthenium atomic fraction in the metal structure is due to better mixing of metals and alloying, hence the liquid phase deposition allows for better alloying of the metals.

5.6.4. Cyclic Voltammetry

Cyclic voltammograms were used to characterize the Pt-Ru catalysts by analysing the changes in shape and pseudo-capacitance between catalysts. The cyclic voltammograms for the catalysts prepared under an argon and vacuum atmosphere are shown in Figures 5-11 and 5-12 respectively, where the first and 50th cycles are shown. Figure 5-13 compares the first cycles of the catalysts, corrected for metal loading and the maximum height.

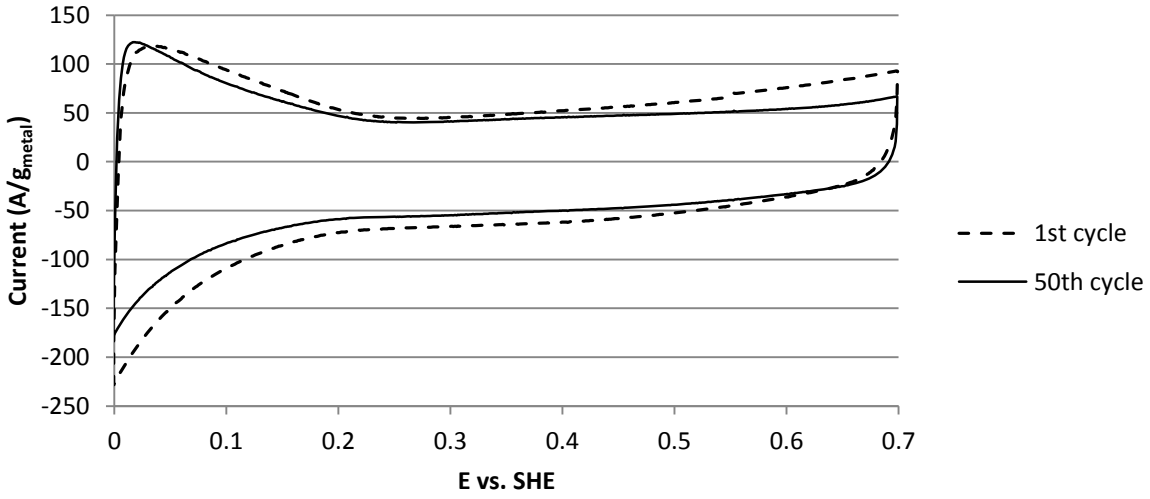

Figure 5-11: First and 50th cyclic voltammetry curves for the catalyst produced under an argon atmosphere at 350 °C for 4 hours.

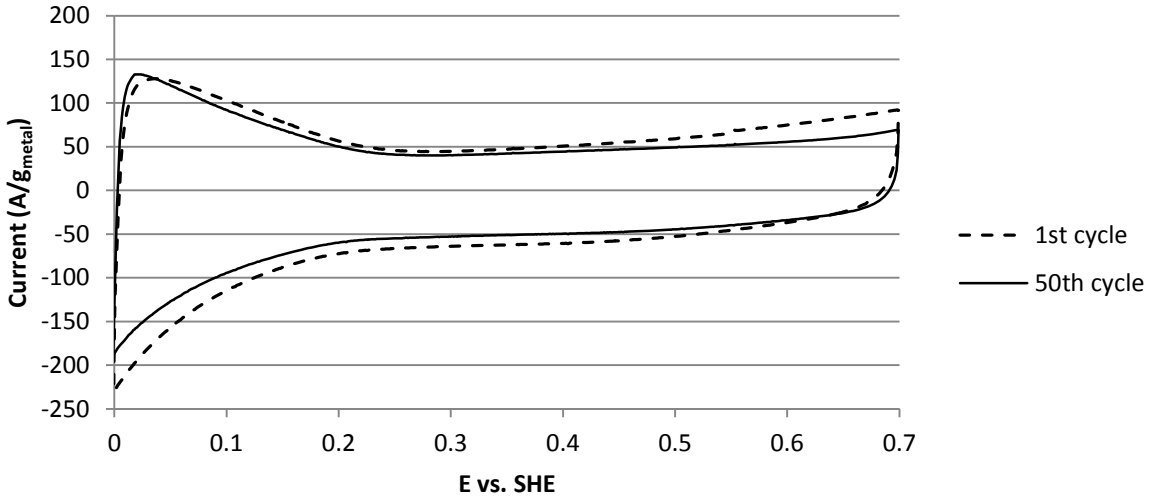

Figure 5-12: First and 50th cyclic voltammetry curves for the catalyst produced under vacuum atmosphere at 350 °C for 4 hours.

Figures 5-11 and 5-12 and show large pseudo-capacitance along the potential range, this is an indication of ruthenium oxide species content, as shown in literature (Sato *et al.*, 2000). The large pseudo-capacitance is due to the multiple oxidation states for oxidation and reduction of ruthenium which allows for ruthenium oxide to be oxidised and reduced to varying forms, some which can continue to be reduced and oxidised (Sato *et al.*, 2000). Zheng *et al*. (1995) described the cyclic voltammetry curve of RuO_2 in a H_2SO_4 electrolyte as mirror like and featureless which describes the figures well. The difference between the 1st and 50th cycle, for both catalysts, can be attributed to ruthenium oxide species reduction to non-reducible ruthenium oxides (Maillard *et al.,* 2002) thus a decrease in pseudo-capacitance is seen.

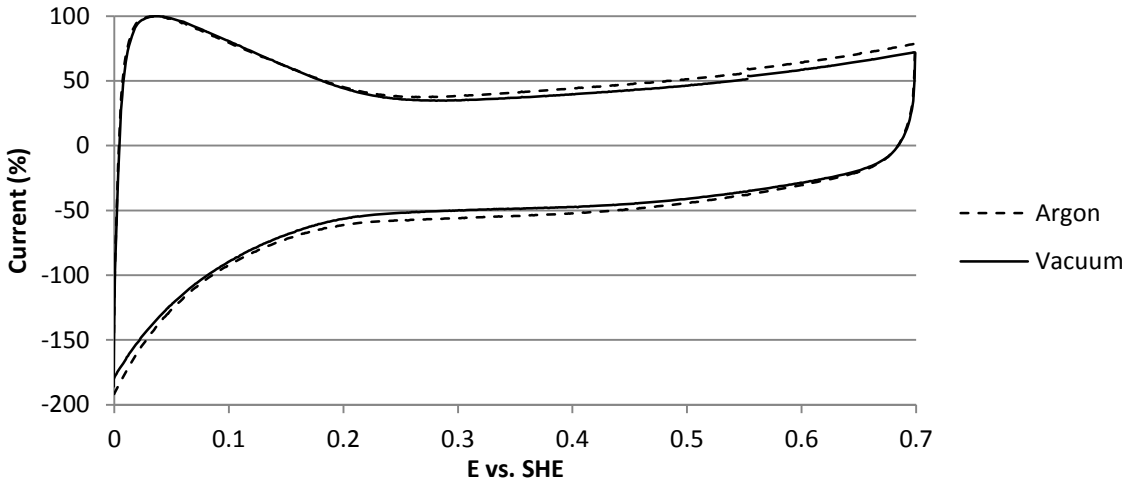

Figure 5-13: First cyclic voltammograms for the catalysts produced under argon and vacuum atmosphere at 350 °C for 4 hours.

The cyclic voltammetry curves shown in Figure 5-13 are very similar, indicating a similar ruthenium oxide content. The catalyst prepared under an argon atmosphere has a slightly larger pseudo-capacitance than the catalyst produced under a vacuum atmosphere indicating a slightly larger ruthenium oxide content in the argon prepared catalyst.

5.6.5. CO Stripping Voltammetry

CO Stripping voltammetry was used to determine the ECSA of the catalysts prepared under argon and vacuum atmospheres, the results are illustrated in Table 5-19. The ECSA of all catalysts were calculated assuming a charge of 0.42 $mC.cm^{-2}$ per CO monolayer adsorbed on the Pt-Ru surface.

Table 5-19: ECSA and expected ECSA of catalysts prepared under different atmospheres.

Catalyst atmosphere	Expected ECSA (m^2/g) for Pt-Ru	Expected ECSA (m^2/g) for Pt-RuO_2	ECSA (m^2/g)
Argon	138	180	175
Vacuum	165	215	201

The ECSA values calculated in the above table are in accordance with the particle size difference. Since the particle size of the catalyst prepared in a vacuum atmosphere is smaller than the catalyst prepared in an inert environment, the former would have a higher surface to volume ratio resulting in a higher ECSA. The similarity between expected ECSA and actual ECSA confirmed the assumption that the ruthenium in the catalyst exists as ruthenium oxide rather than ruthenium metal.

Electrochemical characterisation tests for CO oxidation activity were performed and the onset potential, current at 0.5 V vs. SHE normalized for total metal mass and finally intrinsic current at 0.5 V vs. SHE is reported.

Table 5-20: Electrochemical results for CO oxidation on catalysts prepared under different atmospheres.

Catalyst atmosphere	Onset potential (V vs. SHE)	Current at 0.5 V vs. SHE (A/g_{metal})	Current at 0.5 V vs. SHE (mA/cm^2)
Argon	0.411	33.6	2.3
Vacuum	0.429	17.1	1.2

The CO tolerance of a catalyst can be seen by the onset potential, since onset potential is directly proportional to activation energy of the CO oxidation reaction. Therefore, lower activation energy is

translated into a higher activity and thus a more CO tolerant catalyst. Contrary to the high ECSA of the vacuum prepared catalyst, the argon prepared catalyst is more active for CO oxidation than the vacuum catalyst. This could be attributed to the degree of alloying in the argon prepared catalyst as this is more suited to CO tolerance or the particle morphology differences attributed to decomposition from the vapour phase vs. liquid phase. Another explanation for this difference could be that the argon prepared catalyst contains more ruthenium oxide than the vacuum prepared catalyst, as indicated by the cyclic voltammograms, and this has been shown in literature to improve CO tolerance (Over & Muhler, 2003 and Kim *et al.,* 2000).

5.6.6. Methanol Oxidation

Electrochemical characterisation tests for methanol oxidation activity were performed and the onset potential, current at 0.5 V vs. SHE normalized for total metal mass and finally intrinsic current at 0.5 V vs. SHE is reported. Figure 5-14 is the methanol oxidation voltammetry graph isolating the onset potential.

Table 5-21: Electrochemical results for methanol oxidation on catalysts prepared under different atmospheres.

Catalyst atmosphere	Onset potential (V vs. SHE)	Current at 0.5 V vs. SHE (A/g_{metal})	Current at 0.5 V vs. SHE (mA/cm^2)
Argon	0.288	95.0	6.6
Vacuum	0.290	63.8	4.6

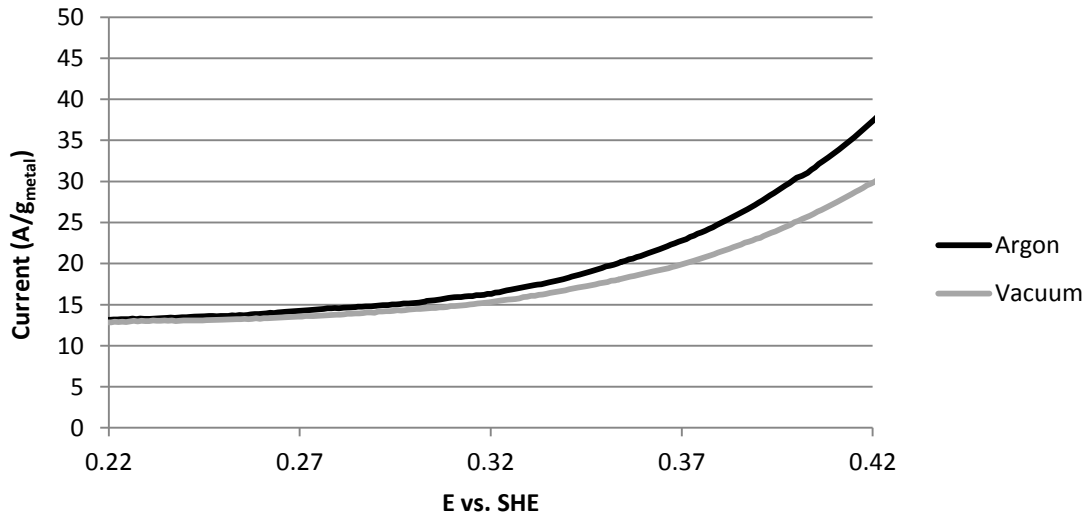

Figure 5-14: Electrochemical graphs for methanol oxidation onset potential on catalysts prepared under different atmospheres.

In accordance with CO tolerance results in section 5.6.5., the catalyst prepared in an argon environment is more active for methanol oxidation. As in CO tolerance, this increased activity for methanol oxidation could be attributed to the differences in the degree of alloying and ruthenium oxide content between the catalysts or the particle morphology differences in the catalysts due to the decomposition phase of the precursors. This finding is well explained in literature on ruthenium oxide on methanol oxidation (Bock *et al*., 2005, Long *et al.,* 2000, Rolison *et al*., 1999) (Frelink *et al.,* 1995a, 1995b & 1996), in accordance with CO tolerance, has shown the importance of ruthenium oxide on methanol oxidation activity.

5.6.7. Chronoamperometry

The importance of chronoamperometry is to establish the catalyst stability in a pseudo-fuel cell environment. Chronoamperometry experiments were carried out on the catalysts prepared under argon and vacuum atmospheres. The current after 30 minutes normalised for total metal mass and the percentage drop from 30 seconds to 30 minutes is reported in Table 5-22.

Table 5-22: Electrochemical results chronoamperometry on catalysts prepared under different atmospheres.

Catalyst atmosphere	Current at 30 minutes (A/g_{metal})	Drop in current (%)
Argon	37.7	42.2
Vacuum	23.5	50.6

Final chronoamperometry currents for the prepared catalysts follow well from the methanol oxidation currents recorded in section 5.6.6. A drop in current during a chronoamperometry test is an indication of the stability of the catalyst (Wang *et al.*, 2005). This instability could be due to catalyst degradation by ruthenium dissolution (Gancs *et al*. 2007).

The catalyst prepared in a vacuum atmosphere had a greater drop in current from 30 seconds to 30 minutes when compared to the catalyst prepared under an argon atmosphere. This additional drop in current could be due to the smaller particle size of the vacuum prepared catalyst undergoing more sintering during the chronoamperometry experiment.

5.6.8. Summary of Atmosphere Influence

The catalyst preparation atmosphere plays a significant role in CO tolerance, methanol oxidation activity and stability of the catalyst. The precursors in the argon environment decomposed from a liquid form, whilst the precursors under a vacuum environment decomposed from the vapour phase.

This change in decomposition phase influenced the particle size and catalyst morphology leading to a higher ruthenium content in the argon prepared catalyst than in the vacuum prepared catalyst.

This change in morphology relayed into an increased activity for methanol and CO oxidation as shown in literature by many researchers, as well as increased stability in chronoamperometry experiments for the catalyst produced in an argon environment. Therefore, catalysts produced in the subsequent sections were made under an argon atmosphere.

5.7. Operating Temperature Influence

Pt-Ru/C catalysts in this section were produced under argon at different operating temperatures ranging from 300 °C to 700 °C with an operating time of 4 hours, 50 wt% total metal loading, and a Pt:Ru molar ratio of 50:50. Physical and electrochemical characterisations of these catalysts are detailed below, followed by a summary in section 5.7.8.

5.7.1. TEM and EDX

TEM images for the catalysts prepared at a temperature of 350 °C for differing operating times is illustrated below:

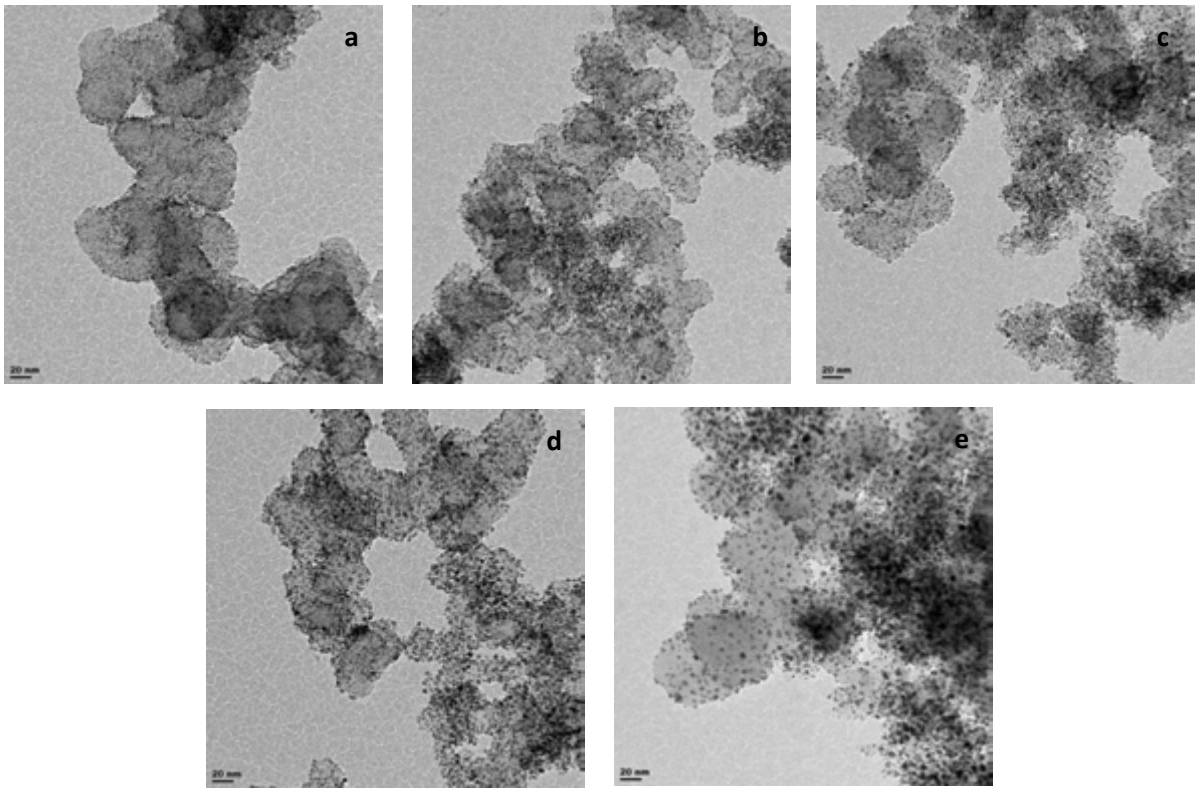

Figure 5-15: TEM images at 20 nm resolution of Pt-Ru/C catalysts produced for 4 hours under argon at a) 300 °C b) 350 °C c) 450 °C d) 600 °C e) 700 °C

The TEM images show well dispersed particles across all operating temperatures, however the particle size visibly increases between temperatures 300 °C to 700 °C. The average particle sizes measured from TEM are shown in Table 5-23, followed by a particle size distribution graph in Figure 5-16. The particle distribution graph re-iterates the visible increase in particle size changes as operating temperature increases.

Table 5-23: Average particle size from TEM imaging of catalysts made under argon at different operating temperatures for 4 hours.

Operating temperature (°C)	Average Particle Size (nm)
300	2.50
350	3.01
450	2.75
600	2.86
700	4.24

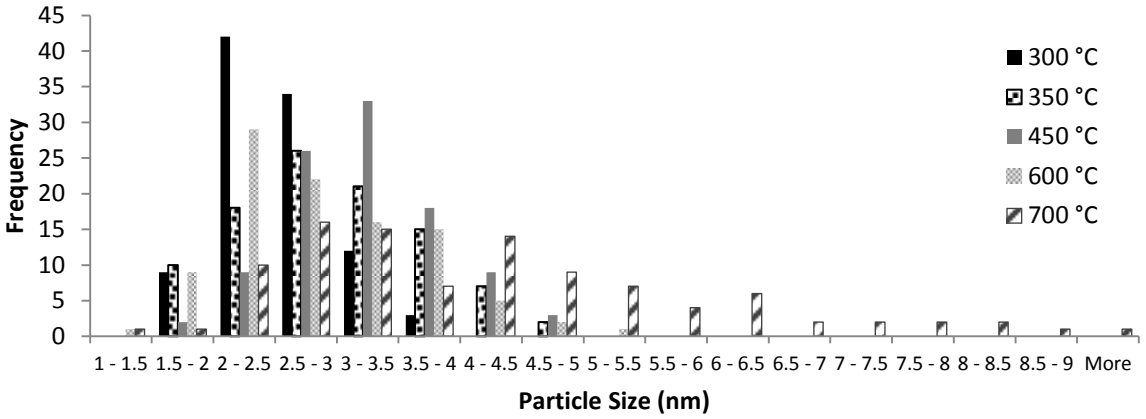

Figure 5-16: Particle size distribution graph of particles measured from TEM imaging of catalysts made under argon at different operating temperatures for 4 hours.

An increase in catalyst particle size is observed as operating temperature increases since high temperatures causes sintering of the catalyst particles, resulting in larger catalyst particles at higher temperatures.

EDX analysis of Pt and Ru in total metal of the different operating time prepared catalysts are compared to expected results in Table 5-24. The EDX values calculated are within a reasonable range of the expected metal percentages.

Table 5-24: Expected Pt and Ru mol% in total metal compared to EDX analysis results of catalysts made under argon at different operating temperatures for 4 hours.

Operating temperature (°C)	Expected (mol%)		EDX result (mol%)	
	Pt	Ru	Pt	Ru
300	50.0	50.0	49.7	50.3
350	50.0	50.0	53.6	46.4
450	50.0	50.0	48.8	51.2
600	50.0	50.0	55.2	44.8
700	50.0	50.0	55.8	44.2

5.7.2. TGA

The TGA characterisation was used to determine the total metal loading of each catalyst. The table below details the expected versus TGA results on total metal loading. These results are in a sensible range to the expected metal loading.

Table 5-25: Expected and TGA total metal loading of catalysts made under argon at different operating temperatures for 4 hours.

Operating temperature (°C)	Expected metal loading (wt%)	TGA metal loading (wt%)
300	50.0	50.2
350	50.0	49.5
450	50.0	50.4
600	50.0	50.1
700	50.0	50.2

5.7.3. XRD

XRD analysis was carried out on the different operating temperature prepared catalysts and the diffraction pattern is illustrated in Figure 5-17:

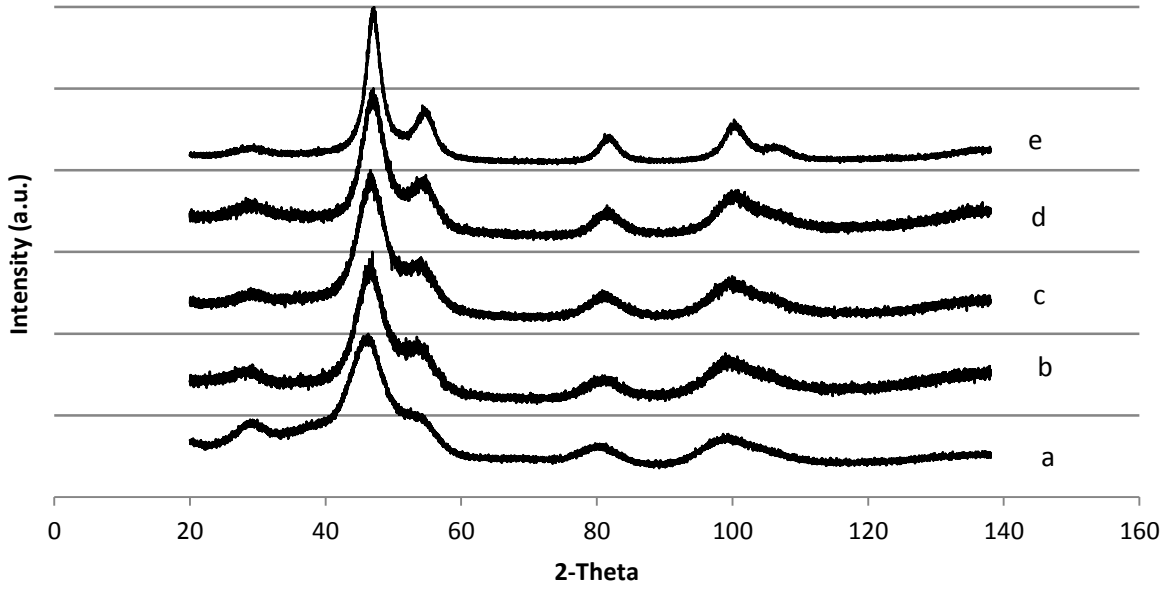

Figure 5-17: XRD graphs of Pt-Ru/C catalysts produced for 4 hours under argon at a) 300 °C b) 350 °C c) 450 °C d) 600 °C e) 700 °C

Using diffraction peaks (111) and (220) the crystallite size of each prepared catalysts was determined and the results are shown in Table 5-26.

Table 5-26: Crystallite size calculated using peaks (111) and (220) of XRD for catalysts made under argon at different operating temperatures for 4 hours.

Operating temperature (°C)	Average crystallite size (nm)
300	2.19
350	2.80
450	2.82
600	3.44
700	4.32

The crystallite sizes determined from XRD correspond to those seen in the TEM analysis. The trend of increasing size with increasing temperature is also observed here. This confirms that the TEM pictures are representative for the catalyst and it is unlikely that large agglomerates exist in the material. The lattice constant and ruthenium atomic fraction in Pt-Ru, calculated using the d-spacing of (111) and (220) peaks, is reported in Table 5-27.

Table 5-27: Average lattice constant and Ru alloyed calculated using peaks (111) and (220) of XRD for catalysts made under argon at different operating temperatures for 4 hours.

Operating temperature (°C)	Average lattice constant	Average Ru atomic fraction in Pt-Ru (%)
300	3.938	5.56
350	3.914	25.3
450	3.898	38.0
600	3.887	47.1
700	3.878	53.6

It can be seen from Table 5-27 that average lattice constant decreases with increasing operating temperature, causing a significant increase in ruthenium fraction included in the platinum lattice as seen in literature (Antolini & Cardellini, 2001). Antolini & Cardellini (2001) concluded the interaction of Ru with the carbon support hinders the formation of an alloy with Pt in the absence of thermal treatment. When thermally untreated Ru exists as an amorphous structure and when taken to higher temperatures the Ru alloyed to form Pt-Ru. High temperatures could lead to sintering of the particles and therefore encourage further alloying of the Pt-Ru particles, thus increasing the ruthenium fraction in the Pt-Ru particles and decrease in lattice spacing.

5.7.4. Cyclic Voltammetry

Cyclic voltammograms were used to characterize the Pt-Ru catalysts by analysing the changes in shape and pseudo-capacitance between catalysts. The cyclic voltammograms for the catalysts prepared at 300 °C and 700 °C are shown in Figures 5-18 and 5-19 respectively, where the first and 50^{th} cycles are shown. The cyclic voltammograms for the catalysts produced at other temperatures are shown in the Appendix. Figure 5-20 compares the first cycles of the catalysts produced at different temperatures, corrected for metal loading and the maximum height.

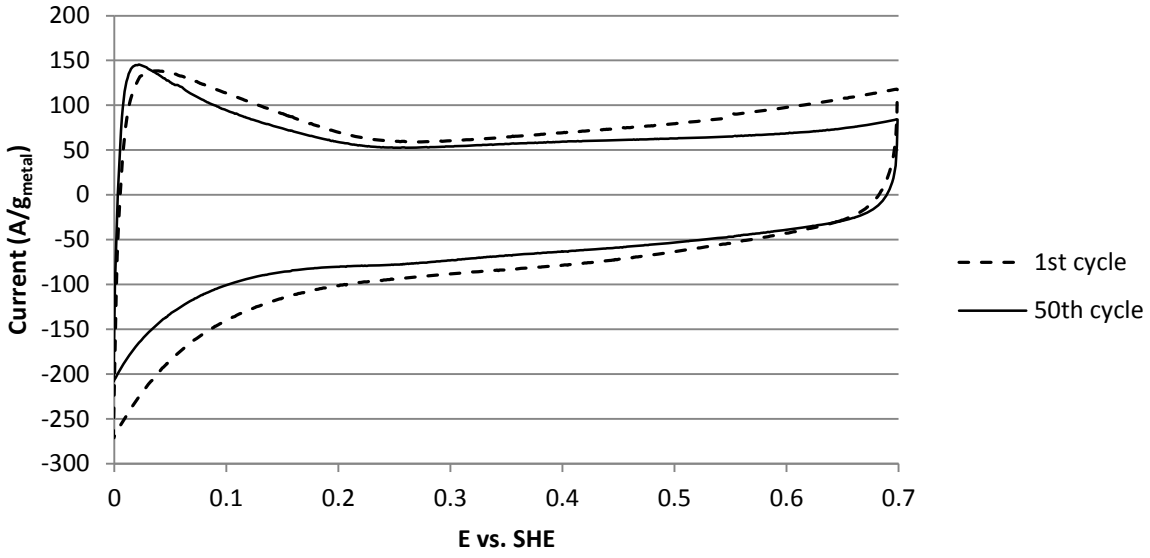

Figure 5-18: First and 50th cyclic voltammetry curves for the catalyst produced under an argon atmosphere at 300 °C for 4 hours.

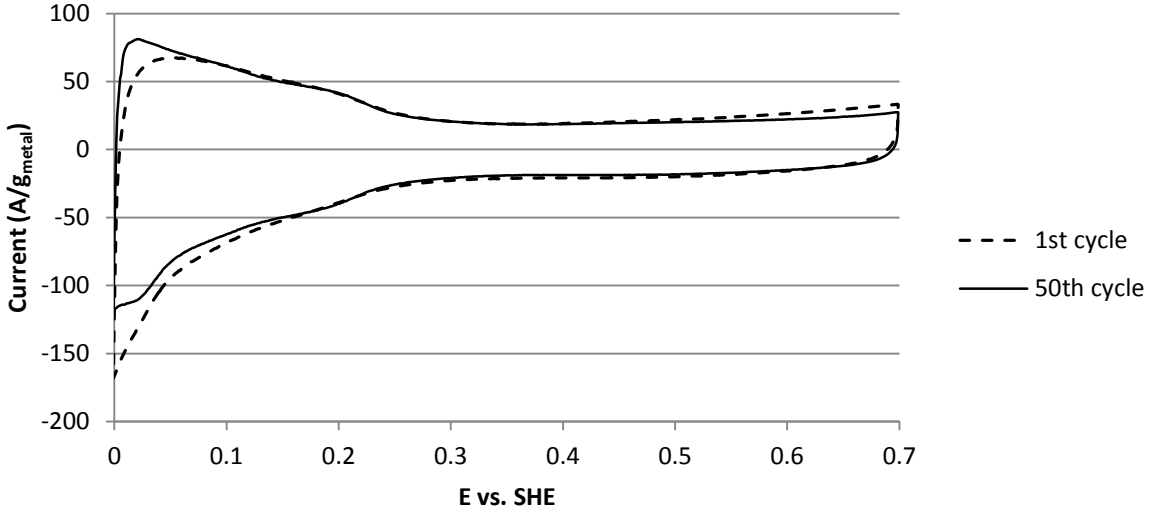

Figure 5-19: First and 50th cyclic voltammetry curves for the catalyst produced under an argon atmosphere at 700 °C for 4 hours.

Figures 5-18 and 5-19 show the vast difference in catalyst composition between the catalysts produced at 300 °C and 700 °C. The cyclic voltammogram of the catalyst prepared at 300 °C has a more featureless curve and a large pseudo-capacitance, indicating a high ruthenium oxide content (Sato *et al.*, 2000). The catalyst produced at 700 °C has defining platinum features and a small pseudo-capacitance, indicating a lower ruthenium oxide content. In addition, the 1st and 50th cycle of the catalyst produced at 300 °C shows some content has been reduced to a non-reducible state

whilst the catalyst produced at 700 °C does not show much change between the 1st and 50th cycle indicating the ruthenium is already in a non-reducible ruthenium oxide or ruthenium metal state (Maillard *et al.,* 2002).

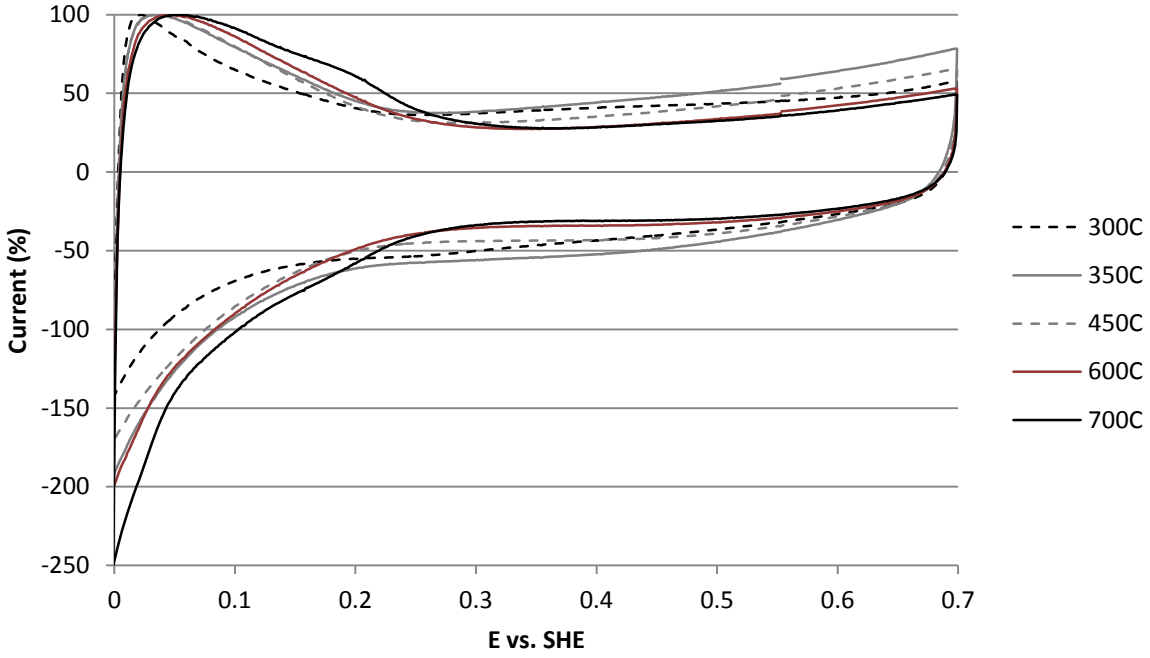

Figure 5-20: First cyclic voltammograms for the catalysts produced under an argon atmosphere at different temperatures for 4 hours.

Figure 5-20 allows for a better comparison between the catalysts, it is once again seen that the catalyst produced at 300 °C demonstrates a more featureless curve with a large pseudo-capacitance while the catalyst produced at 700 °C has a smaller pseudo-capacitance. Figure 5-20 gives a strong indication that catalysts produced at high temperatures contain less ruthenium oxides on the surface while catalysts produced at low temperatures contain a high ruthenium oxide content, with the highest ruthenium oxide content being the catalyst produced at 350 °C.

5.7.5. CO Stripping Voltammetry

ECSA of the catalysts prepared at different operating times were determined using CO stripping voltammetry and the results are shown in Table 5-28.

Table 5-28: ECSA and expected ECSA of catalysts made under argon at different operating temperatures for 4 hours.

Operating temperature (°C)	Expected ECSA (m^2/g) for Pt-Ru	Expected ECSA (m^2/g) for Pt-RuO_2	ECSA (m^2/g)
300	177	230	218

350	138	180	175
450	137	179	175
600	112	146	103
700	89	117	75.7

As expected, the ECSA of the catalysts is inversely proportional to the particle size since an increase in particle size reduces the surface to volume ratio of the prepared catalyst. The expected ECSA is based on the surface area calculated from particle size, therefore it is foreseeable the actual ECSA will be slightly smaller than the predicted ECSA. In addition, since the expected ECSA is based on an amorphous ruthenium oxide structure, deviation from the expected ECSA of Pt-RuO_2 increases as less ruthenium oxide exists in the structure and a Pt-Ru alloy is formed. The ECSA for the catalysts prepared at high temperatures follows the estimated ECSA of Pt-Ru structure, as confirmed in literature (Antolini & Cardellini, 2001) and by the cyclic voltammograms in section 5.7.4.

The CO stripping onset potential, current at 0.5 V vs. SHE normalized for total metal mass and finally intrinsic current at 0.5 V vs. SHE is illustrated in the Table 5-29.

Table 5-29: Electrochemical results for CO oxidation on catalysts made under argon at different operating temperatures for 4 hours.

Operating temperature (°C)	**Onset potential (V vs. SHE)**	**Current at 0.5 V vs. SHE (A/g_{metal})**	**Current at 0.5 V vs. SHE (mA/cm^2)**
300	0.417	23.3	1.4
350	0.411	33.6	2.3
450	0.430	20.5	1.6
600	0.450	11.2	1.3
700	0.455	10.8	1.7

The optimum catalyst preparation operating temperature in this series for CO tolerance was found to be 350 °C since the catalyst prepared at this temperature has the lowest onset potential and highest current per active surface area at 0.5 V vs. SHE (mA/cm^2). The CO oxidation onset potential is influenced by morphology of the catalyst, as this is a vital component in the activity of the catalyst for CO oxidation. Effects such as ruthenium oxides, degree of alloying, particle size and morphology play a large role in activity, although not well understood in literature. As temperature is increased the particle size increases and ruthenium oxide content decreased, therefore the crystalline

structure changes which translates into different active sites for CO oxidation. As ruthenium oxides decrease (Antolini & Cardellini, 2001) the CO tolerance decreases as described in literature (Over & Muhler, 2003) The increase in CO oxidation onset potential is also partly due to the increasing ruthenium content in the Pt-Ru structure and decrease in ruthenium oxide content with an optimum degree of alloying in this series at 350 °C as well as temperature effects on the morphology of the catalyst.

5.7.6. Methanol Oxidation

Electrochemical characterisation tests for methanol oxidation activity were performed and the onset potential, current at 0.5 V vs. SHE normalized for total metal mass and finally intrinsic current at 0.5 V vs. SHE is reported. These results are shown in Table 5-30 and the methanol oxidation voltammogram for each catalyst is shown in Figure 5-21.

Table 5-30: Electrochemical results for methanol oxidation on catalysts made under argon at different operating temperatures for 4 hours.

Operating temperature (°C)	Onset Potential (V vs. SHE)	Current at 0.5 V vs. SHE (A/g_{metal})	Current at 0.5 V vs. SHE (mA/cm^2)
300	0.282	82.0	4.9
350	0.278	95.0	6.6
450	0.303	59.8	4.6
600	0.329	30.9	3.6
700	0.343	41.5	6.4

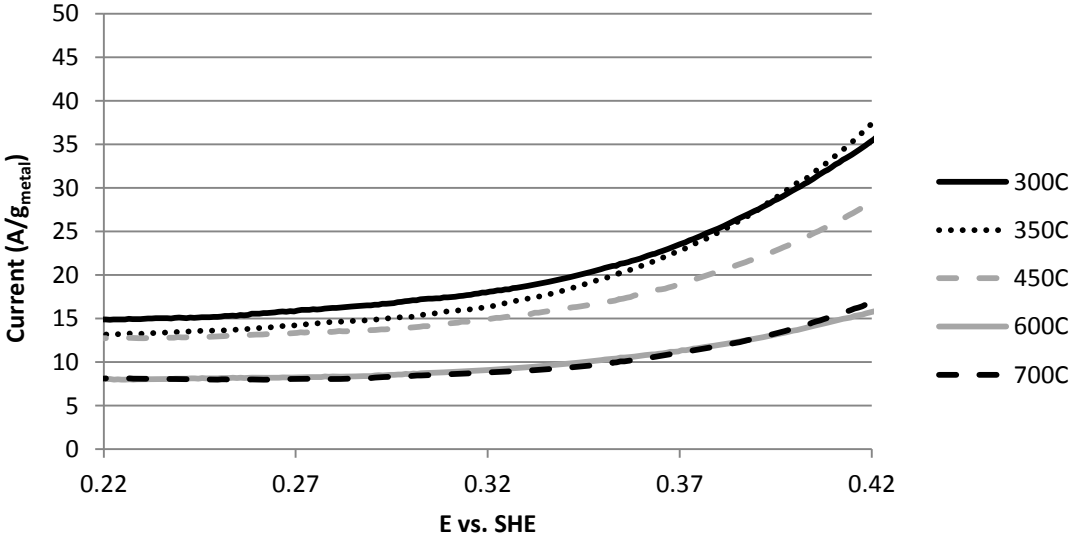

Figure 5-21: Electrochemical graphs for methanol oxidation onset potential on catalysts prepared under argon at different operating temperatures for 4 hours.

Correspondingly to the CO tolerance in section 5.7.5, the operating temperature with the best results according to onset potential for methanol oxidation is 350 °C. Once again, this is most probably due to morphology and ruthenium oxide changes as the temperature of the reactor increases. In addition, the particle size increased as temperature is increased, therefore the crystalline structure changes to contain fewer corners and kinks, and this translates into different active sites for methanol oxidation. Methanol oxidation has been shown to take place preferably on rough surfaces (Hoster *et al.* 2001) this type of surface could be produced at low temperatures rather than high temperatures. This trend can also be seen in the specific current, where the highest current i.e. the most active surface was observed for 350 °C. In addition, the increasing onset potential could be due to the increasing ruthenium content in the Pt-Ru structure, with an optimum degree of alloying in this series at 350 °C as well as temperature effects on the morphology of the catalyst.

5.7.7. Chronoamperometry

Chronoamperometry experiments were carried out on the catalysts prepared with varying operating temperatures. The current after 30 minutes normalised for total metal mass and the percentage drop from 30 seconds to 30 minutes is reported in Table 5-31.

Table 5-31: Electrochemical results for chronoamperometry on catalysts made under argon at different operating temperatures for 4 hours.

Operating temperature (°C)	Current at 30 minutes (A/g_{metal})	Drop in current (%)
300	33.9	46.2
350	37.8	42.2
450	23.2	48.8
600	10.8	53.4
700	15.1	56.3

The chronoamperometry experiment follows the same trend as the methanol oxidation experiment, showing the consistence of these results. It is important to note the decrease in catalyst stability as operating temperature increases. The increased temperature must therefore produce a catalyst morphology which is less stable than catalysts produced at lower temperatures.

5.7.8. Summary of Temperature Influence

Preparation temperature plays a significant role in the prepared catalyst's morphology, particle size, stability and activity for CO and methanol oxidation.

As the preparation temperature increases, the particle size significantly increases causing the ECSA of the catalysts to pointedly decrease. This decrease in active surface area as temperature increases is due to the decrease in ruthenium oxides on the surface which translates into a decrease in activity for both CO and methanol oxidation as seen in CO stripping, methanol oxidation cyclic voltammograms and chronoamperometry results. In addition, an increase in preparation temperature translates into an increase in degree of alloying, as seen in Table 5-27. This increase in alloying does not translate into an increase in activity, indicating inverse proportionality. This result is both agreed with and contested by various researchers as seen in section 2.3.2.2 and section 2.3.3 This increase in ruthenium content in the platinum structure could be due to the sintering of particles, therefore additional mixing occurs of both metals in the structure.

Taking these factors and section 5.6 into consideration, the operating atmosphere of argon and temperature of 350 °C was identified as the optimum atmosphere and temperature respectively for this study in the range tested and these conditions are used in the subsequent sections of the project.

5.8. Operating Time Influence

The findings in section 5.7 where carried through the project, therefore the Pt-Ru catalysts produced hereinafter are produced at a temperature of 350 °C. Pt-Ru/C catalysts in this section were produced under argon at a temperature of 350 °C, with different operating times ranging from 30 minutes to 8 hours. 50 wt% total metal loading, and a Pt:Ru molar ratio of 50:50 were targeted. Physical and electrochemical characterisations of these catalysts are detailed below, followed by a summary in section 5.8.8.

5.8.1. TEM and EDX

TEM images for the catalysts prepared at a temperature of 350 °C for different operating times is illustrated below:

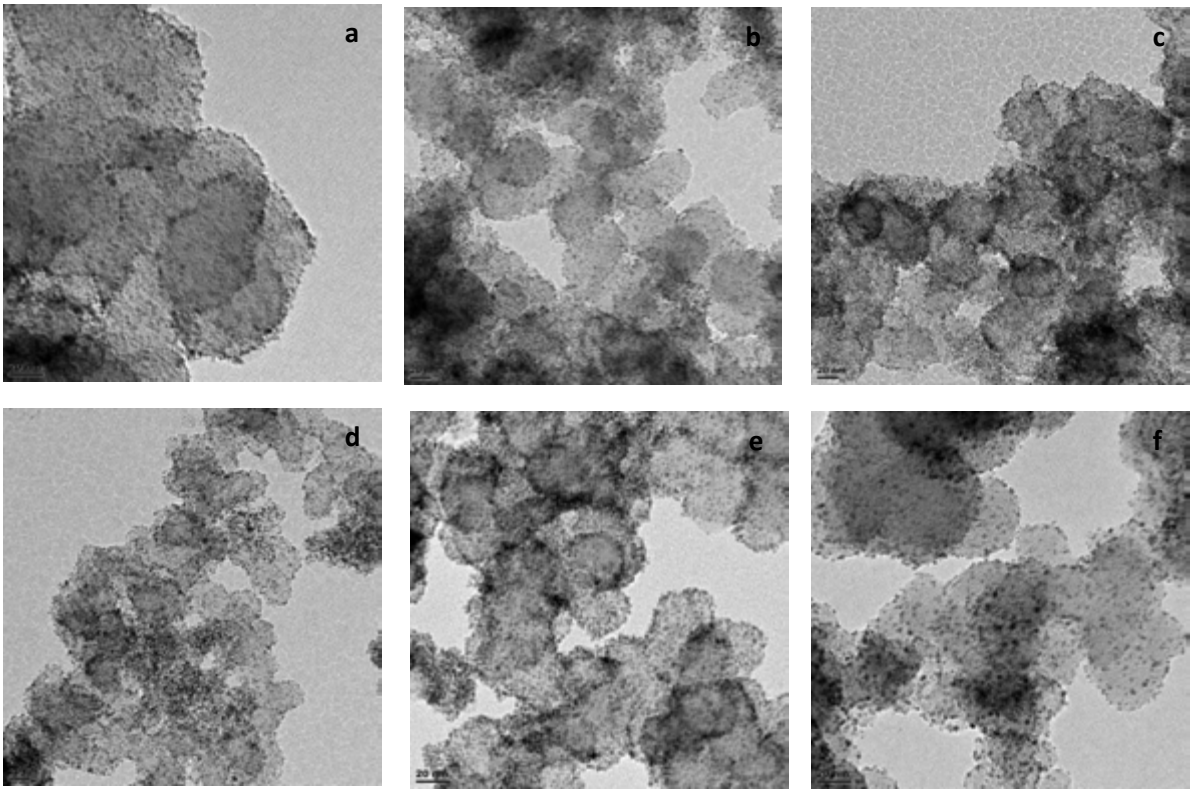

Figure 5-22: TEM images at 20 nm resolution of Pt-Ru/C catalysts produced at 350 °C under argon for a) 30 minutes b) 1 hour c) 2 hours d) 4 hours e) 6 hours and f) 8 hours.

Table 5-32: Average particle size from TEM imaging of catalysts made under argon at 350 °C at different operating times.

Operating time	Average particle size (nm)
30 minutes	2.60
1 hour	2.29
2 hours	2.33
4 hours	3.01
6 hours	2.54
8 hours	2.58

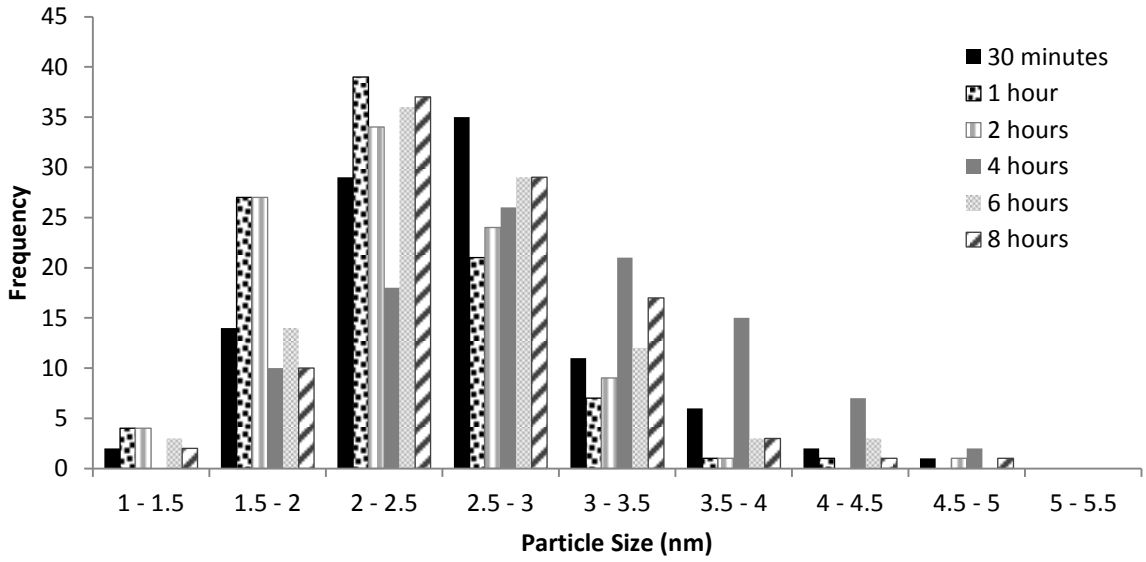

Figure 5-23: Particle size distribution graph of particles measured from TEM images of catalysts made under argon at 350 °C at different operating times.

The TEM images show well dispersed particles and similar, small catalyst particles across all reactor operating times. The average particle sizes measured from TEM are shown in Table 5-32, followed by a particle size distribution graph in Figure 5-23. The particle size distribution, in accordance with particle size, is comparable across the catalysts, as no noticeable trend is observed. This suggests that in terms of particle size, temperature is a more dominant factor as opposed to operating time.

EDX analysis of Pt and Ru in total metal of the different operating time prepared catalysts are compared to expected results in the Table 5-33. The measured EDX values are within a reasonable range of the expected metal percentages.

Table 5-33: Expected Pt and Ru mol% in total metal compared to EDX analysis results of catalysts made under argon at 350 °C at different operating times.

Operating time	Expected (mol%)		EDX result (mol%)	
	Pt	Ru	Pt	Ru
30 minutes	50.0	50.0	52.0	48.0
1 hour	50.0	50.0	50.3	49.7
2 hours	50.0	50.0	48.4	51.6
4 hours	50.0	50.0	53.6	46.4
6 hours	50.0	50.0	52.6	46.4
8 hours	50.0	50.0	53.2	46.8

5.8.2. TGA

The TGA characterisation was used to determine the total metal loading of each catalyst. The table below details the expected versus TGA results on total metal loading. These results are in a sensible range to the expected metal loading.

Table 5-34: Expected and TGA total metal loading of catalysts made under argon at 350 °C at different operating times.

Operating time	Expected metal loading (wt%)	TGA metal loading (wt%)
30 minutes	50.0	52.7
1 hour	50.0	47.0
2 hours	50.0	48.6
4 hours	50.0	49.5
6 hours	50.0	50.3
8 hours	50.0	52.0

5.8.3. XRD

XRD analysis was carried out on the different operating time prepared catalysts and the diffraction pattern is illustrated in Figure 5-24:

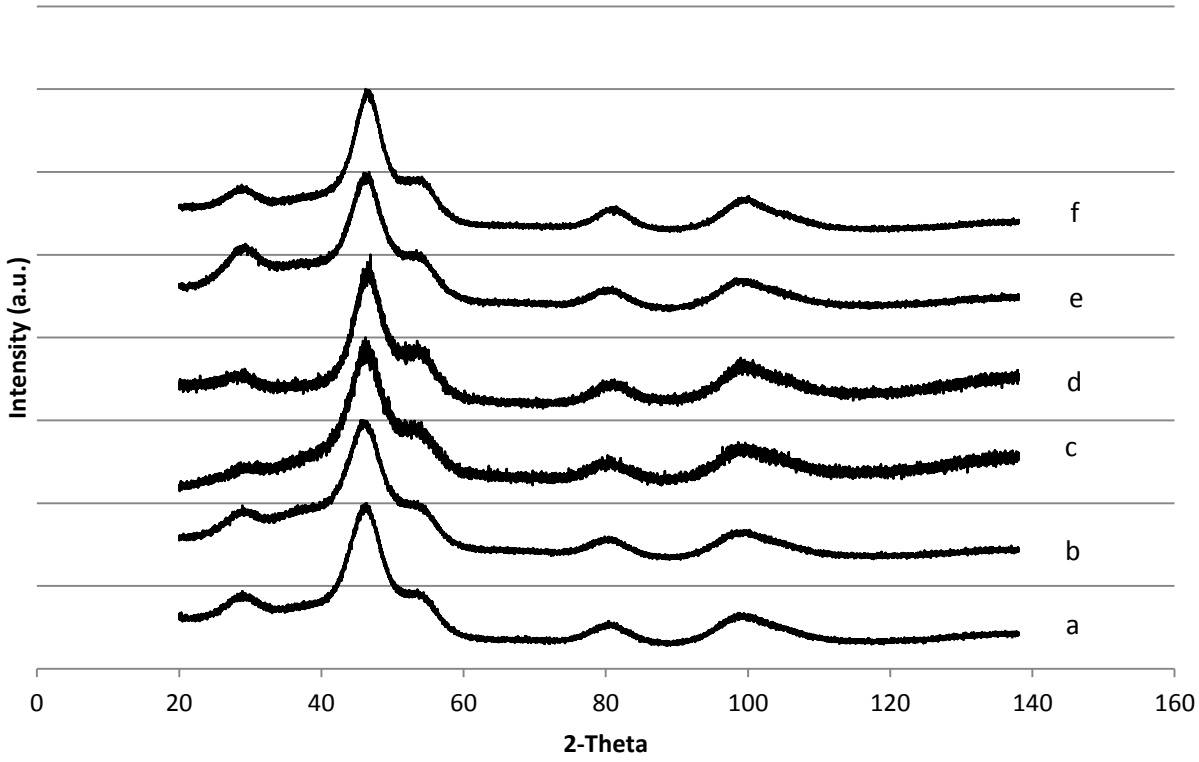

Figure 5-24: XRD graphs of Pt-Ru/C catalysts produced at 350 °C for under argon for a) 30 minutes b) 1 hour c) 2 hours d) 4 hours e) 6 hours and f) 8 hours.

Crystallite size was calculated using diffraction peaks (111) and (220). The results are shown in Table 5-35. The crystallite sizes determined from XRD graphs are similar and show the same trend to the TEM particle sizes measured.

Table 5-35: Average crystallite size calculated using peaks (111) and (220) of XRD for catalysts made under argon at 350 °C at different operating times.

Operating time	Average crystallite size (nm)
30 minutes	2.24
1 hour	2.18
2 hours	2.66
4 hours	2.80
6 hours	2.31
8 hours	2.51

The lattice constant and Ru alloyed, calculated using the d-spacing of (111) and (220) peaks, is reported below:

Table 5-36: Average Lattice constant and Ru alloyed calculated using peaks (111) and (220) of XRD for catalysts made under argon at 350 °C at different operating times.

Operating Time	Average lattice constant	Average Ru atomic fraction in Pt-Ru (%)
30 minutes	3.922	18.7
1 hour	3.923	17.6
2 hours	3.925	16.5
4 hours	3.914	25.3
6 hours	3.924	16.6
8 hours	3.910	27.9

The ruthenium atomic fraction in the platinum structure does not have a significant trend versus the operating time. This shows the operating time does not particularly influence the alloying of the catalyst as significantly as operating temperature. Figure 5-24 shows the crystallite structure remains unchanged throughout varying operating times, suggesting the ruthenium content is constant over the different operating times.

5.8.4. Cyclic Voltammetry

Cyclic voltammograms were used to characterize the Pt-Ru catalysts by analysing the changes in shape and pseudo-capacitance between catalysts. The cyclic voltammograms for the catalysts prepared with an operating time of 30 minutes and 8 hours are shown in Figures 5-25 and 5-26 respectively, where the first and 50^{th} cycles are shown. The cyclic voltammograms for the catalysts produced under different operating times are shown in the Appendix. Figure 5-27 compares the first cycles of the catalysts produced with different operating times, corrected for metal loading and the maximum height.

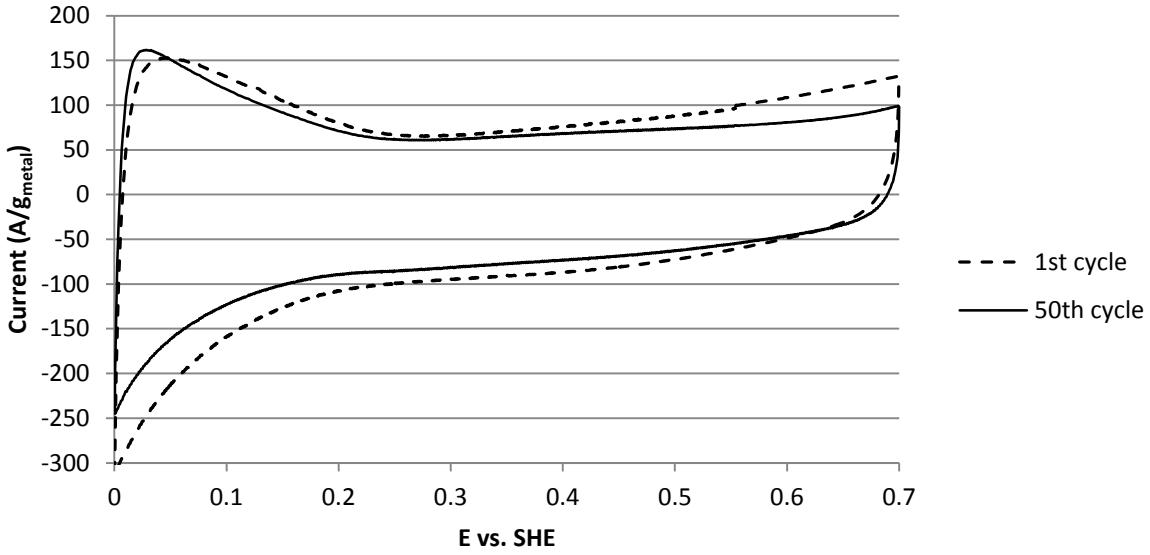

Figure 5-25: First and 50th cyclic voltammetry curves for the catalyst produced under an argon atmosphere at 350 °C for 30 minutes.

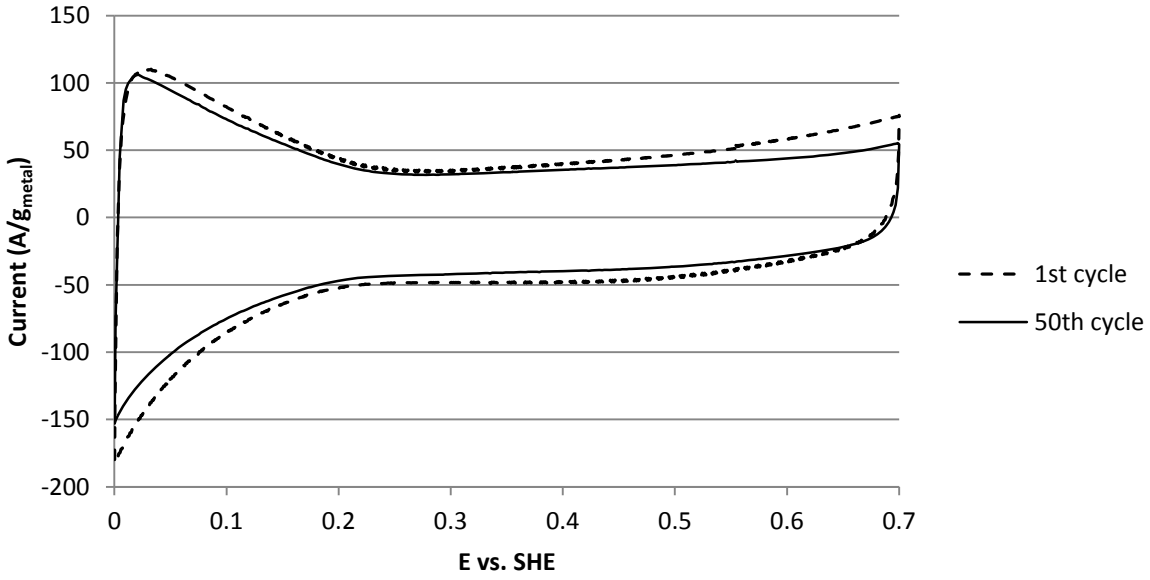

Figure 5-26: First and 50th cyclic voltammetry curves for the catalyst produced under an argon atmosphere at 350 °C for 8 hours.

Figures 5-25 and 5-26 and show large pseudo-capacitance along the potential range and featureless curves, this indicates a high ruthenium oxide content, as shown in literature (Sato *et al.*, 2000) (Zheng *et al*., 1995). The difference between the 1st and 50th cycle, for both catalysts, can be attributed to ruthenium oxide species reduction to non-reducible ruthenium oxides (Maillard *et al.,* 2002) thus a decrease in pseudo-capacitance is seen.

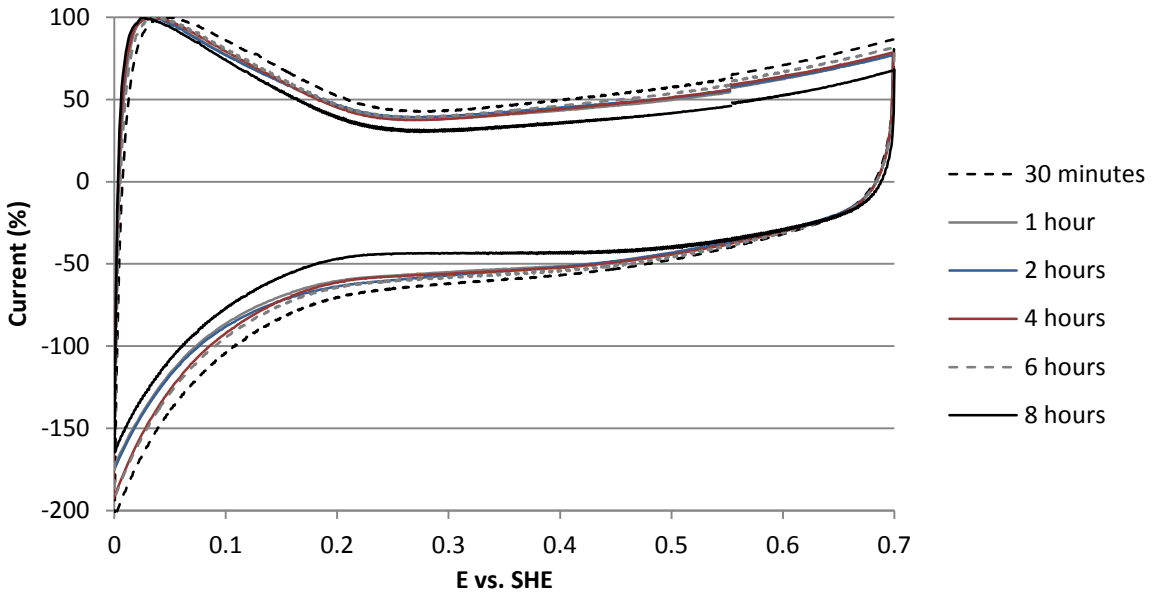

Figure 5-27: First cyclic voltammograms for the catalysts produced under an argon atmosphere at 350 °C for different operating times.

The cyclic voltammetry curves shown in Figure 5-27 are mirror like and featureless with large pseudo-capacitance, indicating a high ruthenium oxide content. The catalyst prepared with a 30 minute operating time has a larger pseudo-capacitance than the catalyst produced with a 8 hour operating time, indicating a larger ruthenium oxide content in the catalyst produced with an operating time of 30 minutes. This shows the operating time effect on the ruthenium oxide content on the surface, as longer operating times decreases the ruthenium oxide content. However, the intermediate operating times do not show a significant trend and the operating time effect on ruthenium oxide content does not affect the ruthenium oxide content to the same degree as operating temperature.

5.8.5. CO Stripping Voltammetry

ECSA of the catalysts prepared at different operating times were determined using CO stripping voltammetry and the results are shown in Table 5-37.

Table 5-37: ECSA and expected ECSA of catalysts made under argon at 350 °C at different operating times.

Operating time	Expected ECSA (m^2/g) for Pt-Ru	Expected ECSA (m^2/g) for Pt-RuO_2	ECSA (m^2/g)
30 minutes	173	225	270
1 hour	177	231	222

2 hours	145	189	225
4 hours	138	180	175
6 hours	167	218	195
8 hours	154	201	146

Table 5-37 clearly shows the ECSA trend, as the reactor operating time increases the ECSA of the catalyst decreases. This trend is not due to particle size, as particle size and surface area don't differ much, but rather a change from Pt-RuO_2 to Pt-Ru as seen from the expected ECSA. At short operating times the actual ECSA closely resembles that of the expected ECSA for Pt-RuO_2 whilst the longer operating times actual ECSA more closely resembles the expected ECSA for Pt-Ru. This shows that increased time in the reactor at a high temperature reduces the ruthenium oxides on the surface.

The CO stripping onset potential, current at 0.5 V vs. SHE normalized for total metal mass and finally intrinsic current at 0.5 V vs. SHE is illustrated below:

Table 5-38: Electrochemical results for CO oxidation on catalysts made under argon at 350 °C at different operating times.

Operating time	Onset potential (V vs. SHE)	Current at 0.5 V vs. SHE (A/g_{metal})	Current at 0.5 V vs. SHE (mA/cm^2)
30 minutes	0.386	44.8	2.1
1 hour	0.406	47.1	2.8
2 hours	0.398	52.6	3.2
4 hours	0.411	33.6	2.3
6 hours	0.404	46.7	3.0
8 hours	0.420	57.1	4.8

Table 5-38 shows the CO oxidation onset potential increases and activity towards CO oxidation decreases as the reactor operating time increases. This decrease in activity is most probably due to a decrease in ruthenium oxide content, since ruthenium oxides assist in CO oxidation (Over & Muhler, 2003).

5.8.6. Methanol Oxidation

Electrochemical characterisation tests for methanol oxidation activity were performed and the onset potential, current at 0.5 V vs. SHE normalized for total metal mass and finally intrinsic current at 0.5

V vs. SHE is reported. Figure 5-28 is the methanol oxidation voltammogram isolating the onset potential range.

Table 5-39: Electrochemical results for methanol oxidation on catalysts made under argon at 350 °C at different operating times.

Operating time	Onset potential (V vs. SHE)	Current at 0.5 V vs. SHE (A/g_{metal})	Current at 0.5 V vs. SHE (mA/cm^2)
30 minutes	0.267	121	5.6
1 hour	0.280	106	6.2
2 hours	0.282	98.5	5.9
4 hours	0.278	95.0	6.6
6 hours	0.281	91.5	5.8
8 hours	0.292	81.6	6.8

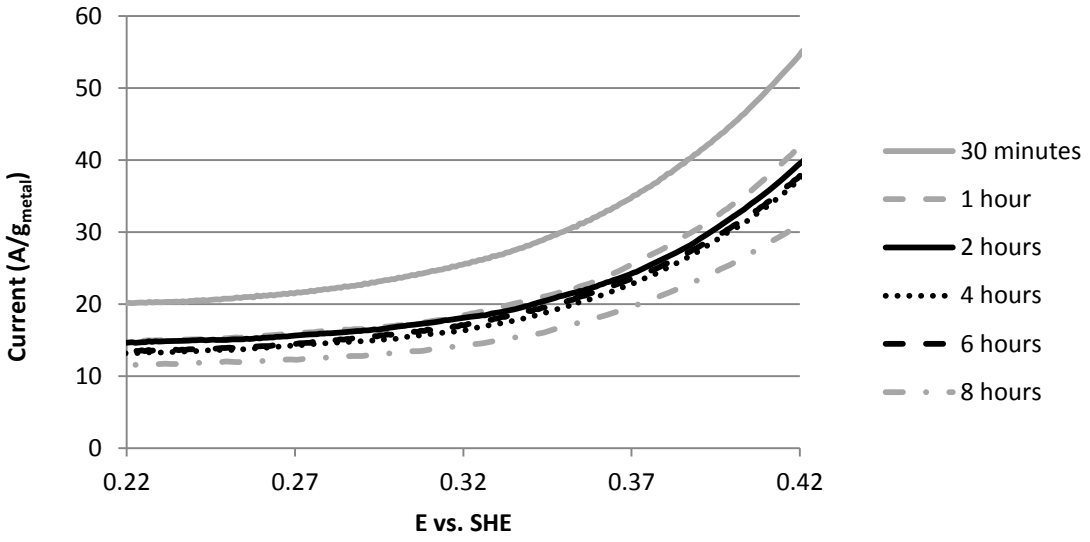

Figure 5-28: Electrochemical graphs for methanol oxidation onset potential on catalysts prepared under argon at 350 °C at different operating times.

Correspondingly to the CO tolerance trend found in section 5.8.5., methanol oxidation onset potential increases as operating time increases and the methanol oxidation onset potential and can be explained by a decrease in ruthenium oxide content as operating time increases. Bock *et al*. (2005) found that ruthenium oxides are vital in increasing the activity for methanol oxidation. The most active catalyst in the range tested for methanol oxidation is found to be the catalyst prepared at 350 °C for 30 minutes. Comparing the current at 0.5 V vs. SHE (A/g_{metal}) to the current at 0.5 V vs.

SHE ($\mu A/m^2$) it can be seen that there is an increase in activity at short operating times, further confirming the best catalyst within the range tested for CO tolerance is the catalyst with an operating time of 30 minutes.

5.8.7. Chronoamperometry

Chronoamperometry experiments were carried out on the catalysts prepared with varying operating times. The current after 30 minutes normalised for total metal mass and the percentage drop from 30 seconds to 30 minutes is reported in Table 5-40.

Table 5-40: Electrochemical results for chronoamperometry on catalysts made under argon at 350 °C at different operating times.

Operating time	Current at 30 minutes (A/g_{metal})	Drop in current (%)
30 minutes	66.9	37.9
1 hour	56.9	38.1
2 hours	53.8	35.2
4 hours	37.8	45.4
6 hours	46.2	39.1
8 hours	42.5	40.3

The final chronoamperometry current decreases as the reactor time increases. These results of the chronoamperometry are in line with methanol oxidation results, however the percentage drop in current does not seem to be influenced by operating temperature. These results show there could be a link between physical characterisations such as degree of alloying or particle size in the stability of the catalyst.

5.8.8. Summary of Time Influence

The reactor operating time plays an important role in catalyst activity since the ECSA is significantly influenced by this factor. As the time the precursors and catalyst spend in the reactor is increased the ECSA of the catalysts decreases, therefore decreasing the current at 0.5 V vs. SHE for CO and methanol oxidation.

The reactor operating time did not significantly affect the degree of alloying in the catalysts or the particle size of the catalysts. However, the electrochemical activities of the catalysts were affected by operating time and these could be explained by the decrease in ruthenium oxide content as operating time is increased. Short operating times had increased activity for methanol and CO oxidation which lead to the shortest time of 30 minutes as the best performing catalyst in this range.

5.9. Pt:Ru Ratio Influence

The findings in previous sections where carried through the project, therefore the Pt-Ru catalysts produced hereinafter are produced under argon at a temperature of 350 °C for a period of 30 minutes. Pt-Ru/C catalysts produced in this section have a 50 wt% total metal loading, with Pt:Ru molar ratio's ranging from 40:60 – 90:10. Physical and electrochemical characterisations of these catalysts are detailed below, followed by a summary in section 5.9.8.

5.9.1. TEM and EDX

TEM images for the catalysts prepared at a temperature of 350 °C for differing Pt:Ru ratios is illustrated in Figure 5-29. The TEM images show well dispersed particles across all catalyst Pt- Ru ratios, however as the platinum percentage in the metal increases a visible increase in catalyst particle size of observed. The average particle sizes measured from TEM are shown in Table 5-41, followed by a particle size distribution graph in Figure 5-30. The particle size distribution, in accordance with particle size shows a shift to larger particle sizes as platinum percentage in the metal increases.

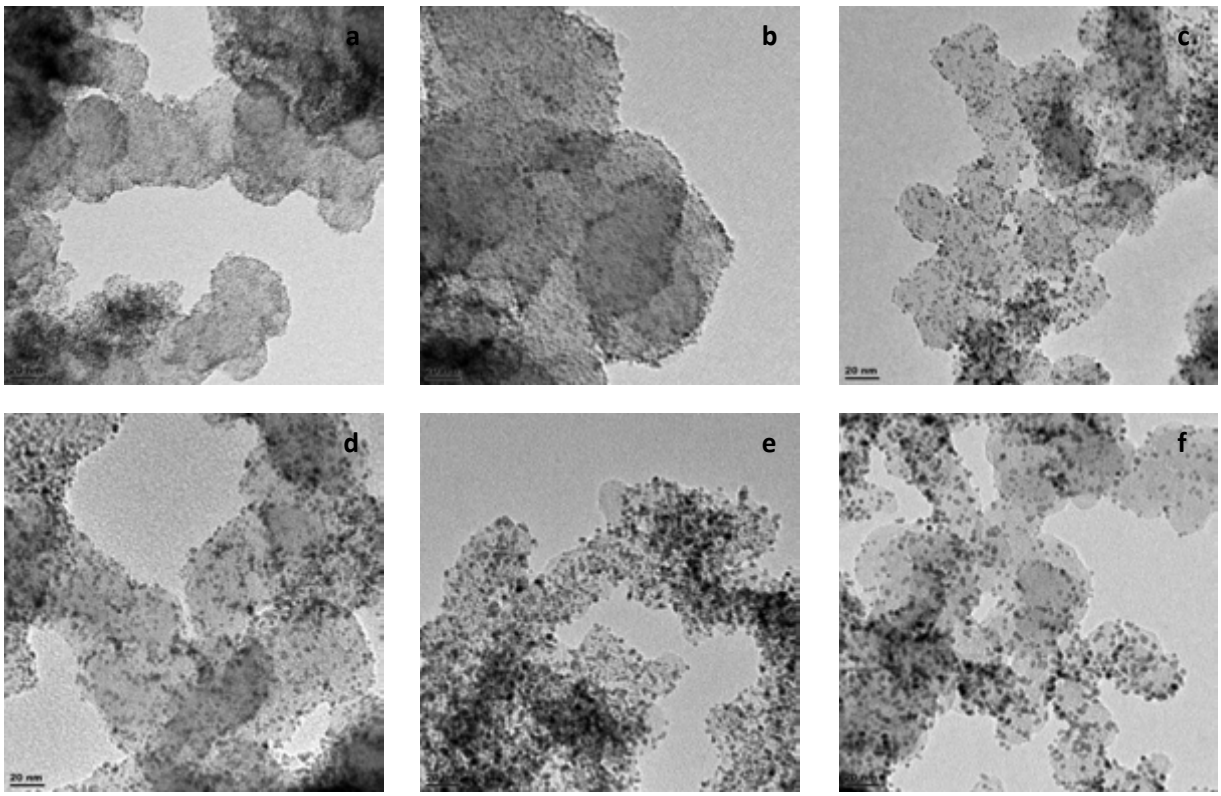

Figure 5-29: TEM images at 20 nm resolution of Pt-Ru/C catalysts produced at 350 °C for 30 minutes under argon with Pt:Ru ratios of a) 40:60 b) 50:50 c) 60:40 d) 75:25 e) 80:20 f) 90:10.

Table 5-41: Average particle size from TEM imaging of catalysts made under argon at 350 °C for 30 minutes with different Pt:Ru ratios.

Pt in total metal (%)	Average particle size (nm)
40	1.78
50	2.60
60	2.64
75	2.70
80	2.65
90	2.80

The increase in particle size is predominantly due the sizes of the metals included. Platinum is a larger atom (1.39 Å) and therefore has a larger particle size in a cluster, however ruthenium is a much smaller atom (1.34 Å) and when included into the platinum cluster the particle size is decreased.

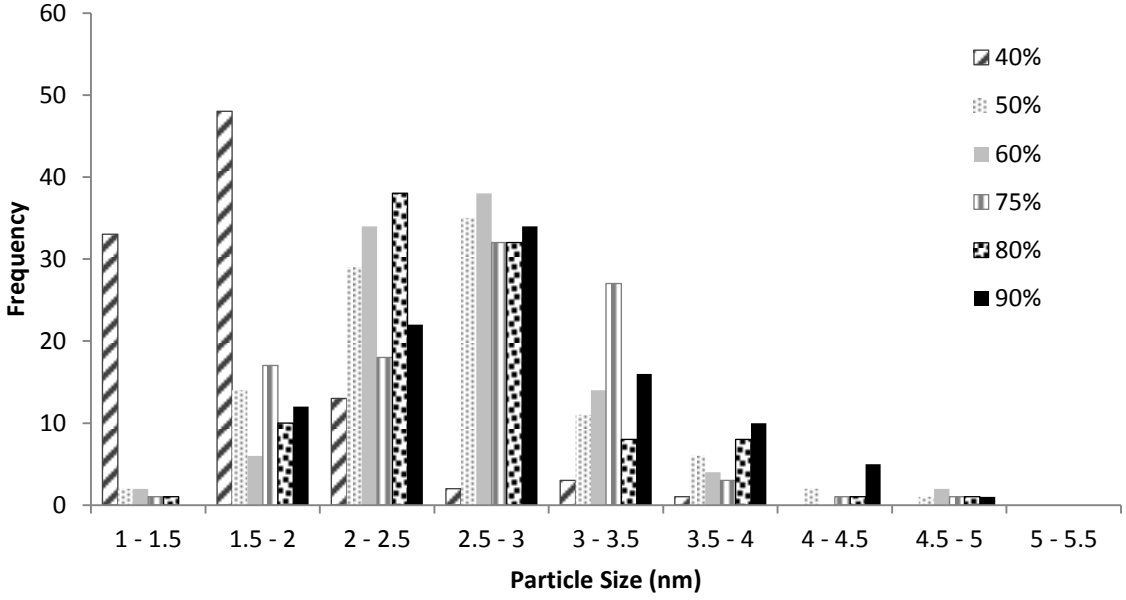

Figure 5-30: Particle size distribution graph of particles measured from TEM imaging of catalysts made under argon at 350 °C for 30 minutes with differing Pt % in total metal loading.

The particle size distribution graph is a good representation of the particle size range for each catalyst. It is noticeable that the particles with high ruthenium content have particle sizes in the

lower range, while catalysts with a low ruthenium content have catalyst particle sizes in the higher range. This is as expected as platinum atoms are larger.

EDX analysis of Pt and Ru in total metal of different ratio prepared catalysts is compared to expected results in the table below. The EDX values calculated are within an acceptable range of the expected metal percentages.

Table 5-42: Expected Pt and Ru mol% in total metal compared to EDX analysis results of catalysts made under argon at 350 °C for 30 minutes with different Pt:Ru ratios.

Pt in total metal (%)	Expected (mol%)		EDX result (mol%)	
	Pt	Ru	Pt	Ru
40	40	60	42.4	57.6
50	50	50	52.0	48.0
60	60	40	60.3	39.7
75	75	25	76.8	23.2
80	80	20	81.6	18.4
90	90	10	90.2	9.85

5.9.2. TGA

The TGA characterisation was used to determine the total metal loading of each catalyst. The table below details the expected versus TGA results on total metal loading. These results are in a sensible range to the expected metal loading.

Table 5-43: Expected and TGA total metal loading of catalysts made under argon at 350 °C for 30 minutes with differing Pt:Ru ratios.

Pt in total metal (%)	Expected metal loading (wt%)	TGA metal loading (wt%)
40	50.0	51.3
50	50.0	52.7
60	50.0	51.8
75	50.0	53.1
80	50.0	53.7
90	50.0	49.6

5.9.3. XRD

XRD analysis was carried out on the different ratio prepared catalysts and the diffraction pattern is illustrated in Figure 5-31:

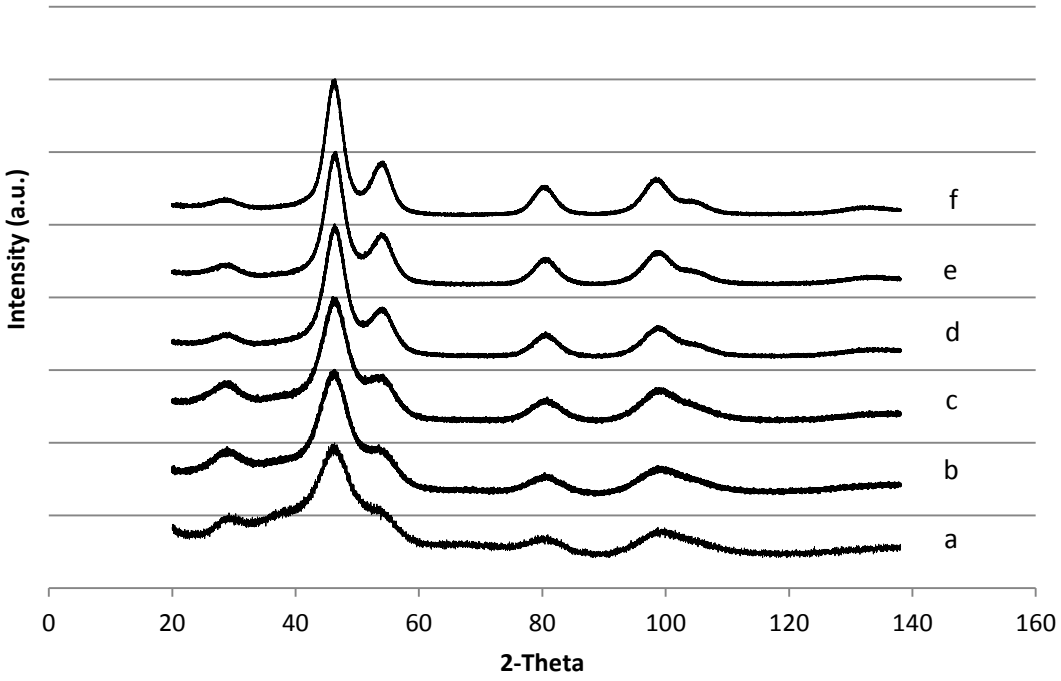

Figure 5-31: XRD graphs of Pt-Ru/C catalysts produced at 350 °C for 30 minutes under argon with Pt:Ru ratios of a) 40:60 b) 50:50 c) 60:40 d) 75:25 e) 80:20 f) 90:10.

Diffraction peaks (111) and (220) were used to determine the crystallite size of each prepared catalyst, the results are shown in Table 5-44.

Table 5-44: Average crystallite size calculated using peaks (111) and (220) of XRD for catalysts made under argon at 350 °C for 30 minutes with differing Pt:Ru ratios.

Pt in total metal (%)	Average crystallite size (nm)
40	2.09
50	2.24
60	2.42
75	2.80
80	2.98
90	3.15

The average catalyst crystallite sizes calculated from XRD peaks are in accordance with TEM measured particles and follow the same trend as found in TEM images.

As expected, the catalyst with the higher platinum content shows typical platinum diffraction pattern. As ruthenium content increases the pattern changes to have less defined peaks and a more amorphous structure. The Lattice constant, calculated using the d-spacing of (111) and (220) peaks, is reported in Table 5-45.

Table 5-45: Average lattice constant and Ru atomic fraction alloyed calculated using peaks (111) and (220) of XRD for catalysts made under argon at 350 °C for 30 minutes with differing Pt:Ru ratios.

Pt in total metal (%)	Average lattice constant	Average Ru atomic fraction in Pt-Ru (%)
40	3.919	21.4
50	3.922	18.7
60	3.924	17.1
75	3.926	15.6
80	3.927	15.1
90	3.930	12.5

The ruthenium atomic fraction in Pt-Ru decreases as the platinum percentage in the total metal increases. In accordance, the average lattice constant decreases as the ruthenium percentage in the metal increases. This is due to the small ruthenium particle size effect on decreasing the total particle size when included into the structure.

5.9.4. Cyclic Voltammetry

Cyclic voltammograms were used to characterize the Pt-Ru catalysts by analysing the changes in shape and pseudo-capacitance between catalysts. The cyclic voltammograms for the catalysts prepared with Pt:Ru ratios of 40:60 and 90:10 are shown in Figures 5-32- and 5-33 respectively, where the first and 50^{th} cycles are shown. The cyclic voltammograms for the intermediate catalysts produced are shown in the Appendix. Figure 5-34 compares the first cycles of the catalysts produced with different Pt:Ru ratios, corrected for metal loading and the maximum height.

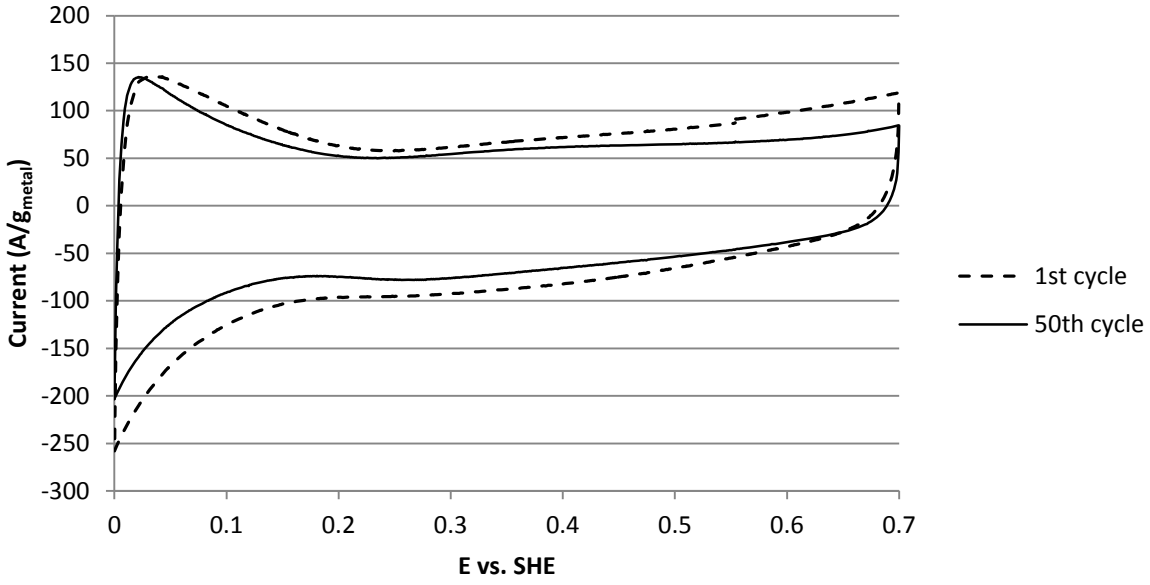

Figure 5-32: First and 50th cyclic voltammetry curves for the catalyst with a Pt:Ru ratio of 40:60 produced under an argon atmosphere at 350 °C for 30minutes.

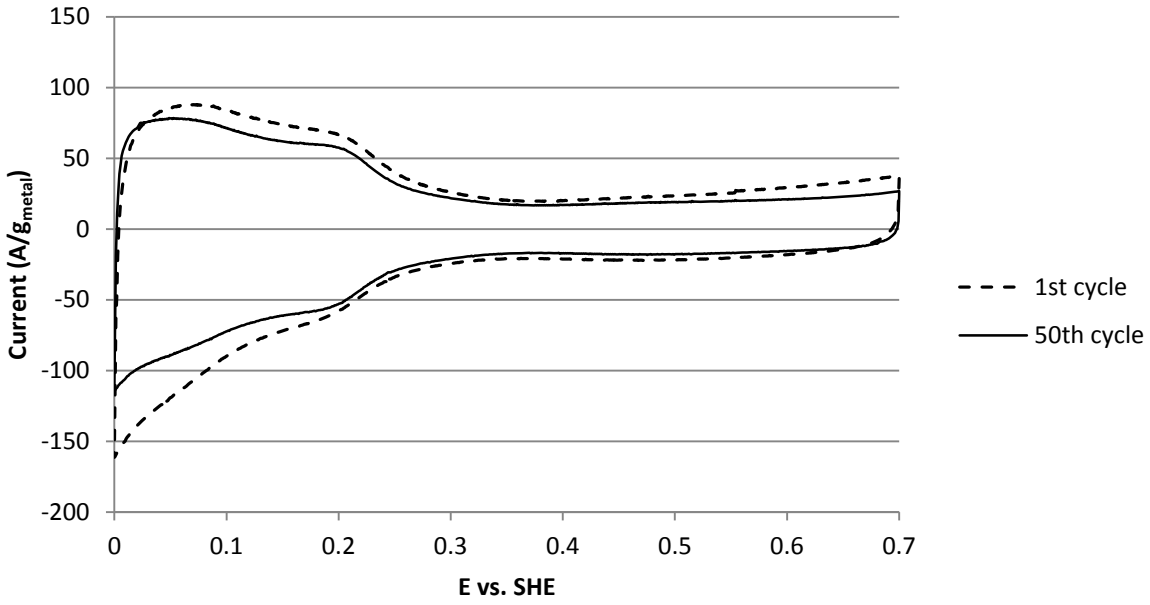

Figure 5-33: First and 50th cyclic voltammetry curves for the catalyst with a Pt:Ru ratio of 90:10 produced under an argon atmosphere at 350 °C for 30minutes.

Figures 5-32 and 5-33 show the difference in catalyst composition between the catalysts with a Pt:Ru ratio of 40:60 and 90:10 The cyclic voltammogram of the 40:60 ratio catalyst has a more featureless cyclic voltammogram and a large pseudo-capacitance, indicating a high ruthenium oxide content

(Sato *et al.*, 2000). The 90:10 ratio catalyst has defining platinum features and a small pseudo-capacitance, indicating a lower ruthenium oxide content.

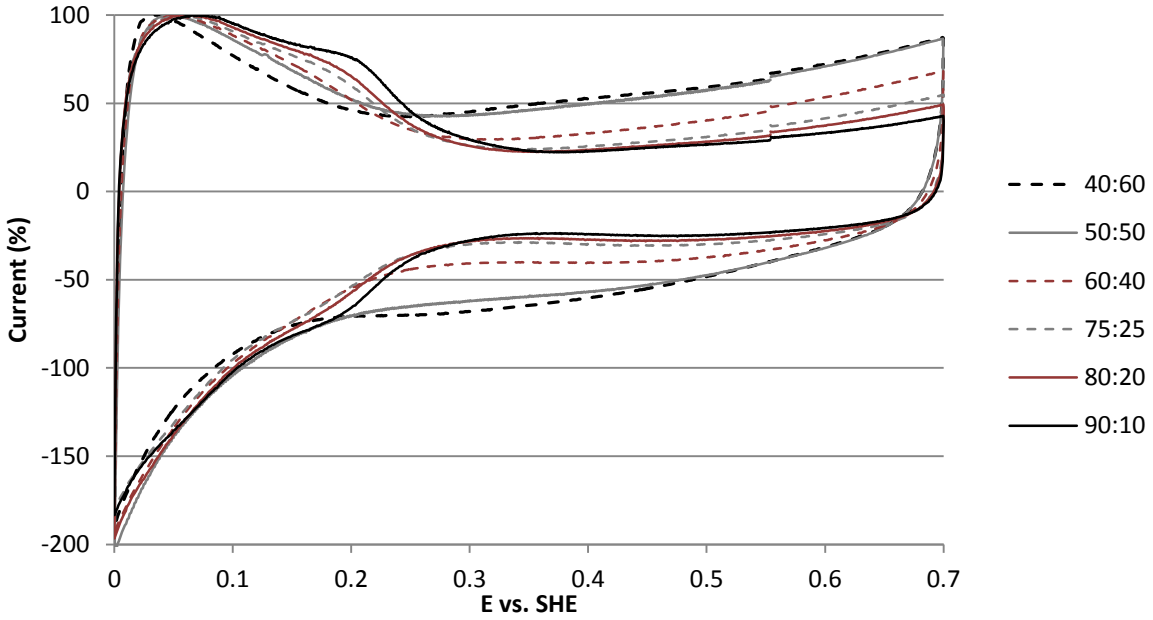

Figure 5-34: First cyclic voltammograms for the catalysts with different Pt:Ru ratios produced under an argon atmosphere at 350 °C for 30 minutes.

Figure 5-34 allows for a better comparison between the different Pt:Ru ratio catalysts, it is once again seen that the 40:60 ratio catalyst demonstrates a more featureless curve with a large pseudo-capacitance while the 90:10 ratio catalyst has a smaller pseudo-capacitance. This is an indication of the trend, as the platinum content increases the ruthenium oxide content in the catalyst decreases.

5.9.5. CO Stripping Voltammetry

ECSA of the catalysts prepared with different Pt:Ru ratios were determined using CO stripping voltammetry and the results are shown in Table 5-46.

Table 5-46: ECSA and expected ECSA of catalysts made under argon at 350 °C for 30 minutes with differing Pt:Ru ratios.

Pt in total metal (%)	Expected ECSA (m^2/g) for Pt-Ru	Expected ECSA (m^2/g) for Pt-RuO_2	ECSA (m^2/g)
40	194	269	267
50	173	225	270
60	151	186	158

75	120	136	88.7
80	109	120	69.1
90	95.9	101	59.4

The expected ECSA for Pt-RuO_2 deviation from actual ECSA increases since the assumption of ruthenium existing as ruthenium oxide no longer holds true. However, the actual ECSA also remains to be much lower than expected for Pt-Ru. This result cannot be explained with the current physical characterisation and could be attributed to the morphology of the platinum structure.

The ECSA of the prepared catalysts decreases as the platinum in the total metal increases, predominantly due to the increase in catalyst particle size as platinum in total metal increases.

The CO stripping onset potential, current at 0.5 V vs. SHE normalized for total metal mass and finally intrinsic current at 0.5 V vs. SHE is illustrated in the Table 5-47.

Table 5-47: Electrochemical results for CO oxidation on catalysts made under argon at 350 °C for 30 minutes with differing Pt:Ru ratios.

Pt in total metal (%)	Onset Potential (V vs. SHE)	Current at 0.5 V vs. SHE (A/g_{metal})	Current at 0.5 V vs. SHE (mA/cm^2)
40	0.392	44.0	2.5
50	0.386	44.8	2.1
60	0.449	16.0	1.1
75	0.470	5.55	0.5
80	0.460	6.67	0.8
90	0.476	4.16	0.5

Table 5-47 shows the ideal Pt:Ru ratio for CO oxidation to be 50:50 as this has the lowest CO oxidation onset potential as well as the highest current at 0.5 V vs. SHE (A/g_{metal}). This is in accordance with previous studies as shown in section 2.3.3 as the ratio plays a role in the bifunctional mechanism and this is the optimum ratio for the rate determining step (Gasteiger *et al.*, 1994a):

$$Ru - OH + Pt - CO \rightarrow Pt + Ru + CO_2 + H^+ + e^-$$

5.9.6. Methanol Oxidation

Electrochemical characterisation tests for methanol oxidation activity were performed and the onset potential, current at 0.5 V vs. SHE normalized for total metal mass and finally intrinsic current at 0.5 V vs. SHE is reported. These results are shown in Table 5-48 and Figure 5-35 shows the electrochemical graphs with emphasis on the onset potential.

Table 5-48: Electrochemical results for methanol oxidation on catalysts made under argon at 350 °C for 30 minutes with differing Pt:Ru ratios.

Pt in total metal (%)	Onset Potential (V vs. SHE)	Current at 0.5 V vs. SHE (A/g_{metal})	Current at 0.5 V vs. SHE (mA/cm^2)
40	0.268	77.7	4.5
50	0.267	121	5.6
60	0.269	123	8.5
75	0.268	113	10.8
80	0.297	49.8	5.8
90	0.347	38.1	4.6

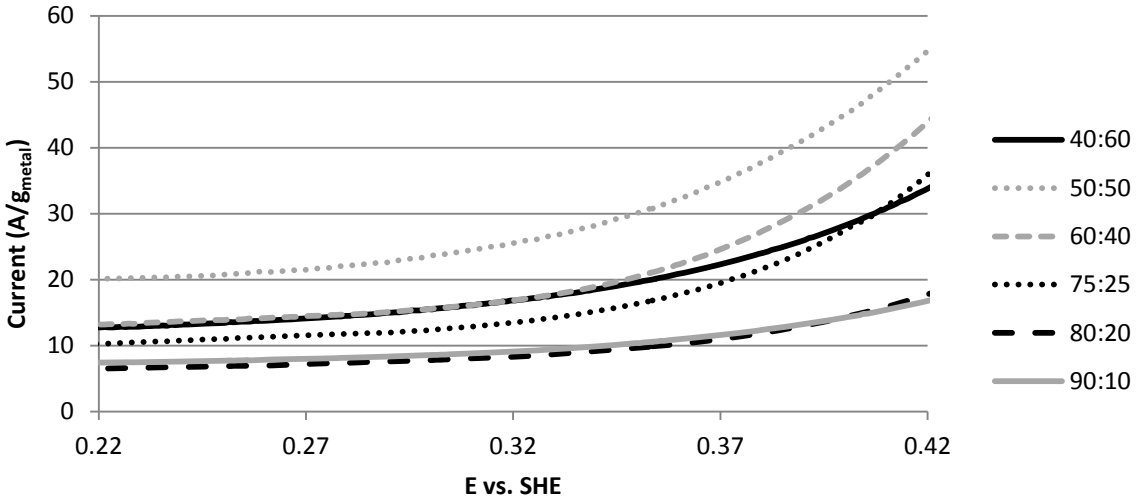

Figure 5-35: Electrochemical graphs for methanol oxidation onset potential on catalysts prepared under argon at 350 °C for 30 minutes with differing Pt:Ru ratios.

An interesting result is the methanol oxidation onset potential between Pt:Ru ratios 40:60, 50:50, 60:40 and 75:25 as these are nearly identical. The second indication of activity for methanol oxidation is the current at 0.5 V vs. SHE (A/g_{metal}), since this is of importance in an operating fuel cell. Thus, the catalysts with a Pt:Ru ratios of 60:40 and 50:50 are seen to be the most active catalysts in

the given range for methanol oxidation. As shown in section 2.3.2.2, the literature on optimum Pt:Ru ratio varies for different researchers since catalyst preparation (Zhang, 2008) and electrochemical testing conditions play a significant role in optimum ratio (Lizcano-Valbuena *et al.,* 2002). It is however, expected that catalysts with a high ruthenium oxide content would perform better for methanol oxidation than catalysts with less ruthenium oxide as shown in literature (Lasch *et al.,* 2003). The degree of alloying itself can play a significant role, although contested between researchers.

5.9.7. Chronoamperometry

Chronoamperometry experiments were carried out on the catalysts prepared with varying Pt:Ru ratio. The current after 30 minutes normalised for total metal mass and the percentage drop from 30 seconds to 30 minutes is reported in Table 5-49. These experiments share insight into methanol oxidation activity.

Table 5-49: Electrochemical results for methanol oxidation chronoamperometry on catalysts made under argon at 350 °C for 30 minutes with differing Pt:Ru ratios.

Pt in total metal (%)	Current at 30 minutes (A/g_{metal})	Drop in current (%)
40	35.2	43.4
50	66.9	37.9
60	70.4	42.7
75	59.8	49.1
80	21.9	57.9
90	13.7	62.5

Table 5-49 clearly shows the highest current for methanol oxidation under chronoamperometry experimental settings is found to be catalysts with ratios of 50:50 and 60:40. The stability of the catalysts tends to decrease as the platinum percentage increases, as seen in literature this is due to the reduced alloying of Ru within the platinum structure. Liu & Zhang (2009) found alloyed ruthenium to be more stable in the presence of methanol than unalloyed ruthenium. The chronoamperometry results shown above confirm the findings in section 5.9.6., showing a Pt:Ru ratio of either 50:50 or 60:40 to be the optimum ratio in this range for methanol oxidation. Chronoamperometry adds information on stability which allows the best performing catalyst in this range to be narrowed down. The Pt:Ru ratio of 50:50 is the most stable catalyst and therefore it can be concluded that the 50:50 ratio is the best catalyst in this experimental range.

5.9.8. Summary of Metal Ratio Influence

The Pt:Ru metal ratio has an influence on catalyst particle size due to the incorporation of a smaller ruthenium atom into the larger platinum structure. Thus, the catalyst particle size decreases as the ruthenium percentage increases. This decrease in catalyst particle size as ruthenium percentage increases translates into an increase in ECSA as particle size decreases due to the increase in surface to volume ratio and ruthenium oxide species.

Analysis of the XRD curves shows that the degree of alloying is proportional to the catalyst Pt:Ru ratio. However, the gradient is gradual and the ruthenium atomic fraction ranges from 12.5 - 21.4 across the platinum percentages in the metal. The cyclic voltammograms and expected ECSA suggests a high ruthenium oxide content in the lower platinum ratios and less ruthenium oxide in the higher platinum ratios by a more crystalline pattern.

A Pt:Ru ratio of 50:50 was the most active catalyst for CO oxidation, as seen from the CO stripping voltammetry data and this ratio is confirmed by researchers such as Gasteiger *et al.* (1995), Giorgi *et al.* (2001) and Lin *et al.* (1999). The CO oxidation data demonstrates that CO tolerance of a catalyst is highly sensitive to Pt:Ru ratio. From the methanol oxidation data it can be seen that onset potential for methanol oxidation is not highly dependent on Pt:Ru ratio, as values for the ratios 40:60, 50:50, 60:40 and 75:25 are nearly identical despite slightly changing degree of alloying. Further analysis of the catalysts with varying Pt:Ru ratios found the 50:50 catalyst to be more stable in the presence of methanol than the other ratios and thus this catalyst is determined to be the best performing catalyst in the given parameters. This result is also in accordance with some literature (Aricò *et al*. 2009), although this is a contested ratio as seen in section 2.3.2.2.

5.10. Prepared Catalyst and Commercial Catalysts

This section serves to compare the best performing prepared catalyst with the commercial catalysts described in section 5.1. The tables below detail the results on two commercial Pt-Ru/C catalysts and the best performing prepared catalyst using CO stripping voltammetry, methanol oxidation and chronoamperometry experiments. Commercial catalyst 1 is a 60 wt% Pt-Ru/C (Pt:Ru, 1:1) catalyst and commercial catalyst 2 is a 54 wt% Pt-Ru/C (Pt:Ru, 1:1.5) catalyst. The prepared catalyst with the best performance is the 50 wt% Pt-Ru/C catalyst produced under argon at 350 °C for an operating time of 30 minutes and a Pt:Ru ratio of 50:50.

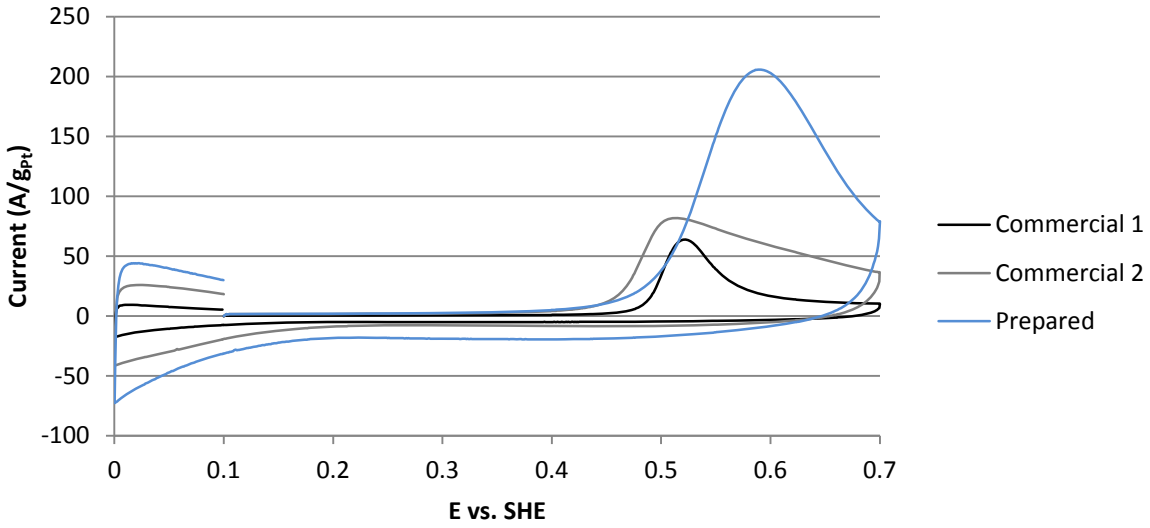

Figure 5-36: First sweep of CO stripping voltammograms of commercial catalysts and prepared catalyst.

Table 5-50: ECSA of commercial catalysts and prepared catalyst measured using CO stripping voltammetry.

Commercial catalyst	wt% Metal	ECSA (m^2/g)
Commercial 1	60	40.3
Commercial 2	54	105
Prepared	52.7	270

The ECSA of the prepared catalyst is significantly larger than that of the commercial catalysts, this is predominantly due to the existence of a high content of ruthenium oxide on the surface of the prepared catalyst.

Table 5-51: Electrochemical results for CO oxidation on commercial and prepared catalysts.

Commercial catalyst	Onset Potential (V vs. SHE)	Current at 0.5 V vs. SHE (A/g_{metal})	Current at 0.5 V vs. SHE (mA/cm^2)
Commercial 1	0.454	35.4	8.6
Commercial 2	0.398	77.8	8.6
Prepared	0.386	44.8	2.1

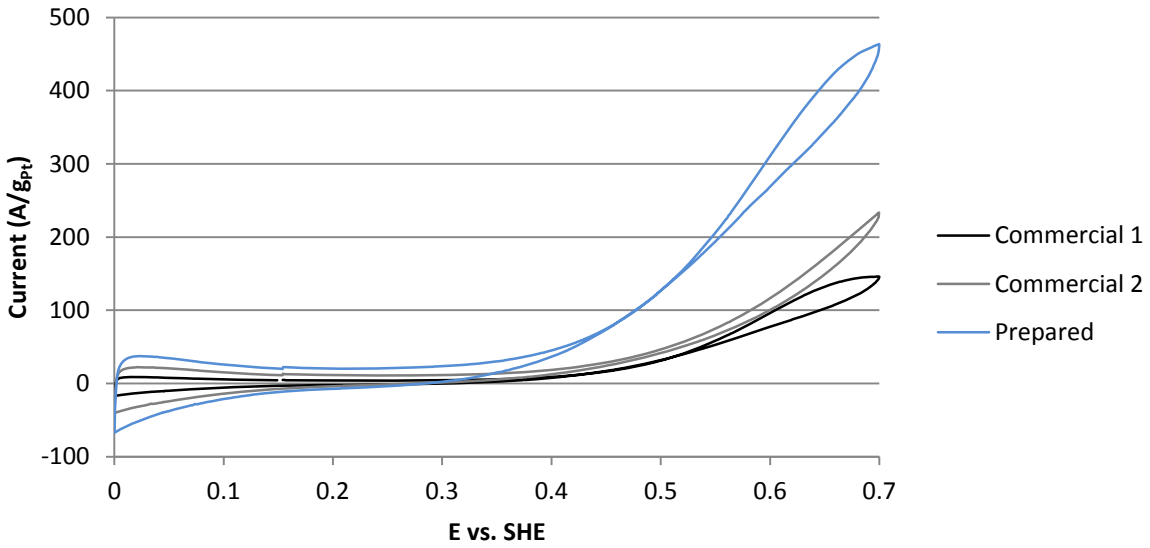

Figure 5-37: Methanol oxidation cyclic voltammograms of commercial catalysts and prepared catalysts.

In accordance with literature described in previous sections, the CO tolerance of a catalyst with a high ruthenium oxide content is higher than that of a catalyst with less ruthenium oxide. This counts for the lower onset potential for the prepared catalyst vs. the commercial catalysts. The currents at 0.5 V vs. SHE for the commercial catalysts are higher than that of the prepared catalyst because the peak height is smaller and thus shifted to the left, while the prepared catalyst peak height is large and stretched across a wider plane.

Table 5-52: Electrochemical results for methanol oxidation on commercial catalysts.

Commercial catalyst	Onset Potential (V vs. SHE)	Current at 0.5 V vs. SHE (A/g_{metal})	Current at 0.5 V vs. SHE (mA/cm^2)
Commercial 1	0.328	31.2	7.6
Commercial 2	0.328	46.8	5.2
Prepared	0.267	121	5.6

Following from CO tolerance data, methanol oxidation onset potential for the prepared catalyst is lower than the commercial catalysts. This is also due to the higher ruthenium oxide content, small particles and optimally alloyed Pt-Ru particles.

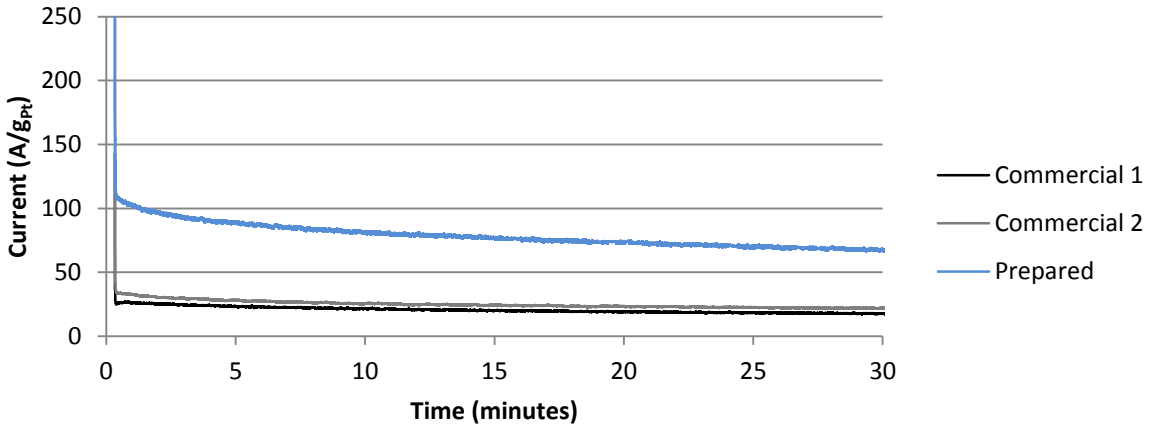

Figure 5-38: Chronoamperometry curves for commercial catalysts and prepared catalysts.

Table 5-53: Chronoamperometry results on commercial catalysts.

Commercial catalyst	Current at 30 minutes (A/g_{metal})	Drop in current (%)
Commercial 1	17.5	32.6
Commercial 2	21.9	34.9
Prepared	66.9	37.9

The commercial catalysts show a slightly more stable Pt-Ru/C catalyst, Liu & Zhang (2009) found catalysts with ruthenium alloyed are more stable than catalysts with unalloyed ruthenium. Therefore, this increased stability is most probably due to the alloyed nature of these catalysts vs. the relatively unalloyed nature of the prepared catalyst, however the difference in stability is not significant.

This section has shown the best catalyst prepared in this work is more active for CO and methanol oxidation than commercial catalysts. In addition, the catalyst particle sizes produced are small, have an ideal morphology for oxidation and produce a high active surface area when compared to the commercial catalysts.

6. CONCLUSIONS

This study involved the systematic investigation of operating atmosphere, temperature, time and Pt:Ru ratio in catalyst preparation by chemical deposition. The results have proven to be in line with findings in the literature and confirmed reproducibility of the preparation method and testing method.

An interesting finding was the difference in activity between deposition from precursors in vapour and liquid phase. This could be explained by a higher ruthenium oxide content in an argon atmosphere versus vacuum which leads to in increased activity for CO and methanol oxidation, as seen in literature. This change in morphology, most probably including more surface oxides, improved the activity for CO and methanol oxidation, and the stability of the catalyst.

The operating temperature of the furnace had a significant effect of the prepared catalysts. High temperatures caused sintering of the catalyst particles and therefore a decrease in ECSA. In addition, at high operating temperatures the platinum and ruthenium particles were more alloyed than at low operating temperatures and less ruthenium oxides existed. The poor CO and methanol oxidation activity at high operating temperatures was not solely attributed to low ECSA, but was also due to increased alloying or decreased ruthenium oxides on the surface. This finding is in accordance with literature stating unalloyed Pt-Ru is more active for methanol oxidation than alloyed Pt-Ru and ruthenium oxides are essential for high methanol oxidation activity. However, the optimum reactor temperature in the range investigated in the study, was not the lowest temperature of 300 °C but is rather 350 °C. The catalyst produced at 300 °C has an extremely low degree of alloying but does not have the highest activity for CO or methanol oxidation. It is thus believed that an optimum degree of alloying exists, the reason for this is currently unclear. Furthermore, chronoamperometry results show an increased instability of catalysts produced at high temperatures which is an additional indication that high temperatures have a negative influence on the morphology of the catalysts.

The operating time of the furnace did not seem to have a significant impact on the particle size or degree of alloying, however the ECSA of the prepared catalysts decreased with increasing time in the reactor. This indicated that time spent at a high temperature negatively affected the prepared catalyst's morphology by reducing the active surface area, activity for CO oxidation and methanol oxidation by reducing the ruthenium oxide content. Therefore, the best operating time for catalyst preparation was found to be 30 minutes at operating temperature of 350 °C. It is interesting to note the stability of the catalysts prepared at different operating times had similar catalyst stabilities, this could be due to the similar degrees of alloying as it was constant.

The Pt:Ru ratio plays a vital role in the bifunctional mechanism and, as seen in literature, is specific to each individual method. As the platinum concentration decreased, the particle size decreased and ECSA increased. The particle size decrease is due to the incorporation of smaller ruthenium atoms into the platinum structure, this change can be seen in the increase lattice spacing of the catalysts. The influence of the Pt:Ru ratio yielded interesting results for activity as the optimum ratio for CO oxidation was not found to be the optimum ratio for methanol oxidation. The methanol oxidation onset potential was similar across the Pt:Ru ratio range of 40:60 – 75:25, whilst CO oxidation onset potential had a clear minimum at 50:50. This shows the CO oxidation onset potential is more sensitive to changes in Pt:Ru ratio than methanol oxidation. Methanol oxidation current at 0.5 V vs. RHE ($\mu A/m^2$) and chronoamperometry experiments showed a Pt:Ru ratio of 50:50 to be the optimum.

The literature on Pt-Ru catalyst particles is contradictory due to multiple factors affecting the optimum composition, morphology and preparation method. Therefore it is important for each researcher to investigate their own optimum conditions and confirm parallels with literature and the reaction mechanisms. Papers by Waszczuk *et al*. (2001) and Chrzanowski & Wieckowski (1998) confirm the more unalloyed Pt-Ru particles perform better for methanol oxidation, while Bock *et al*. (2005) and Long *et al*. (2000) detail the positive influence of ruthenium oxides on CO tolerance and methanol oxidation. The optimum ratio for CO tolerance and methanol oxidation ranges throughout literature. This study could serve as additional information to add to the bank of knowledge on Pt-Ru preparation by chemical deposition, in order to further the understanding of these catalysts.

The suggested future work based on these findings are to identify the degree of alloying influence on the methanol oxidation, as seen in the temperature study. This is of importance since the results hinted towards an optimum around 25 % Ru in Pt-Ru, showing the degree of alloying on methanol oxidation is not a simple question of unalloyed vs. fully alloyed. Secondly, there are unanswered questions surrounding the ruthenium content on the surface. It is important to investigate this claim further by HR-TEM, TEM diffraction patterns or XPS studies. It is important to note that the reaction conditions were optimised for a Pt:Ru molar ratio of 1:1, and this could vary for a platinum ratio higher than this, as the precursor decomposition temperature for platinum is lower than that of ruthenium and this could influence the optimum reactor conditions for the different Pt:Ru ratios. Therefore further investigation is needed to ensure these optimum reactor conditions hold for the different Pt:Ru ratios. Since the pressure study of the catalyst preparation method showed promising results towards a methanol oxidation for catalysts prepared at a higher pressure, further investigations are needed into various argon pressures during preparation in order to optimise this

preparation aspect. Lastly, additional preparation temperature studies are suggested to explore the lower temperature range in order to gain more insight into a more accurate optimum preparation temperature.

7. APPENDIX

7.1. Temperature Effect on Cyclic Voltammograms

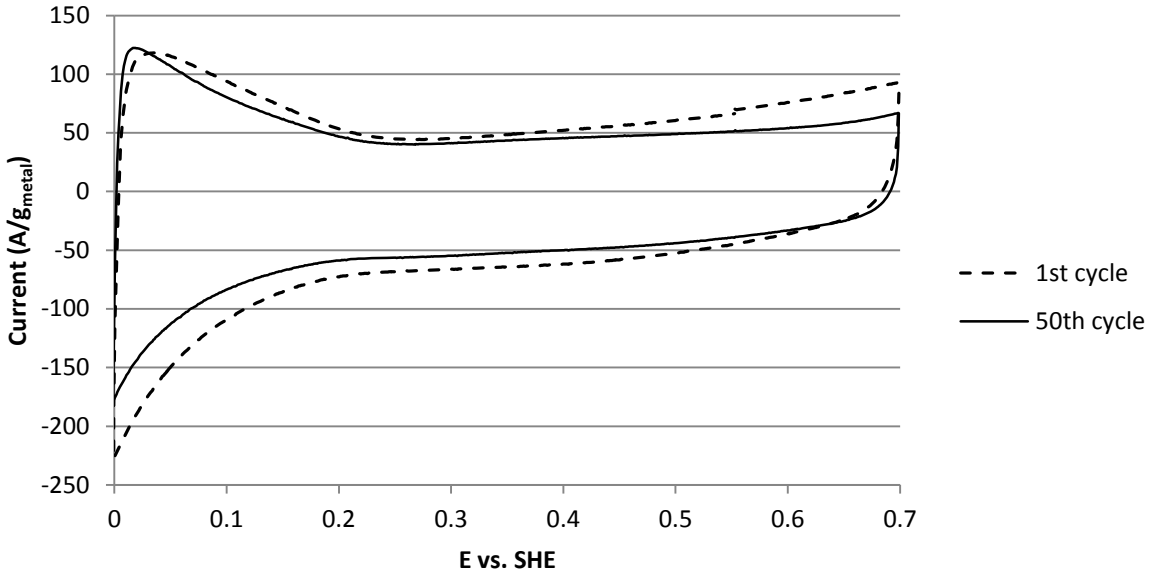

Figure 7-1: First and 50th cyclic voltammetry curves for the catalyst produced under an argon atmosphere at 350 °C for 4 hours.

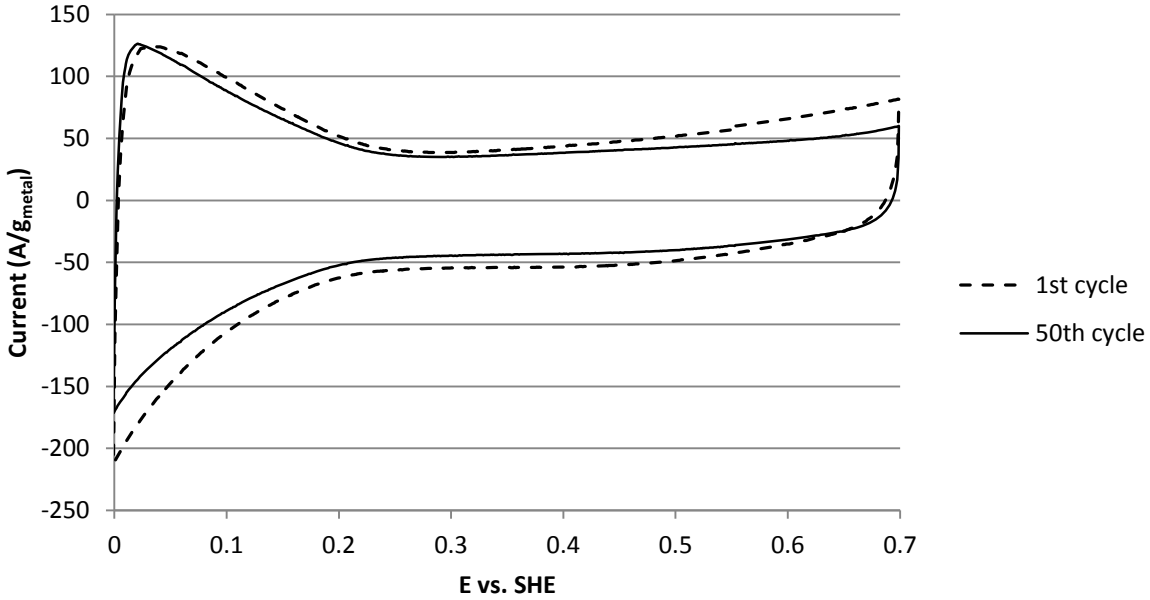

Figure 7-2: First and 50th cyclic voltammetry curves for the catalyst produced under an argon atmosphere at 450 °C for 4 hours.

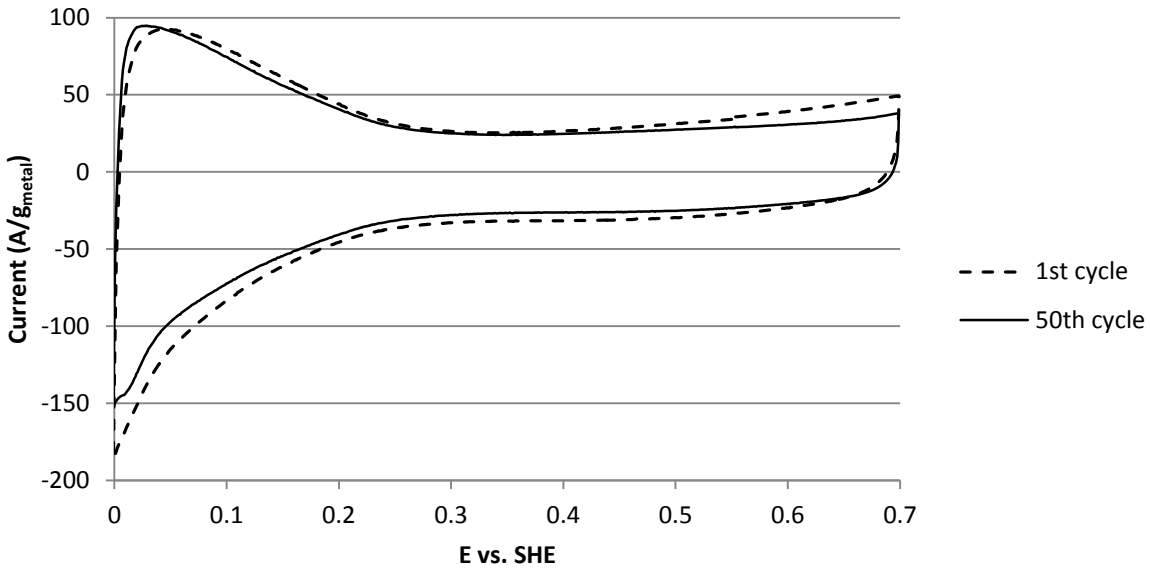

Figure 7-3: First and 50th cyclic voltammetry curves for the catalyst produced under an argon atmosphere at 600 °C for 4 hours.

7.2. Time Effect on Cyclic Voltammograms

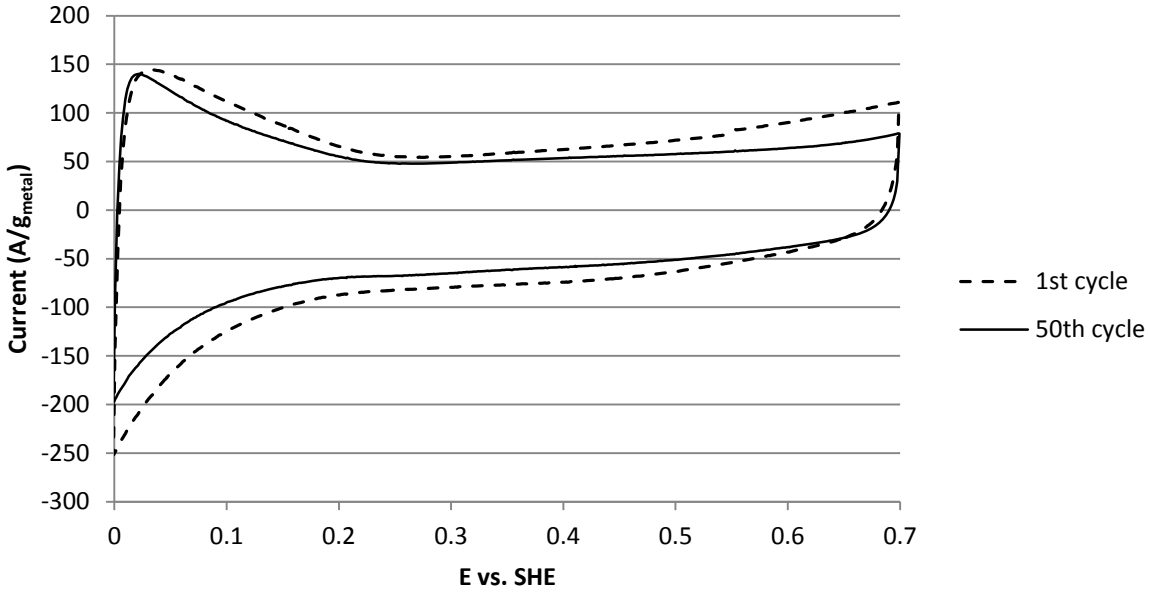

Figure 7-4: First and 50th cyclic voltammetry curves for the catalyst produced under an argon atmosphere at 350 °C for 1 hour.

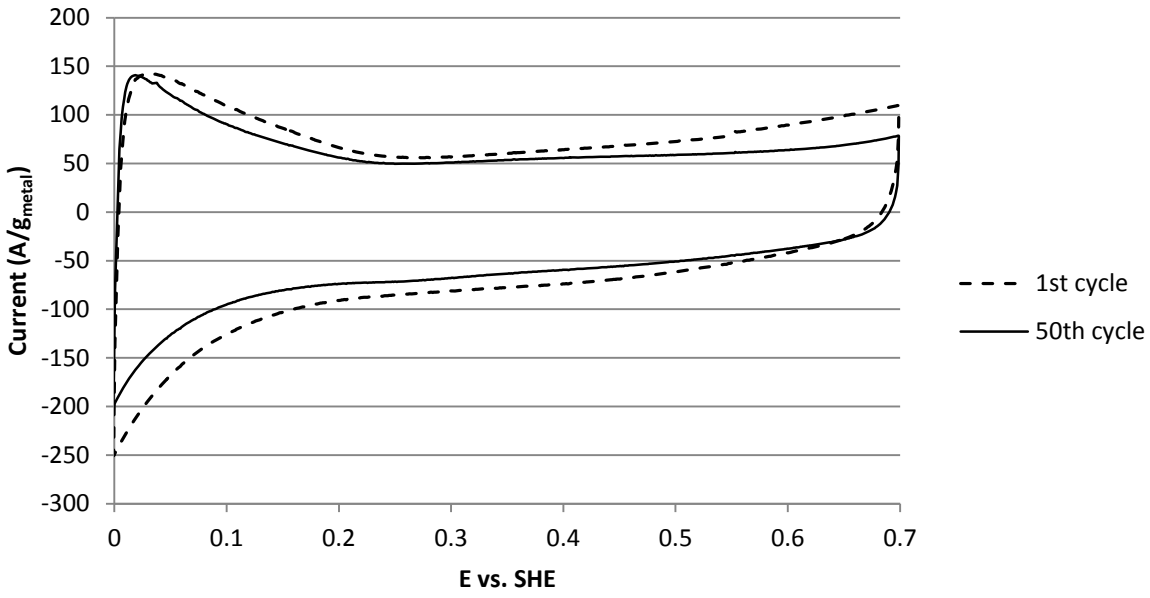

Figure 7-5: First and 50th cyclic voltammetry curves for the catalyst produced under an argon atmosphere at 350 °C for 2 hours.

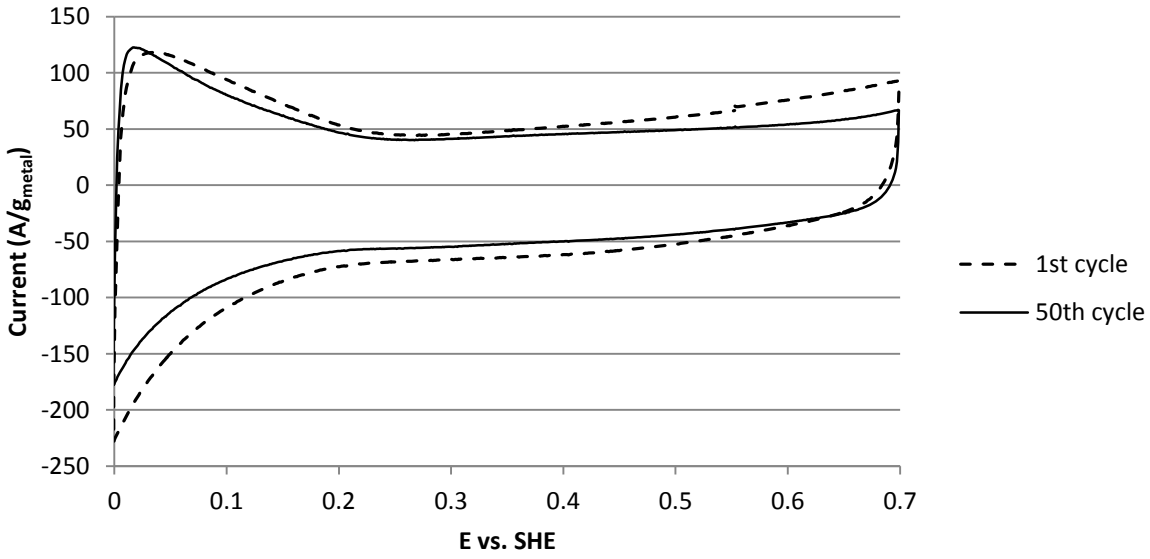

Figure 7-6: First and 50th cyclic voltammetry curves for the catalyst produced under an argon atmosphere at 350 °C for 4 hours.

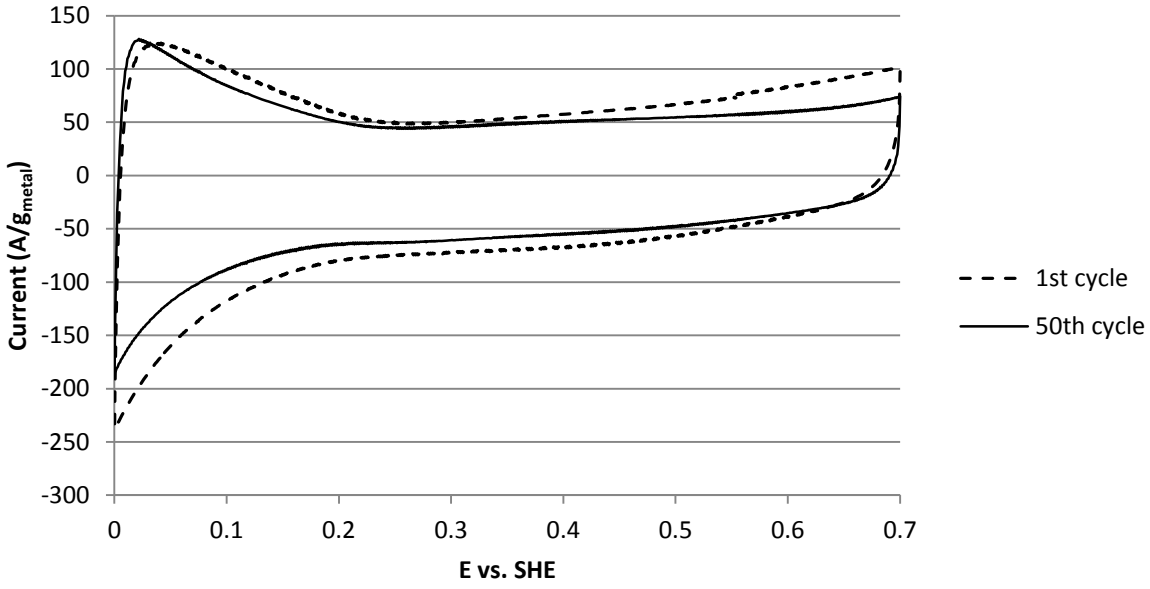

Figure 7-7: First and 50th cyclic voltammetry curves for the catalyst produced under an argon atmosphere at 350 °C for 6 hours.

7.3. Pt:Ru Ratio Effect on Cyclic Voltammograms

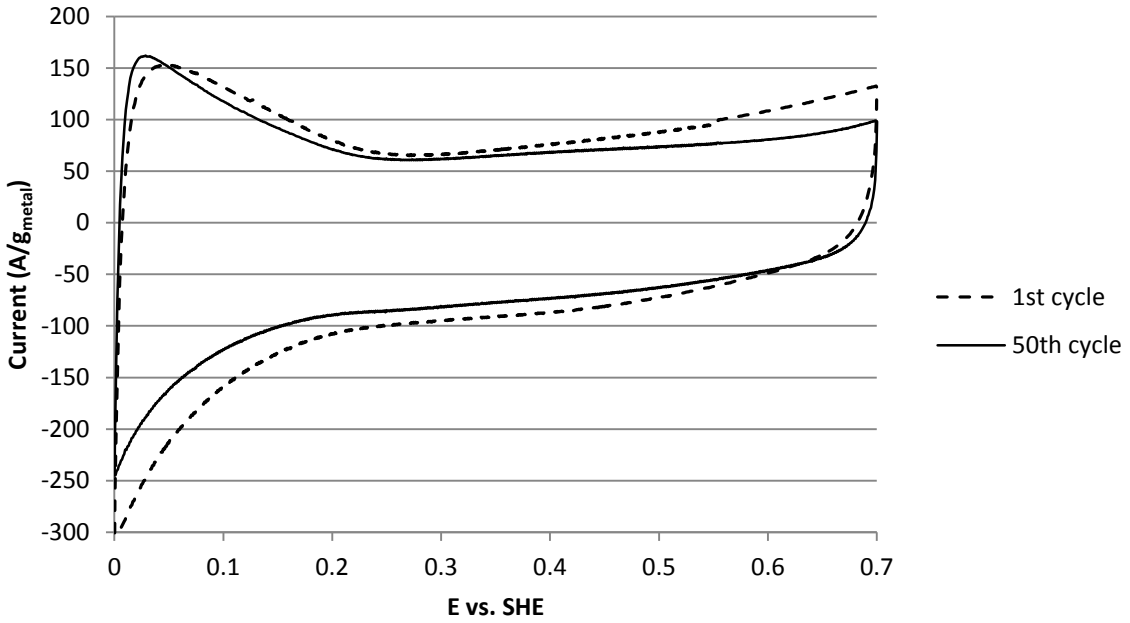

Figure 7-8: First and 50th cyclic voltammetry curves for the catalyst with a Pt:Ru ratio of 50:50 produced under an argon atmosphere at 350 °C for 30 minutes.

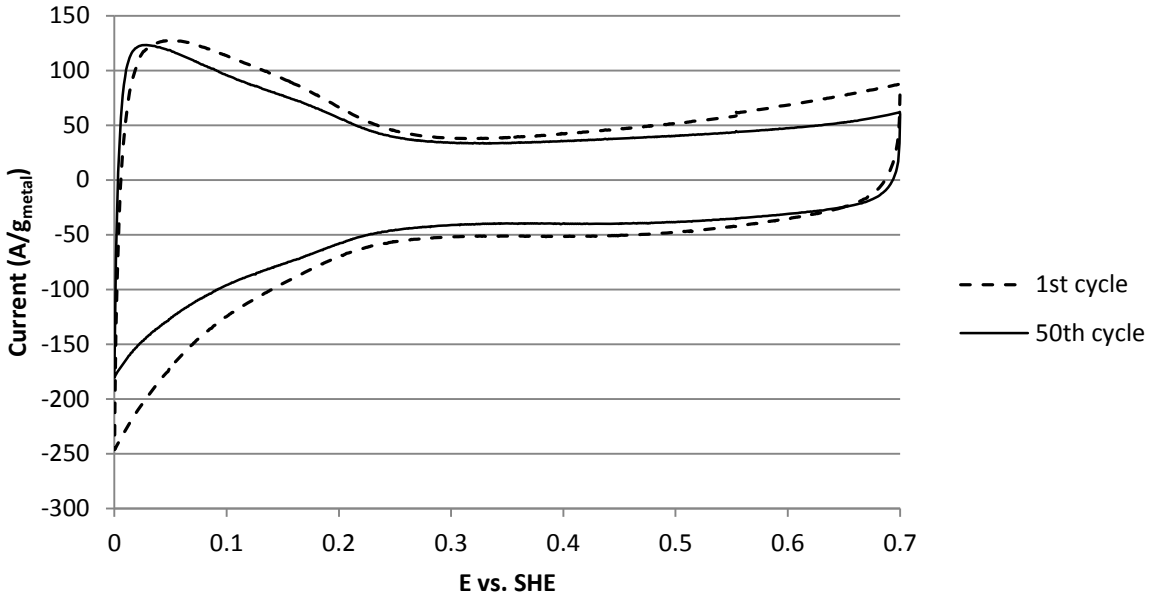

Figure 7-9: First and 50th cyclic voltammetry curves for the catalyst with a Pt:Ru ratio of 60:40 produced under an argon atmosphere at 350 °C for 30 minutes.

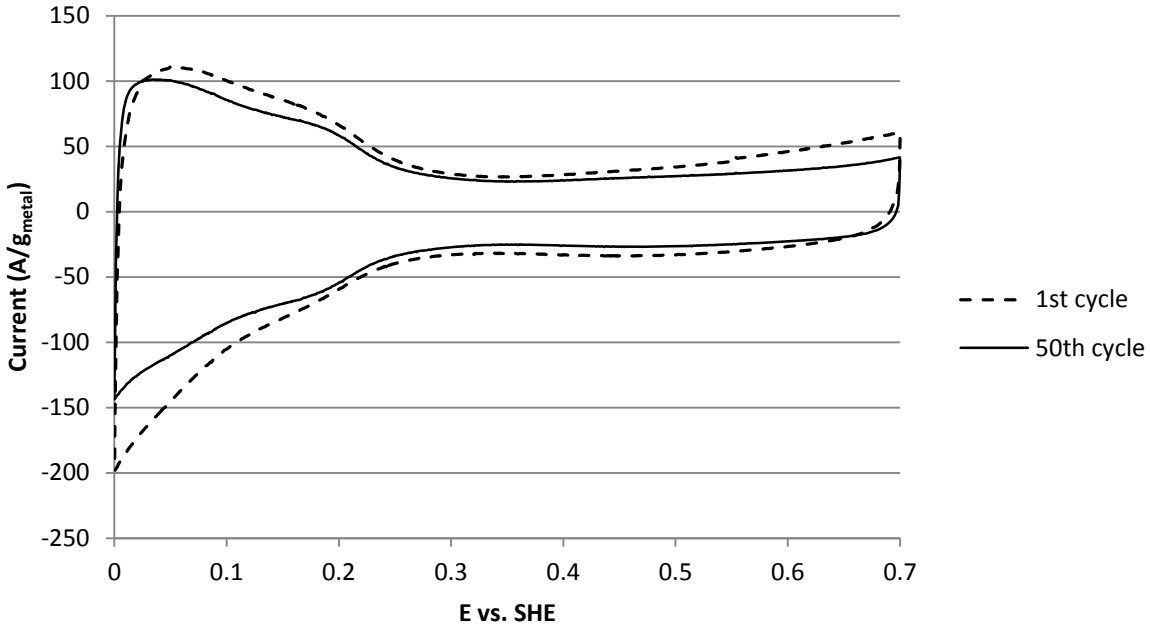

Figure 7-10: First and 50th cyclic voltammetry curves for the catalyst with a Pt:Ru ratio of 75:25 produced under an argon atmosphere at 350 °C for 30 minutes.

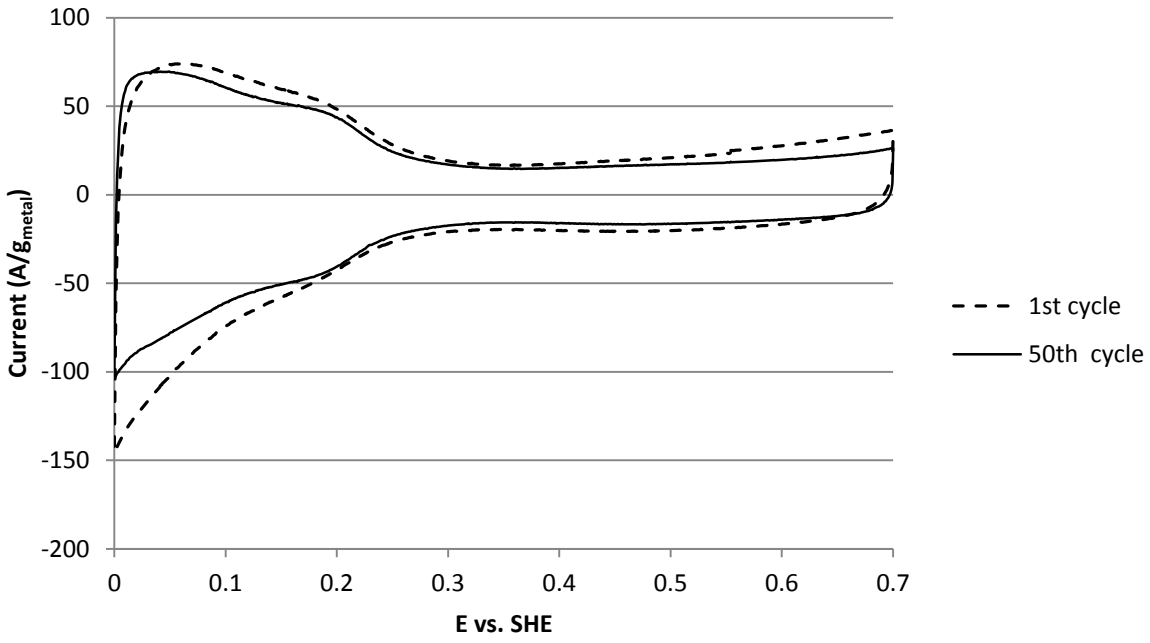

Figure 7-11: First and 50th cyclic voltammetry curves for the catalyst with a Pt:Ru ratio of 80:20 produced under an argon atmosphere at 350 °C for 30 minutes.

8. REFERENCES

Antolini, E. & Cardellini, F. 2001. Formation of carbon supported PtRu alloys: an XRD analysis. *Journal of Alloys and Compounds.* 315(1–2):118-122.

Aricò, A.S., Antonucci, P.L., Modica, E., Baglio, V., Kim, H. & Antonucci, V. 2002. Effect of Pt-Ru alloy composition on high-temperature methanol electro-oxidation. *Electrochimica Acta*. 47(22–23): 3723-3732.

Aricò, A.S., Baglio, V. & Antonucci, V. 2009. Direct Methanol Fuel Cells: History, Status and Perspectives. *Electrocatalysis of Direct Methanol Fuel Cells.* H. Liu & J. Zhang, Eds. 1-78.

Aricò, A.S., Baglio, V., Di Blasi, A., Modica, E., Antonucci, P.L. & Antonucci, V. 2003. Analysis of the high-temperature methanol oxidation behaviour at carbon-supported Pt–Ru catalysts. *Journal of Electroanalytical Chemistry.* 557(0):167-176.

Aricò, A.S., Srinivasan, S. & Antonucci, V. 2001. DMFCs: From Fundamental Aspects to Technology Development. *Fuel Cells.* 1(2):133-161.

Auer, E., Freund, A., Pietsch, J. & Tacke, T. 1998. Carbons as supports for industrial precious metal catalysts. *Applied Catalysis A: General.* 173(2):259-271.

Bahlawane, N., Kohse-Hoinghaus, K., Premkumar, P.A. & Lenoble, D. 2012. Advances in the deposition chemistry of metal-containing thin films using gas phase processes. *Chemical Science.* 3(4):929-941.

Barnard, A.S. 2013. Modeling polydispersive ensembles of diamond nanoparticles. *Nanotechnology*. 24(8): 085703.

Battiston, G.A., Gerbasi, R. & Rodriguez, A. 2005. A Novel Study of the Growth and Resistivity of Nanocrystalline Pt Films Obtained from $Pt(acac)_2$ in the Presence of Oxygen or Water Vapor. *Chemical Vapor Deposition.* 11(3):130-135.

Behling, N.H. 2012. *Fuel Cells: Current Technology Challenges and Future Research Needs.* Elsevier.

Bock, C., Blakely, M.A. & MacDougall, B. 2005. Characteristics of adsorbed CO and CH_3OH oxidation reactions for complex Pt/Ru catalyst systems. *Electrochimica Acta.* 50(12):2401-2414.

Brett, C.M.A., Oliveira Brett, A.M.C.F., Fisher, A.C. & Compton, R.G. 1992. Potential step chronoamperometry at the wall-jet electrode: experimental. *Journal of Electroanalytical Chemistry.* 334(1–2):57-64.

Cabot Corporation 2013. *Vulcan XC-72R.* Available: http://www.cabot-corp.com/Specialty-Carbon-Blacks/Adhesives-and-Sealants/Products/PR200808140923AM3985/ [07/05/2013].

Carmo, M., dos Santos, A.R., Poco, J.G.R. & Linardi, M. 2007. Physical and electrochemical evaluation of commercial carbon black as electrocatalysts supports for DMFC applications. *Journal of Power Sources.*173(2):860-866.

Chen, W., Sun, G., Liang, Z., Mao, Q., Li, H., Wang, G., Xin, Q., Chang, H. et al. 2006. The stability of a PtRu/C electrocatalyst at anode potentials in a direct methanol fuel cell. *Journal of Power Sources.* 160(2):933-939.

Chrzanowski, W. & Wieckowski, A. 1998. Surface Structure Effects in Platinum/Ruthenium Methanol Oxidation Electrocatalysis. *Langmuir.* 14(8):1967-1970.

Climent, V. & Feliu, J. 2011. Thirty years of platinum single crystal electrochemistry. *Journal of Solid State Electrochemistry.* 15(7-8):1297-1315.

Compton, R.G. 1987. *Electrode Kinetics: Reactions.* Elsevier Science.

Conway, B.E. & Pell, W.G. 2003. Double-layer and pseudocapacitance types of electrochemical capacitors and their applications to the development of hybrid devices. *Journal of Solid State Electrochemistry*. 7(9): 637-644.

Cornell University 2014. *Electrochemical Performance for Ordered Intermetallics.* Available: http://abruna.chem.cornell.edu/Projdescp/electrocatalysis-beta.htm [18/02/2014].

Coutanceau, C., Rakotondrainibé, A.F., Lima, A., Garnier, E., Pronier, S., Léger, J. & Lamy, C. 2004. Preparation of Pt-Ru bimetallic anodes by galvanostatic pulse electrodeposition: characterization and application to the direct methanol fuel cell. *Journal of Applied Electrochemistry.* 34(1):61-66.

da Silva, D.F., Oliveira Neto, A., Pino, E.S., Brandalise, M., Linardi, M., Spinacé, E.V. 2007. PtRu/C electrocatalysts prepared using electron beam irradiation. *Materials Research.* 10(4):367-370.

Dhar, H.P., Christner, L.G. & Kush, A.K. 1987. Nature of CO Adsorption during H_2 Oxidation in Relation to Modeling for CO Poisoning of a Fuel Cell Anode. *Journal of the Electrochemical Society.* 134(12):3021-3026.

Dinh, H.N., Ren, X., Garzon, F.H., Piotr Zelenay & Gottesfeld, S. 2000. Electrocatalysis in direct methanol fuel cells: in-situ probing of PtRu anode catalyst surfaces. *Journal of Electroanalytical Chemistry*. 491(1–2): 222-233.

Egerton, R.F. 2011. *Electron Energy-Loss Spectroscopy in an Electron Microscope.* Third Edition ed. London: Springer-Verlag London Limited.

Erkey, C. 2009. Preparation of metallic supported nanoparticles and films using supercritical fluid deposition. *The Journal of Supercritical Fluids.* 47(3): 517-522.

Fabbri, E., Taylor, S., Rabis, A., Levecque, P., Conrad, O., Kötz, R. & Schmidt, T.J. 2014. The Effect of Platinum Nanoparticle Distribution on Oxygen Electroreduction Activity and Selectivity. *Chemcatchem.* :n/a-n/a.

Frelink, T., Visscher, W., Cox, A.P. & van Veen, J.A.R. 1995a. Ellipsometry and dems study of the electrooxidation of methanol at Pt and Ru- and Sn- promoted Pt. *Electrochimica Acta.* 40(10):1537-1543.

Frelink, T., Visscher, W. & van Veen, J. A. R. 1996. Measurement of the Ru Surface Content of Electrocodeposited PtRu Electrodes with the Electrochemical Quartz Crystal Microbalance: Implications for Methanol and CO Electrooxidation. *Langmuir.* 12(15):3702-3708.

Frelink, T., Visscher, W. & van Veen, J.A.R. 1995b. On the role of Ru and Sn as promotors of methanol electro-oxidation over Pt. *Surface Science.* 335(0):353-360.

Gancs, L., Hakim, N., Hult, B. & Mukerjee, S. 2006. Dissolution of Ru from PtRu Electrocatalysts and its Consequences in DMFCs. *ECS Transactions.* 3(1):607-618.

Gancs, L., Hult, B.N., Hakim, N. & Mukerjee, S. 2007. *The Impact of Ru Contamination of a Pt／C Electrocatalyst on Its Oxygen-Reducing Activity.*

Gao, L., Abeysiri, M.C. & Winfield, Z.C. 2012. Evaluating the Energy Consumption and Emissions of Direct Alcohol Fuel Cells. *International Journal of Energy Science (IJES).* 2(5):211-2016.

Garcia, J.R.V. & Goto, T. 2003. Chemical Vapor Deposition of Iridium, Platinum, Rhodium and Palladium. *Materials Transactions.* 44(9):1717-1728.

Gasteiger, H.A., Markovic, N., Ross, P.N. & Cairns, E.J. 1994a. Carbon monoxide electrooxidation on well-characterized platinum-ruthenium alloys. *The Journal of Physical Chemistry.* 98(2):617-625.

Gasteiger, H.A., Markovic, N., Ross, P.N. & Cairns, E.J. 1994b. Temperature-Dependent Methanol Electro-Oxidation on Well-Characterized Pt-Ru Alloys. *Journal of the Electrochemical Society.* 141(7):1795-1803.

Gasteiger, H.A., Markovic, N.M. & Ross, P.N. 1995. H2 and CO Electrooxidation on Well-Characterized Pt, Ru, and Pt-Ru. 1. Rotating Disk Electrode Studies of the Pure Gases Including Temperature Effects*. The Journal of Physical Chemistry*. 99(20): 8290-8301.

Gavrilov, A.N., Savinova, E.R., Simonov, P.A., Zaikovskii, V.I., Cherepanova, S.V., Tsirlina, G.A. & Parmon, V.N. 2007. On the influence of the metal loading on the structure of carbon-supported PtRu catalysts and their electrocatalytic activities in CO and methanol electrooxidation. *Physical Chemistry Chemical Physics.* 9(40):5476-5489.

Gilman, S. 1964. The Mechanism of Electrochemical Oxidation of Carbon Monoxide and Methanol on Platinum. II. The "Reactant-Pair"□ Mechanism for Electrochemical Oxidation of Carbon Monoxide and Methanol.*The Journal of Physical Chemistry.* 68(1):70-80.

Giorgi, L., Pozio, A., Bracchini, C., Giorgi, R. & Turtù, S. 2001. H2 and H2/CO oxidation mechanism on Pt/C, Ru/C and Pt–Ru/C electrocatalysts. *Journal of Applied Electrochemistry.* 31(3):325-334.

Green, M.L., Gross, M.E., Papa, L.E., Schnoes, K.J. & Brasen, D. 1985. Chemical Vapor Deposition of Ruthenium and Ruthenium Dioxide Films. *Journal of the Electrochemical Society.* 132(11):2677-2685.

Hamann, C.H., Hamnett, A. & Vielstich, W. 2007. *Electrochemistry.* Wiley.

Hamnett, A. 1997. Mechanism and electrocatalysis in the direct methanol fuel cell. *Catalysis Today.* 38(4):445-457.

Han, K., Lee, J. & Kim, H. 2006. Preparation and characterization of high metal content Pt–Ru alloy catalysts on various carbon blacks for DMFCs. *Electrochimica Acta.* 52(4):1697-1702.

Hoster, H., Iwasita, T., Baumgärtner, H. & Vielstich, W. 2001. Current-Time Behavior of Smooth and Porous PtRu Surfaces for Methanol Oxidation. *Journal of the Electrochemical Society.* 148(5):A496-A501.

Hubert, H., Devouard, B., Garvie, L.A.J., O'Keeffe, M., Buseck, P.R., Petuskey, W.T. & McMillan, P.F. 1998. *An element of decagonal sphere packing.* Available:http://www.nature.com/nature/journal/v391/n6665/fig_tab/391376a0_F1.html [18/02/2014].

Igumenov, I.K., Semyannikov, P.P., Trubin, S.V., Morozova, N.B., Gelfond, N.V., Mischenko, A.V. & Norman, J.A. 2007. Approach to control deposition of ultra thin films from metal organic precursors: Ru deposition.*Surface and Coatings Technology.* 201(22–23):9003-9008.

Inaba, M. 2009. Durability of Electrocatalysts in Polymer Electrolyte Fuel Cells. *ECS Transactions.* 25(1):573-581.

Iwasita, T., Hoster, H., John-Anacker, A., Lin, W.F. & Vielstich, W. 2000. Methanol Oxidation on PtRu Electrodes. Influence of Surface Structure and Pt-Ru Atom Distribution. *Langmuir.* 16(2):522-529.

Jeon, M.K., Lee, K.R., Oh, K.S., Hong, D.S., Won, J.Y., Li, S. & Woo, S.I. 2006. Current density dependence on performance degradation of direct methanol fuel cells. *Journal of Power Sources.* 158(2):1344-1347.

Jones, A.C. & Hitchman, M.L. 2009. *Chemical Vapour Deposition: Precursors, Processes and Applications.* Royal Society of Chemistry.

Jusys, Z., Kaiser, J. & Behm, R.J. 2002. Composition and activity of high surface area PtRu catalysts towards adsorbed CO and methanol electrooxidation: A DEMS study. *Electrochimica Acta.* 47(22–23):3693-3706.

Kim, Y.D., Over, H., Krabbes, G. & Ertl, G. 2000. Identification of RuO_2 as the active phase in CO oxidation on oxygen-rich ruthenium surfaces. *Topics in Catalysis.* 14(1-4):95-100.

Kinoshita, K. 1990. Particle Size Effects for Oxygen Reduction on Highly Dispersed Platinum in Acid Electrolytes. *Journal of the Electrochemical Society.* 137(3):845-848.

Knights, S.D., Colbow, K.M., St-Pierre, J. & Wilkinson, D.P. 2004. Aging mechanisms and lifetime of PEFC and DMFC. *Journal of Power Sources.* 127(1–2):127-134.

Kotov, N.A. 2006. Materials science: Carbon sheet solutions. *Nature.* 442(7100):254-255.

KU Leuven 2010. *X-ray diffraction – Bruker D8 Discover.* Available: http://fys.kuleuven.be/iks/nvsf/experimental-facilities/x-ray-diffraction-2013-bruker-d8-discover [10/05/2013].

Lasch, K., Jörissen, L., Friedrich, K.A. & Garche, J. 2003. The function of ruthenium oxides in Pt-Ru catalysts for methanol electro-oxidation at low temperatures. *Journal of Solid State Electrochemistry.* 7(9):619-625.

Lasch, K., Jörissen, L. & Garche, J. 1999. The effect of metal oxides as co-catalysts for the electro-oxidation of methanol on platinum–ruthenium. *Journal of Power Sources.* 84(2):225-230.

Li, L. & Xing, Y. 2009. Methanol Electro-Oxidation on Pt-Ru Alloy Nanoparticles Supported on Carbon Nanotubes. *Energies.* 2(3):789-804.

Lin, M., Huang, H., Liu, Y., Liang, C., Fei, S., Chen, X. & Ni, C. 2013. High loading of uniformly dispersed Pt nanoparticles on polydopamine coated carbon nanotubes and its application in simultaneous determination of dopamine and uric acid. *Nanotechnology.* 24(6):065501.

Lin, S.D., Hsiao, T., Chang, J. & Lin, A.S. 1999. Morphology of Carbon Supported Pt-Ru Electrocatalyst and the CO Tolerance of Anodes for PEM Fuel Cells. *The Journal of Physical Chemistry B*. 103(1): 97-103.

Liu, H. & Zhang, J. 2009. *Electrocatalysis of Direct Methanol Fuel Cells: From Fundamentals to Applications.* Wiley.

Liu, H., Song, C., Zhang, L., Zhang, J., Wang, H. & Wilkinson, D.P. 2006. A review of anode catalysis in the direct methanol fuel cell. *Journal of Power Sources.* 155(2):95-110.

Lizcano-Valbuena, W.H., Paganin, V.A. & Gonzalez, E.R. 2002. Methanol electro-oxidation on gas diffusion electrodes prepared with Pt-Ru/C catalysts. *Electrochimica Acta.* 47(22–23):3715-3722.

Long, D.P., Blackburn, J.M. & Watkins, J.J. 2000. Chemical Fluid Deposition: A Hybrid Technique for Low-Temperature Metallization. *Advanced Materials.* 12(12): 913-915.

Long, J.W., Stroud, R.M., Swider-Lyons, K. & Rolison, D.R. 2000. How To Make Electrocatalysts More Active for Direct Methanol OxidationAvoid PtRu Bimetallic Alloys! *The Journal of Physical Chemistry B.*104(42):9772-9776.

Lu, C. & Masel, R.I. 2001. The Effect of Ruthenium on the Binding of CO, H_2, and H_2O on Pt(110). *The Journal of Physical Chemistry B.* 105(40):9793-9797.

Maillard, F., Gloaguen, F. & Leger, J. 2003. Preparation of methanol oxidation electrocatalysts: ruthenium deposition on carbon-supported platinum nanoparticles. Journal of Applied Electrochemistry. 33(1): 1-8.

Maillard, F., Schreier, S., Hanzlik, M., Savinova, E.R., Weinkauf, S. & Stimming, U. 2005. Influence of particle agglomeration on the catalytic activity of carbon-supported Pt nanoparticles in CO monolayer oxidation.*Physical Chemistry Chemical Physics.* 7(2):385-393.

Maiyalagan, T. 2008. Electrochemical synthesis, characterization and electro-oxidation of methanol on platinum nanoparticles supported poly(o-phenylenediamine) nanotubes. *Journal of Power Sources.*179(2):443-450.

Mayrhofer, K.J.J., Blizanac, B.B., Arenz, M., Stamenkovic, V.R., Ross, P.N. & Markovic, N.M. 2005. The Impact of Geometric and Surface Electronic Properties of Pt-Catalysts on the Particle Size Effect in Electrocatalysis. *The Journal of Physical Chemistry B.* 109(30):14433-14440.

Mayrhofer, K.J.J., Strmcnik, D., Blizanac, B.B., Stamenkovic, V., Arenz, M. & Markovic, N.M. 2008. Measurement of oxygen reduction activities via the rotating disc electrode method: From Pt model surfaces to carbon-supported high surface area catalysts. *Electrochimica Acta.* 53(7):3181-3188.

MiPlaza Materials Analysis 2008. *Inductively Coupled Plasma-Atomic Emission Spectrometry (ICP-AES).* Koninklijke Philips.

Morozova, N., B., Zharkova, G., I., Semyannikov, P., P., Sysoev, S., V., Igumenov, I., K., Fedotova, N., E. & Gelfond, N., V. 2001. Vapor pressure of precursors for CVD on the base of platinum group metals. *The Journal of Physical Chemistry* .IV France. 11Pr3-609; Pr3-616.

Morozova, N.B., Zherikova, K.V., Semyannikov, P.P., Trubin, S.V. & Igumenov, I.K. 2009. Study of temperature dependencies of saturated vapor pressure of ruthenium(III) beta-diketonate derivatives. *Journal of Thermal Analysis and Calorimetry.* 98(2): 395-399.

Neergat, M., Leveratto, D. & Stimming, U. 2002. Catalysts for Direct Methanol Fuel Cells. *Fuel cells.* 2(1):25-30.

Over, H. & Muhler, M. 2003. Catalytic CO oxidation over ruthenium—bridging the pressure gap. *Progress in Surface Science.* 72(1–4):3-17.

Piela, P., Eickes, C., Brosha, E., Garzon, F. & Zelenay, P. 2004. *Ruthenium Crossover in Direct Methanol Fuel Cell with Pt-Ru Black Anode.*

Pletcher, D., Greff, R., Peat, R., Peter, L.M. & Robinson, J. 2001. *Instrumental Methods in Electrochemistry.* First ed. Cambridge: Woodhead Publishing Limited.

Pozio, A., Silva, R.F., De Francesco, M., Cardellini, F. & Giorgi, L. 2002. A novel route to prepare stable Pt–Ru/C electrocatalysts for polymer electrolyte fuel cell. *Electrochimica Acta.* 48(3):255-262.

Radmilovic, V., Gasteiger, H.A. & Ross, P.N. 1995. Structure and Chemical Composition of a Supported Pt-Ru Electrocatalyst for Methanol Oxidation. *Journal of Catalysis.* 154(1):98-106.

Rajalakshmi, N., Lakshmi, N. & Dhathathreyan, K.S. 2008. Nano titanium oxide catalyst support for proton exchange membrane fuel cells. *International Journal of Hydrogen Energy.* 33(24):7521-7526.

Ralph, T.R. & Hogarth, M.P. 2002. Catalysis for Low Temperature Fuel Cells. *Platinum Metals Review.* 46(3):117-135.

Ribeiro, V.A., Correa, O.V., Neto, A.O., Linardi, M. & Spinacé, E.V. 2010. Preparation of PtRuNi/C electrocatalysts by an alcohol-reduction process for electro-oxidation of methanol. *Applied Catalysis A: General.*372(2):162-166.

Rolison, D.R., Hagans, P.L., Swider, K.E. & Long, J.W. 1999. Role of Hydrous Ruthenium Oxide in Pt-Ru Direct Methanol Fuel Cell Anode Electrocatalysts: The Importance of Mixed Electron/Proton Conductivity. *Langmuir.* 15(3):774-779.

Santos, E. & Schmickler, W. 2011. *Catalysis in Electrochemistry: From Fundamental Aspects to Strategies for Fuel Cell Development.* Wiley.

Sato, Y., Yomogida, K., Nanaumi, T., Kobayakawa, K., Ohsawa, Y. & Kawai, M. 2000. Electrochemical Behavior of Activated-Carbon Capacitor Materials Loaded with Ruthenium Oxide. *Electrochemical and Solid-State Letters*. 3(3): 113-116.

Schmidt, T.J., Gasteiger, H.A., Stäb, G.D., Urban, P.M., Kolb, D.M. & Behm, R.J. 1998. Characterization of High-Surface-Area Electrocatalysts Using a Rotating Disk Electrode Configuration. *Journal of the Electrochemical Society.* 145(7):2354-2358.

Shah, R.K. 2007. Introduction to Fuel Cells. In S. Basu, Ed. *Recent Trends in Fuel Cell Science and Technology*. Springer New York. 1-9.

Shao, M. 2013. *Electrocatalysis in Fuel Cells: A Non- and Low- Platinum Approach.* Springer.

Sharma, S. & Pollet, B.G. 2012. Support materials for PEMFC and DMFC electrocatalysts—A review. *Journal of Power Sources.* 208(0):96-119.

Sinha, P.K., Mukherjee, P.P. & Wang, C. 2007. Impact of GDL structure and wettability on water management in polymer electrolyte fuel cells. *Journal of Materials Chemistry*. 17(30):3089-3103.

Spinace, E.V., Indelicato do Vale, L.A., Oliveira Neto, A. & Linardi, M. 2007. Preparation of PtRu/C Anode Electrocatalysts using NaBH4 as Reducing Agent and OH- ions as Stabilizing Agent. *ECS Transactions.*5(1):89-94.

Stamenkovic, V., Grgur, B.N., Ross, P.N. & Markovic, N.M. 2005. *Oxygen Reduction Reaction on Pt and Pt-Bimetallic Electrodes Covered by CO: Mechanism of the Air Bleed Effect with Reformate.*

Stevens, D.A., Rouleau, J.M., Mar, R.E., Bonakdarpour, A., Atanasoski, R.T., Schmoeckel, A.K., Debe, M.K. & Dahn, J.R. 2007. Characterization and PEMFC Testing of $Pt_{1-x}M_x$ (M = Ru , Mo , Co , Ta , Au , Sn) Anode Electrocatalyst Composition Spreads. *Journal of the Electrochemical Society.* 154(6):B566-B576.

Thurier, C. & Doppelt, P. 2008. Platinum OMCVD processes and precursor chemistry. *Coordination Chemistry Reviews.* 252(1–2):155-169.

Vielstich, W., Lamm, A. & Gasteiger, H.A. Eds. 2003. *Handbook of Fuel Cells- Fundamentals, Technology and Applications*. 4th ed. England: WILEY.

Vielstich, W., Yokokawa, H. & Gasteiger, H.A. 2009. *Handbook of Fuel Cells: fundamentals technology and applications. Advances in electrocatalysis, materials, diagnostics and durability : Part 1.* Wiley.

Vigier, F., Coutanceau, C., Hahn, F., Belgsir, E.M. & Lamy, C. 2004. On the mechanism of ethanol electro-oxidation on Pt and PtSn catalysts: electrochemical and in situ IR reflectance spectroscopy studies. *Journal of Electroanalytical Chemistry.* 563(1):81-89.

Vogel, W., Britz, P., Bönnemann, H., Rothe, J. & Hormes, J. 1997. Structure and Chemical Composition of Surfactant-Stabilized PtRu Alloy Colloids. *The Journal of Physical Chemistry B.* 101(51):11029-11036.

Wang, Z.B., Yin, G.P. & Shi, P.F. 2005. Stable Pt–Ru/C Catalysts Prepared from New Precursors by Thermal Reduction for Direct Methanol Fuel Cell. *Journal of the Electrochemical Society.* 152(12):A2406-A2412.

Wang, Y., Wang, C. & Chen, K.S. 2007. Elucidating differences between carbon paper and carbon cloth in polymer electrolyte fuel cells. *Electrochimica Acta.* 52(12):3965-3975.

Wang, Z., Wang, X., Zuo, P., Yang, B., Yin, G. & Feng, X. 2008. Investigation of the performance decay of anodic PtRu catalyst with working time of direct methanol fuel cells. *Journal of Power Sources.* 181(1):93-100.

Wasmus, S. & Küver, A. 1999. Methanol oxidation and direct methanol fuel cells: a selective review. *Journal of Electroanalytical Chemistry.* 461(1–2):14-31.

Waszczuk, P., Solla-Gullón, J., Kim, H.S., Tong, Y.Y., Montiel, V., Aldaz, A. & Wieckowski, A. 2001. Methanol Electrooxidation on Platinum/Ruthenium Nanoparticle Catalysts. *Journal of Catalysis.* 203(1):1-6.

Watanabe, M. & Motoo, S. 1975. Electrocatalysis by ad-atoms: Part II. Enhancement of the oxidation of methanol on platinum by ruthenium ad-atoms. *Journal of Electroanalytical Chemistry and Interfacial Electrochemistry*. 60(3): 267-273.

Watanabe, M., Uchida, M. & Motoo, S. 1987. Preparation of highly dispersed Pt + Ru alloy clusters and the activity for the electrooxidation of methanol. *Journal of Electroanalytical Chemistry and Interfacial Electrochemistry.* 229(1–2):395-406.

Will, F.G. 1965. Hydrogen Adsorption on Platinum Single Crystal Electrodes: I . Isotherms and Heats of Adsorption. *Journal of the Electrochemical Society.* 112(4):451-455.

Wu, J., Yuan, X.Z., Wang, H., Blanco, M., Martin, J.J. & Zhang, J. 2008. Diagnostic tools in PEM fuel cell research: Part I Electrochemical techniques. *International Journal of Hydrogen Energy.* 33(6):1735-1746.

Xing, L., Hossain, M.A., Tian, M., Beauchemin, D., Adjemian, K. & Jerkiewicz, G. 2014. Platinum Electro-dissolution in Acidic Media upon Potential Cycling. *Electrocatalysis*. 5(1): 96-112.

Yang, L., Yang, W. & Cai, Q. 2007. Well-Dispersed PtAu Nanoparticles Loaded into Anodic Titania Nanotubes: A High Antipoison and Stable Catalyst System for Methanol Oxidation in Alkaline Media. *The Journal of Physical Chemistry C.* 111(44):16613-16617.

Yoda, S., Hasegawa, A., Suda, H., Uchimaru, Y., Haraya, K., Tsuji, T. & Otake, K. 2004. Preparation of a Platinum and Palladium/Polyimide Nanocomposite Film as a Precursor of Metal-Doped Carbon Molecular Sieve Membrane via Supercritical Impregnation. *Chemistry of Materials.* 16(12): 2363-2368.

Zaidi, S.M.J. & Rauf, M.A. 2009. Fuel Cell Fundamentals. In S.M.J. Zaidi & T. Matsuura, Eds. *Polymer Membranes for Fuel Cells.* Springer US. 1-6.

Zhang, H., Wang, X., Zhang, J.L. & Zhang, J.W. 2008. *Electrocatalysts and Catalyst Layers Fundamentals and Applications.* London: Springer.

Zhao, J., Marcy, H.O., Tonge, L.M., Wessels, B.W., Marks, T.J. & Kannewurf, C.R. 1989. Organometallic Chemical Vapor Deposition of Superconducting YBaCuO Films and Post-Deposition Processing. In R. McConnell & S. Wolf, Eds. *Science and Technology of Thin Film Superconductors*. Springer US. 295-299.

Zhao, T., Kreuer, K.D. & Van Nguyen, T. 2007. *Advances in Fuel Cells.* Elsevier Science.

Zheng, J.P., Cygan, P.J. & Jow, T.R. 1995. Hydrous Ruthenium Oxide as an Electrode Material for Electrochemical Capacitors*. Journal of the Electrochemical Society*. 142(8): 2699-2703.